

Technische Universität München
Fakultät für Mathematik

Mathematical Modeling of Quorum Sensing: Two Different Approaches

Meltem Gölgeli Matur

Vollständiger Abdruck der von der Fakultät für Mathematik der Technischen Universität München zur Erlangung des akademischen Grades eines
Doktors der Naturwissenschaften (Dr. rer. nat.)
genehmigten Dissertation.

Vorsitzender: Univ.-Prof. Dr. Daniel Matthes
Prüfer der Dissertation: 1. Univ.-Prof. Dr. Christina Kuttler
2. Univ.-Prof. Dr. Johannes Müller
3. Fordyce A. Davidson, Ph.D., Reader
University of Dundee, Scotland, United Kingdom

Die Dissertation wurde am 02.07.2013 bei der Technischen Universität München eingereicht und durch die Fakultät für Mathematik am 17.09.2013 angenommen.

Abstract

In this PhD thesis, a special case of a bacterial communication system, the so-called Quorum Sensing is modeled, in two different mathematical approaches. First, the transition process among bacterial states affected by the signaling molecule concentration is investigated in a stochastic model and their time dynamic is determined. The suitable parameters are estimated in comparison to experimental data. Next, the spatial distribution of signaling molecules produced by heterogeneously distributed bacteria is described and analyzed by a reaction-diffusion equation. Approximate analytical solutions to this complex system were determined. The modeling results are implemented, simulated and discussed for both approaches.

Zusammenfassung

Im Rahmen dieser Doktorarbeit wird ein Spezialfall bakterieller Kommunikation, das sogenannte Quorum Sensing, mit zwei verschiedenen mathematischen Ansätzen modelliert. Zuerst wird der Transitionsprozess zwischen verschiedenen bakteriellen Zuständen, beeinflusst von Signalmolekülen, mit einem stochastischen Modell untersucht und deren zeitliche Dynamik bestimmt. Passende Parameter werden im Vergleich mit experimentellen Daten geschätzt. Anschließend wird die räumliche Verteilung von Signalmolekülen, die von heterogen verteilten Bakterien produziert werden, durch eine Reaktions - Diffusions Gleichung beschrieben und analysiert. Geeignete approximative Lösungen zu diesem komplexen System werden bestimmt. Die Modellierungsergebnisse für beide Ansätze werden implementiert, simuliert und diskutiert.

Acknowledgments

I would like to express my sincere gratitude to Prof. Dr. Christina Kuttler, Prof. Dr. Johannes Müller and Dr. Burkhard Hense for giving me the opportunity to work with them. It was the greatest chance in my academic life.

I am so thankful to Prof. Dr. Christina Kuttler and Prof. Dr. Johannes Müller for their guidance, patience and constant support. I have really learned a lot from you.

I would like to thank Dr. Burkhard Hense, who was being for me much more than a regular chef during my Ph.D. journey in Helmholtz Center Munich.

Special thanks goes to my family Ferhat, Levent and Sevinc who always stand behind me, no matter what decision I am making. I deeply thank to my friends Judith, Maria and Phaedra who have supported me mentally and emotionally during the last challenging years.

Meltem Gölgeli
Munich, 01.10.2013

Dedicated to Sadettin and Sevinc Gölgeci

Contents

Contents	vii
List of Figures	ix
List of Tables	1
1 Introduction	3
1.1 Motivation and Objectives of the Thesis	4
1.2 Outline of the Thesis	6
2 Quorum Sensing and an Overview of its Mathematical Models	9
2.1 Quorum Sensing and Bacterial Behavior	9
2.2 The Underlying Experiment	11
2.3 A Brief Overview on Mathematical Modeling of QS	15
3 A Stochastic Model of QS	19
3.1 Model Assumptions	19
3.2 A Single Cell Model	19
3.2.1 Stationary States	23
3.2.2 Exact Solution for the Single Cell Model	26
3.3 A Population Model	32
3.3.1 Exact Solution for the Population Model	33
3.4 Implementation of the Explicit Solution for the Parameter Estimation	35
3.4.1 Implementation	36
3.4.2 Parameter Estimation and Numerical Simulations	37
3.5 Conclusions	40
4 Spatial Structure of Cells and their Effect on the AHL Concentration	43
4.1 Model Assumptions	44
4.1.1 Pre-model: Line Shaped Single Cell in 1D	44
4.2 A Single Cell Model in \mathbb{R}^3 with a Linear Source Term	49
4.2.1 Assumptions of the Single Cell Model with a Linear Source Term	49
4.2.2 Suitable Scaling for the Single Cell Model with a Linear Source Term	52

CONTENTS

4.2.3	Single Cell Model with Abiotic AHL Degradation	55
4.2.4	A suitable Approximate Model for a Single Cell in \mathbb{R}^3 with a Linear Source Term	56
4.3	A Population Model in \mathbb{R}^3 with a Linear Source Term and a suitable Approximate Model	61
4.4	A Single Cell Model in \mathbb{R}^3 with a Lipschitz Continuous Source Term	69
4.4.1	Suitable Scaling for the Single Cell Model with a Nonlinear Source Term	70
4.4.2	A Suitable Approximate Model for a Single Cell with a Lipschitz Continuous Source Term	73
4.4.3	Numerical Simulations for a Single Cell	75
4.5	A Population Model in \mathbb{R}^3 with a Lipschitz Continuous Source Term	76
4.5.1	Numerical simulations for N cells	86
4.6	Conclusions	90
5	Discussion	93
	Bibliography	95

List of Figures

2.1	QS-regulated gene transcription of <i>V. fischeri</i>	11
2.2	QS system of <i>P.putida</i> IsoF with the Las based reporter.	12
2.3	A sketch of flow chamber.	13
2.4	A sample picture of the experiment.	13
2.5	Pictures from the experiment.	14
3.1	Possible states of one cell and their transition.	20
3.2	Time course of AHL concentration in active and inactive cell state.	21
3.3	Characteristic curves of an inactive cell.	28
3.4	Suitable initial distribution for $u^-(z, 0)$	29
3.5	Simulation of one inactive cell.	30
3.6	Simulation of one active cell.	32
3.7	Structure of cell transition	33
3.8	Characteristic curves on the $(z - t)$ -grid.	36
3.9	Number of cells without external AHL.	39
3.10	Model (3.26) fitted to experimental data	40
4.1	1D cell on the x-axis.	45
4.2	Numerical simulation of one 'shrinking' cell focused on the intracellular behavior	77
4.3	Numerical simulation of one 'shrinking' cell focused on the changing scale of AHL concentration	78
4.4	Numerical simulation of the vanishing AHL concentration	78
4.5	Numerical simulation of the AHL concentration on the boundary of intra-extra cellular space for different values of L	79
4.6	Numerical simulation of AHL production for two cells	87
4.7	Numerical simulation of approximate AHL concentration for N cells	90

LIST OF FIGURES

List of Tables

3.1	Variables of the model developed in Chapter 3.	21
3.2	Parameters of the model developed in Chapter 3.	22
3.3	Change of AHL concentration and correspondent pdfs in time.	22
3.4	Starting parameter values vs. estimated parameter values.	38
3.5	Starting values for the data based estimation.	39
4.1	Variables of the model in Chapter 4.	50
4.2	Parameters of the models with a linear reaction term.	50
4.3	Parameters of the models with a Lipschitz continuous source term.	69
4.4	Parameters used for numerical simulations in Chapter 4.	76

LIST OF TABLES

1 Introduction

Mathematical modeling of microbiological processes generates an interdisciplinary scientific interest because a model can simplify understanding of biochemical mechanisms in complex dynamical systems by reducing them to the essential subprocesses and may predict the future behavior of the natural systems (Murray [47, 48]). Even the unicellular organisms, e.g. bacteria, utilize a variety of complex biochemical mechanisms to share information about environmental issues. It is widely recognized that bacteria communicate to each other using several mechanisms to facilitate their adaptation to changing environmental conditions (Bassler [6], Eberhard [11], Fuqua et al. [18], Miller and Bassler [41], Nealson et al. [50]).

Quorum sensing is one of the several possible cell to cell communication mechanisms appearing in many bacterial species which indicates a collective behavior of the whole colony by coordinating their gene expression using diffusible signaling molecules (Bassler [6], Fuqua et al. [18], Hense et al. [22]). In this process, each bacterium generally produces signaling molecules and releases them through the cell membrane. Moreover, they detect the accumulation of signaling molecules, continuously. When a critical environmental concentration of signaling molecules is reached, bacteria coordinate their gene expression so that a collective behavior starts for the benefit of the colony (Waters and Bassler [60], Williams [61]). In other words, quorum sensing effectively can control processes like bioluminescence, virulence, biofilm formation, sporulation, antibiotic resistance etc. in various bacterial species allowing the bacteria to act as a multicellular organism (Zhu et al. [64]).

Various mathematical models describing quorum sensing in bacteria can be found in the literature. Nevertheless, the similarities between different quorum sensing mechanisms enable to classify the mathematical models mainly in two different approaches: modeling at the single cell level (Dockery and Keener [10], James et al. [26]) and modeling at the population level (Anguige et al. [1, 2], Gustafsson et al. [21], Ward et al. [59]). The population models can describe either a homogeneously mixed population ([1, 21, 59]) or spatially heterogeneous structures (Hense et al. [23], Melke et al. [39], Müller et al. [45]). Furthermore, the noise under the intercellular dynamics and the random cell transcription enforce developing stochastic models at both single cell and population level that describe bacterial motion, cell division and chemical communications (Goryachev et al. [20], Koerber et al.

[33], Müller et al. [46]).

1.1 Motivation and Objectives of the Thesis

Even though numerous biological and mathematical models of quorum sensing have been studied over the years, the regulation of dynamic cell responses affected by signaling molecule concentration and the interaction between cells influenced by the changes of multiple environmental and cellular factors are still not fully understood. For this reason, there is a strong interest in experimental research for cell to cell communication which can be supported by mathematical models to understand and interpret these processes better. Generally, the analysis of mathematical models and the estimation of the correspondent parameters aims to predict the future behavior of the bacterial colony and can potentially motivate to perform new experimental methods. In this thesis, we study two different mathematical modeling approaches for the quorum sensing mechanism in response to some open problems appeared from experimental researches.

The first modeling approach in this thesis is based on the stochastic dynamics of individual bacterial cells which display a switching behavior from an 'inactive' to an 'active' cell state as a result of quorum sensing. The switching behavior is dependent on the signaling molecule concentration around the cell, i.e., if the concentration reaches a certain threshold around a cell quorum sensing becomes active. Since the signaling molecules are assumed to be present in large amounts, we model their time dependent change in two different states by ordinary differential equations (i.e., deterministically), while we take into account the randomness of the switching process and insert this stochasticity with the probability density functions into the differential equation system. Thus, we determine signaling molecule dependent probability density functions of discrete cell states and explain the dynamics of a bacterial colony in time.

Stochasticity due to switching of the gene status was pioneered in Ko [31] and followed by many others [29, 34, 46]. Our study mainly focuses on the approaches of Lipniacki et al. [34] and Müller et al. [46]. First, Lipniacki et al. [34] combine the ordinary differential equations with a stochastic component for the transcription of mRNA and protein levels in a single cell and obtain a system of first-order partial differential equations for two dimensional probability density functions. Then, Müller et al. [46] introduce a similar stochastic approach for the transcription process between identical cells switching in two discrete states in which the large number of product density (mRNA or protein) is described deterministically.

Hence Müller et al. [46] address the probability density of product concentration (i.e., it means for our case: signaling molecule concentration) in two cell states at time t . In contrast, we investigate the individual dynamics of a bacterial colony of size N in two cell

states (inactive and active) at time t where the cells are considered to switch randomly from the 'inactive' state to the 'active' state dependently on the signaling molecule concentration. Ultimately, our approach intends to explain the switching behavior in a bacterial colony as a result of quorum sensing. Taking up the modeling idea in Müller et al. [46], we introduce a model with partial differential equations including the interaction among a growing bacterial colony. Since we are not interested here in the spatial distribution of cells, our model includes the variables of signaling molecule concentration and time. These partial differential equations turn out to have a unique explicit solution. Further, we compare the model with an experimental data set and estimate correspondent parameter values. In that way, we are able to predict the future behavior of bacteria in such a system and to understand the similar quorum sensing behavior of many other colonies.

In the second part of the thesis, contrary to the first modeling approach, we concern about the spatial distribution of cells and its effect on the signaling molecule concentration. Triggering the positive feedback loop diffusible signaling molecules have also an impact on the behavioral changes of cells as an effect of quorum sensing, e.g. the switching behavior which we have studied in the first modeling approach. However we overlook this possible behavioral change in our model. Müller et al. [45] formulate a similar idea keeping cells as single objects with a spatially homogeneous interior, which enables to describe the total mass of the signaling molecules within the cells by ordinary differential equations. In the exterior, the spatial structure becomes important and a diffusion equation with a decay term represents the diffusion and degradation of the signaling molecules. They give a special attention on diffusion of the signaling molecules through the cell membrane and explain the active diffusion (assuming that the signaling molecules are carried by active pumps located in the cell membrane) of signaling molecules with two different rates (inflow and outflow rates). Although this model appears in linear form, the PDE in medium is defined on a region excluding little holes (the cells), which precludes finding analytical solutions for many cells and costs a high computational effort for a fine discretization around each of the cells, numerically. Avoiding these costs, they scale the cell size to a point which facilitates to find an approximate solution in the stationary state. Here, the scaling behavior of inflow and outflow rates is of special interest, because of the fact considering the mass within the cell (homogeneously distributed structure) but density in the exterior (heterogeneous structure).

Müller and Uecker [44] extended the idea of Müller et al. [45] and presented a model in which cells communicate with each other via diffusion of the signaling molecules in the non stationary case. The model consists of an initial boundary value problem for a parabolic partial differential equation describing the exterior concentration of the signaling molecules, coupled with ordinary differential equations for the masses of the substance within each cell, analogously to Müller et al. [45], whereas Müller and Uecker [44] develop

approximate models and approximation theorems that include the form of an ordinary differential equation or of a delay equation.

Contrary to the approaches in Müller et al. [45] and Müller and Uecker [44], our model is based on a reaction diffusion equation for both exterior and interior of cells where the reaction term contains a nonlinearity because of the quorum sensing process. We assume that the signaling molecules freely diffuse through the cell membrane and each of the spatially scattered identical cells have a way to sense signaling molecules produced by others besides its own internal production. We adopt the idea of shrinking cells and therefore we scale the cells appropriately with the radius $L \rightarrow 0$, which allows us to replace each cell by a point source. As we consider the signaling molecules have a spatially homogeneous distribution within the cell, we scale the production rates in each cell so that we preserve the spatial structure of the heterogeneous medium. Heterogeneity of the signaling molecules in the exterior results from the heterogeneous distribution of cells. Since the signaling molecules are only transported by diffusion, the distance between cells has a strong impact on the sensing process. Indeed, a cell may sense the signaling molecules produced by a neighbor cell much better than produced by one cell located over long distances. It is well known that the concentration of surrounding signaling molecules triggers the positive feedback loop and increases the production within the cell [8]. Under all of these assumptions, we first suggest a single cell model where we can compute a unique explicit solution for the model which leads us to find a suitable approximate system for the N cells case. Subsequently, we obtain approximate solutions for the nonlinear equations under steady state condition and illustrate numerical simulations for the approximate solution. As a result, we investigate a large scale concentration of signaling molecules while the cells were assumed to shrink to a point.

1.2 Outline of the Thesis

This thesis is organized as follows:

In Chapter 2, we briefly introduce the biological background of quorum sensing. Then, we give a detailed account of a gene regulation experiment performed for the biofilm forming bacterial strain *Pseudomonas putida* IsoF. At the end of this chapter we give a short literature review on relevant papers on mathematical modeling of quorum sensing.

In Chapter 3, we analyze the interaction between cells in a stochastic manner and develop a model describing the probability density function of cells in two different cell states. The model approach leads to a system of hyperbolic partial differential equations depending on signaling molecule concentration and time. After solving this hyperbolic partial differential equation system via the method of characteristics explicitly, we estimate a suitable parameter family appropriate to the experimental data by the least squares

method. Moreover, we simulate the solution numerically and show that the developed model meets the experimental data quite well. To conclude this chapter, we summarize the achieved results, interpret the estimated parameter values according to experimental measurements and give an aspect of the future work.

In Chapter 4, we focus on the spatial interaction between cells via signaling molecules and develop a model in form of a reaction diffusion equation. Further, we explore the signaling molecule concentration in space while we assume that the cells shrink to a point source. The scaling concept of the signaling molecule production rates is of interest, because the signaling molecules that are produced within the cell can diffuse freely through the membrane to the spatially structured medium. As it is often not possible to find any explicit or numerical solution to the derived model, we seek a suitable approximation in the steady state which can embody the classical solution. Consequently, we present approximate models and approximation theorems for different typical situations that show the solutions of original and approximative models are close to each other.

2 Quorum Sensing and an Overview of its Mathematical Models

This chapter aims to give an overview of a communication system among bacteria which is known as quorum sensing. Section 2.1 provides a short history of quorum sensing via some selected publications in biology. In order to understand the dynamics of this communication system better we give an experimental example in Section 2.2. To conclude this chapter we present in Section 2.3 some aspects on the mathematical modeling of quorum sensing among many.

2.1 Quorum Sensing and Bacterial Behavior

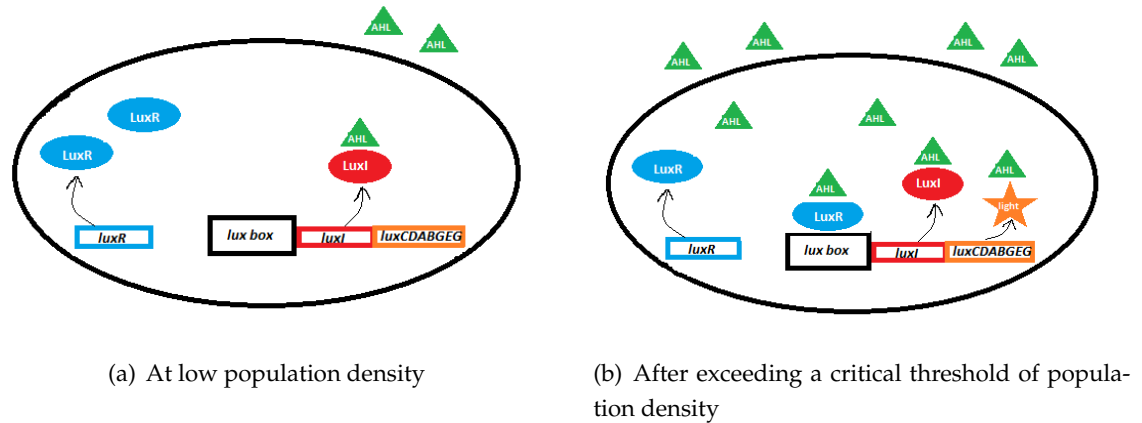
The cell-to-cell communication system is related to the question under which conditions and how bacteria change their gene expression in adaptation to the environment. Many bacterial species have a collective (communal) behavior contrary to their unicellular existence. They communicate with each other using chemical signals which enables them to notice the information about the current signaling molecule concentration. If a colony exceeds a specific threshold of the signaling molecule concentration, all cells act together for the benefit of the whole colony (bioluminescence, biofilm formation, antibiotic resistance, etc.) that gives them greater chances to survive in changing environmental conditions Bassler [6], Waters and Bassler [60].

The cell-cell communication mechanism, often also called quorum sensing (QS), regulates gene expression (production of a DNA protein by a cell) via releasing small signaling molecules, the so-called autoinducers (AIs), which are synthesized within the cell by an AI-synthase (Fuqua et al. [18, 19], Kaplan and Greenberg [28]). Every single bacterium produces AIs in cytoplasm and releases them into environment. AIs around the cell diffuse back from the medium into the cell cytoplasm through the cell membrane (Bassler [6], Waters and Bassler [60]). At low cell densities, AIs are produced by the bacteria at a low level and since the population density increases, bacteria trigger the positive feedback loop and produce more AIs (Kaplan and Greenberg [28]). The bacteria coordinate their behavior by regulating gene expression and start a population-wide response for the benefit of the colony (Jayaraman and Wood [27], Waters and Bassler [60]). For example, AIs

can regulate several processes, like luminescence, building of biofilms or producing toxic substances (Annous et al. [3], Waters and Bassler [60]).

Initially, it was thought that bacteria have a mechanism to sense the AI concentration in the environment and by that get an estimate for the present local population density. When a critical density of population is exceeded bacteria begin then with the transcription of some genes that enables to switch their usual behavior (Fuqua et al. [18]). Recently, it was shown that this process is more complicated and does not depend on their local density only, i.e. their "quorum", but also on the freely diffusible space and other environmental factors. In Redfield [55], the same mechanism was interpreted as "diffusion sensing". The underlying idea is that there is a diffusible space around the cell; it is reasonable to speak about diffusion sensing, because it depends on the diffusible area, if and how fast the AI concentration accumulates and reaches the threshold. For example, in a limited space (in a pore), the diffusion would be limited comparing to a large space (in a river). Both approaches can be unified in terms of "efficiency sensing" which proposes that bacteria are affected by diffusion or advection and by their spatial distribution and local density (Hense et al. [22]). This new concept considers that the bacteria do not only sense the cell density but also cell distribution and diffusion effects in the complex medium, which allows estimating the efficiency of the regulated behavior. Recently, many other hypotheses have been proposed to define quorum sensing, e.g. positional sensing, cumulative gradient sensing etc. Platt and Fuqua [54]. As it is more generic, we will use the term QS to describe several cell interactions throughout the thesis.

As an example of a bacterium with a QS mechanism, we start with the Gram-negative [52] marine species *Vibrio fischeri*, in which the QS was firstly observed about four decades ago (Eberhard [11], Nealson et al. [50]). *V.fischeri* naturally exists either in a free-living planktonic state or in a symbiotic state of certain luminescent fishes or squids (Bassler et al. [7], Fuqua et al. [18]). The host uses this luminescence to attract his prey or defends himself from predators by a light camouflage, the bacteria benefit from the abundance of nutrients in the light organ and by that allow proliferation in enormous numbers in the host (Waters and Bassler [60]). The bacteria luminesce when colonizing with high cell densities in the light organs, but they are usually dark in the free-living state, namely in low cell densities. The main QS regulation system of *V. fischeri* involves two regulatory proteins called LuxI and LuxR (Engebrecht and Silverman [12]). LuxI synthesizes an AI which is known to be an acylated homoserine lactone (AHL) (Eberhard [11]). The AHL is synthesized within the cell, diffuses into the extracellular environment and back into the cell. The LuxR proteins are cytoplasmic AHL receptors and DNA binding transcriptional activators. As we see in Figure 2.1, the *lux box* has two operons which are called *luxR* on the left side of the box and *luxI* on the right side of the box. *luxCDABEG* are genes responsible for bioluminescence (James et al. [26]). When QS starts, AHLs bind to

Figure 2.1: QS-regulated gene transcription of *V. fischeri*.

the LuxR protein receptors. These LuxR-AHL (dimerized) complexes attach to the empty *lux box* and activate target gene transcription. Thus, *luxCDABEG* enabled the light production (Miller and Bassler [41], Waters and Bassler [60]). Further, transcription of the AHL synthase *luxI* creates a positive feedback loop that is thought to contribute to the coordination of a population-wide transition to a high cell density quorum-sensing state (Boyer and Wisniewski-Dyé [8]). This LuxIR-type regulation is typical for a large number of Gram-negative bacteria and acylated homoserine lactones (AHLs), which are found in Gram-negative bacteria of the phylum Proteobacteria. Gram-positive bacteria have typically oligopeptides as AI. There is another class of AIs, the so called AI-2, which has been discovered both in Gram-negative and Gram-positive bacteria. Therefore, it is postulated as universal signal for communication across species (Waters and Bassler [60]).

2.2 The Underlying Experiment

In order to understand the induction dynamics of QS we present an experiment of the biofilm forming bacterial strain *Pseudomonas putida* IsoF in a flow chamber. This experiment was performed by the group of Prof. Dr. J. Rädler, LMU Munich, both under flow and non flow conditions for several AHL concentrations which were added in the flow system (0nM, 10nM, 50nM, 100nM). They analyzed the QS mediated induction dynamics of growing microcolonies and their responses to changing AHL concentrations. The Gram-negative bacterium *P. putida* IsoF was used as a model organism, since it contains only one QS system (Megerle [38], Meyer et al. [40]). The underlying molecular mechanisms of the *P. putida* IsoF QS system have been characterized before and it is known to be similar to *V. fischeri* QS system. The QS system of *P. putida* IsoF consists of the regulatory

activator PpuR and the AHL synthase PpuI (Fekete et al. [16], Steidle et al. [57]).

In the following experiment, they used a so-called Las-based reporter system to monitor the bacterial behavior. The QS system of *P. putida* IsoF with Las-based reporter is schematically shown in Figure 2.2. When the AHL concentration reaches a certain threshold, AHL binds to the activator PpuR. The PpuR/AHL complex activates expression of the AHL synthase PpuI and by that triggers the positive feedback loop, which results in increased AHL production. Gene expression is followed using an AHL sensor which contains a fusion of *lasB* promoter with the green fluorescent protein (GFP). This modification allows the bacteria to fluoresce in their activated state, which can be observed by fluorescence microscopy. Here *gfp* is the gene, which is responsible for fluorescence. When LasR binds to AHL, this complex stimulates the GFP gene expression [38, 40].

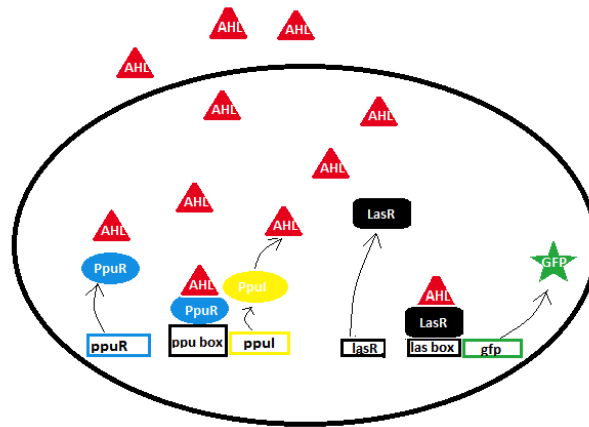


Figure 2.2: QS system of *P.putida* IsoF with Las based reporter.

In Figure 2.3, a sketch of a flow chamber is given, where the bacteria were attached and then observed under both bright field and fluorescence microscopy, respectively. As a result of QS, some of the cells had switched their current state and they are fluorescent, which can be seen under fluorescence microscopy. In that way it is possible to monitor the "switch" of cells and the flow effect during the accumulation of AHL. We will call this "switch of cell state" as activation and a cell active, when it is fluorescent, and the remaining non-fluorescent cells inactive. Black points refer to all bacteria and their positions. Green points refer to bacteria which are activated and can be observed under fluorescence microscopy. We draw four windows as being in flow chamber which represent a unit area, where the pictures are collected from each of them every 20 minutes, simultaneously [38, 40].

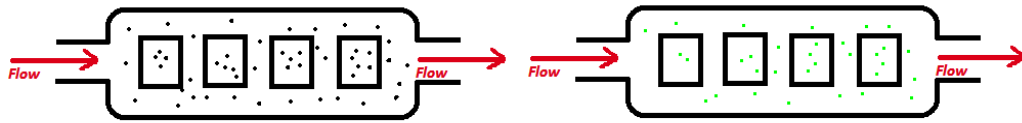


Figure 2.3: A sketch of flow chamber: Left panel - under bright field microscopy and right panel - under fluorescence microscopy.

The picture in Figure 2.4 clearly shows what we have drawn in Figure 2.3. It was taken under non-flow conditions with 0 nM AHL after 6 hours from the begin of the experiment. Further, there are sample pictures in Figure 2.5 from the experiment performed by the group of Prof. Dr. J. Rädler, LMU Munich in non-flow conditions for 0 nM AHL. The pictures on the left column were taken under bright field microscopy and on the right column under the fluorescence microscopy. It is possible to see how many and how strong the bacteria fluoresce comparing the pictures at the same time point.

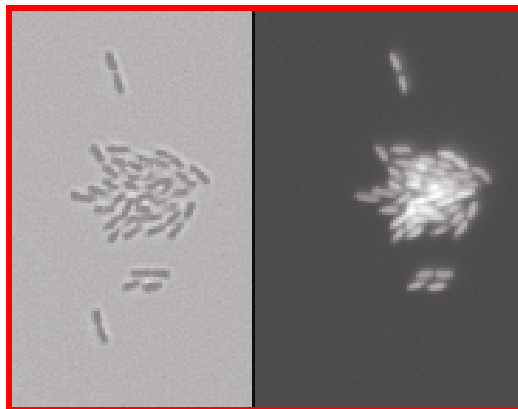


Figure 2.4: Picture of *P.putida* IsoF under bright field and fluorescence microscopy. Picture was taken at 6. hours of the experiment performed by the group of Prof. Dr. J. Rädler, LMU Munich from the second window of the flow chamber.

All these pictures were analyzed with "Imageana", an image analysis program by Prof. Dr. J. Müller, TU München [42]. Imageana compares the pictures from bright field and fluorescence microscopy and measures the area where bacteria are dark or bright. Knowing the average number of bacteria in unit area we converted these data to a raw data set, like the number of active and inactive cells for each time point.

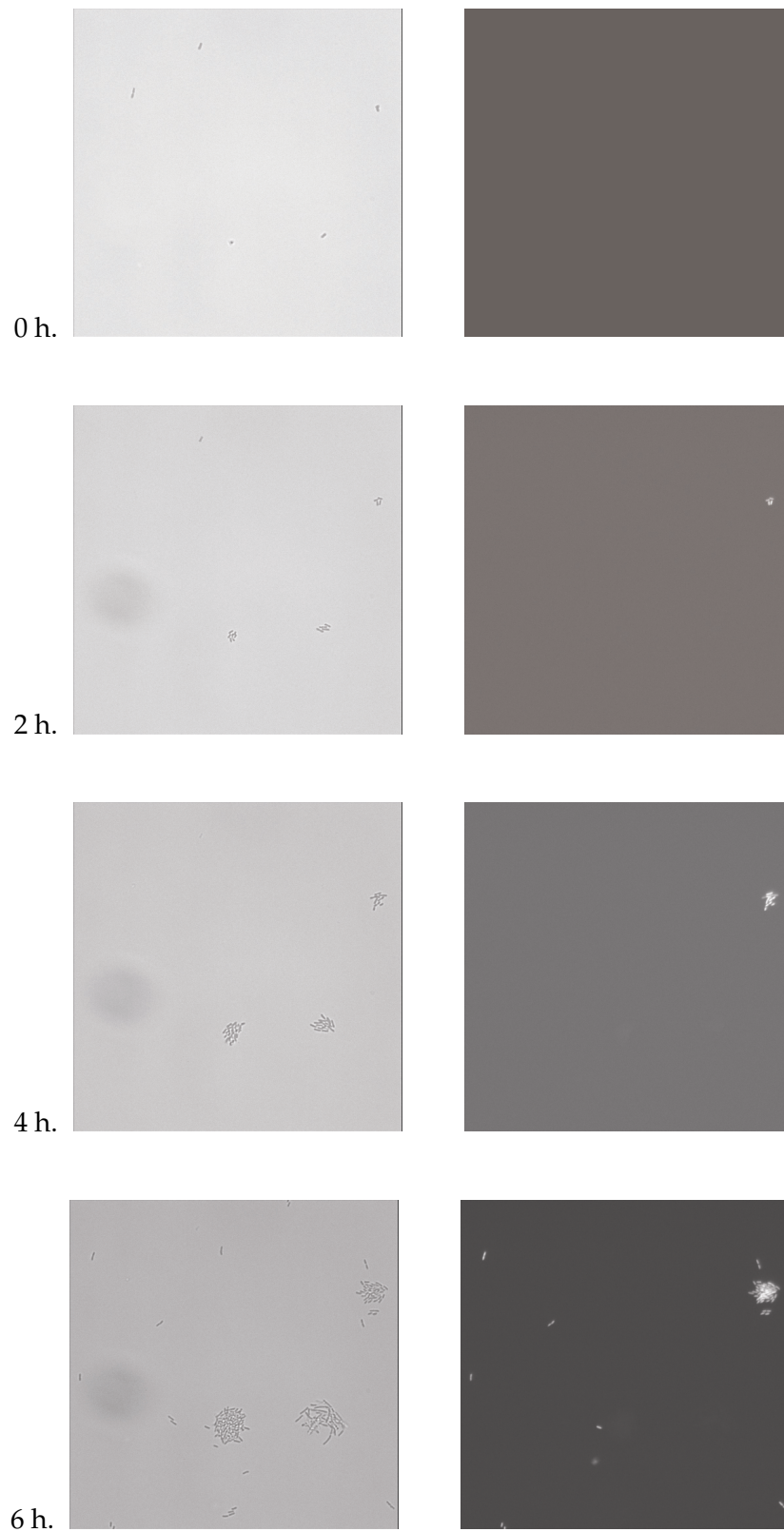


Figure 2.5: Pictures from the experiment: left column under bright field microscopy and right column under fluorescence microscopy.

2.3 A Brief Overview on Mathematical Modeling of QS

The first mathematical model on QS was built up on *V. fischeri* QS system (James et al. [26]). It dealt with the regulation of bioluminescence in *V. fischeri* and focused on the response of a single cell to the external AI concentration. They started with a system of the ordinary nonlinear differential equations (ODEs) for the time dependent changes of AIs, LuxR and LuxR/AI complex concentration within the cell and extended the model by a variable for the external AI concentration to understand the way, in which a cell might respond to surrounding AI concentration. It was concluded that two stable steady states are possible for luminescent and non-luminescent phenotypes. The "switch" between these states are explained due to the change in parameters describing the system dynamics and extracellular AI concentration.

A similar mathematical model was introduced for the bacterial species *Pseudomonas aeruginosa* with two regulatory QS systems, called *las* system and *rhl* system (Dockery and Keener [10]). In that work, they emphasized on the kinetics of the *las* system and described it by an eight-dimensional ODEs with rates in Michaelis-Menten type. They simplified this ODE system by taking into account that some reactions are faster than others. The idea on this was that the enzymes LasR and LasI were living much longer than their producers, respectively lasR mRNA and lasI mRNA. Then, they switched to a partial differential equation (PDE) model, which included the possibility of inhomogeneous distribution of AIs outside of the cell. Starting with a single cell, it was pointed out that the AI production increase (decrease) is dependent on colony size and density.

In Nilsson et al. [51] was presented a model on the change of AHL concentration inside bacterial cells and in a biofilm over time. They showed that the AHL concentration within a cell often exhibits a rapid increase early in population growth. Since they did not consider the spatial variation of AHL molecules and/or the stochasticity in cell transcription, this kind of modeling is only useful for identifying the critical threshold for a single cell to initiate QS.

The first example for a mathematical model on population level in QS was given by (Ward et al. [59]). There, the focus was on the population dynamics for *V. fischeri*, in view of down-regulated and up-regulated subpopulations and their switching behavior with increasing AI production. They used a system of non-linear ODEs and showed through curve fitting techniques for parameter estimation that the solution of systems agree with experimental data. An important view of this paper was pointing out that AI production is much faster in the former than the latter bacterial population. Although they did not consider the spatial variation of AIs, they described the model as a first step towards modeling complex behavior in biological systems and extended their work in Koerber et al. [32] taking into account the spatial distribution of AIs and its effect on QS.

Koerber et al. [32] focused on the medical aspects of QS for the bacteria *Pseudomonas aeruginosa* which is associated with the burn-wound infection. They presented a model for the early stages of a QS correlated infection process in burn-wounds and for the diffusion of AIs in the burn-wounds environment. They defined the cells densities for two states, where QS regulated cells were called "up-regulated" and the other remaining "down-regulated". A system of ODEs referred to the change of cell concentration whereas a reaction-diffusion equation described the change of AI concentration over time. Further, they fitted the model to experimental data by estimating parameters. Thus, they pointed out that the wound environment itself has an important effect upon the QS mechanism.

In the last years, (parallel to the biological developments) mathematical QS models came into question which extended the focus to include stochastic aspects. This enabled to examine the small noise quantities, which can be found for example in Goryachev et al. [20], Koerber et al. [33], Müller et al. [45]. In Koerber et al. [33], they started with a deterministic model for a large bacterial population of a human pathogen *Staphylococcus aureus* within the endosome. Using the information from the first model, they switched to single cell case, where the bacterial cell escapes from an endosome into the cytoplasm and had only two different states (down-regulated and up-regulated). The probability that a bacterium is in the down-regulated state (up-regulated state) was given with a probability density function (pdf) at time t , dependent on the thickness of the endosome membrane, AI concentration and the concentration of the principal degradative exo-enzyme, which were assumed as random variables. It was possible in the model that a down-regulated cell became up-regulated and an up-regulated cell can also drop back to the down-regulated state. The pdfs governed by these model assumptions enable to measure the probability that a bacterium being in one of these states. Taking a Taylor expansion in Δt , they achieved a system of two first order PDEs. From this model they had been able to determine biologically meaningful asymptotic and numerical solutions.

In Goryachev et al. [20], an intracellular model in an *Agrobacterium* population was incorporated into a stochastic population model, which described bacterial motion, cell division and chemical communication. The developed model described the intracellular control network in terms of cell transition related with environmental control. The population model consisted of an intracellular model in which each bacterium was given a unique copy of an intracellular model. This approach allowed monitoring of both the individual cells and population behavior. They first formulated the chemical kinetics of QS with a deterministic view. Further, they complemented two ODEs describing the dynamics of cell density and extracellular AI concentration for the population model. As the QS network is robust to molecular noise, the intracellular model was simulated stochastically. They assumed that bacteria can either randomly move in the medium with a diffusion effect or remain attached (stable). Both forms exchange AI with the surrounding medium and

divide periodically. With the exact Gillespie algorithm and with an self created software, they simulated cell motion, exchange and diffusion of AI.

In Müller et al. [46], a general stochastic model in Gram-negative bacteria was developed which presents the random distribution of a gene product. It was assumed that the only source of variance is due to switching transcription on and off by a random process. Probability density functions were created for two possible gene states, e.g. ON or OFF. They first determined with ODEs the change of the the product density, which can be either mRNA or a protein. According to the model assumptions, they set the probability that a bacterium being in state ON (OFF) with a pdf that includes the change of product density and time. As $\Delta t \rightarrow 0$ they achieved a PDE system which allowed for an explicit solution. They found that certain parameters translates bistable behavior into bimodal distributions, which was supported by experimental results.

The models we have mentioned above are only of a few selected publications among many. In this chapter, we aimed to give a short overview of the progression in mathematical modeling of QS from its beginning. However several modeling aspects of QS can be found in many other works, e.g [16, 17, 23, 30, 58].

3 A Stochastic Model of QS

In this chapter we present a stochastic model of QS in the bacterium *P. putida* IsoF to explore the cell dynamics at the population level. The background and details of the underlying QS experiment and its results were given in Section 2.2. Our stochastic population model describes the bacterial transition between inactive and active cell states affected by surrounding AHL concentration for single cells and determines the AHL dependent probability density functions of both cell states. The model formulation is based on Müller et al. [46] and allows to quantify, e.g., the rates of cell division, activation and AHL degradation.

3.1 Model Assumptions

We assume that at a time point $t \geq 0$, each cell is either in the inactive (I) or in the active (A) state and there is not any interstate. Figure 3.1 shows the cell transition with the one way arrow from the inactive cell (I) to the active cell (A), i.e., the inactive cells can be activated with the rate α , whereas active cells never become inactive. The cell transition occurs as a consequence of a QS process and that is why it is dependent on the intracellular AHL concentration. The β arrows in Figure 3.1 represent that each cell divides independently of its state (active or inactive) with the same rate and the offspring preserves the current state of its parents. There are different rates for the AHL production in each cell state, i.e., an inactive cell (I) produces with the rate m_1 while an active cell (A) produces with the rate $m_1 + m_2$. In both states, AHL is degraded abiotically with the rate γ . We suppose that each element of the parameter set $P = \{\alpha, \beta, \gamma, m_1, m_1 + m_2\}$ is a positive real number and we neglect the possibility that a cell dies or leaves the colony, for simplicity.

3.2 A Single Cell Model

Primarily, we develop a model for the case of a single cell that includes the deterministic AHL production dynamics within the cell and a stochastic process describing the transition from inactive to active. Let us denote the two possible cell states inactive (I) and active (A) as shown in Figure 3.1. We describe the AHL concentration by z and the change of the AHL concentration in time by corresponding ODEs (with the initial condition $z(0) = z_0$)

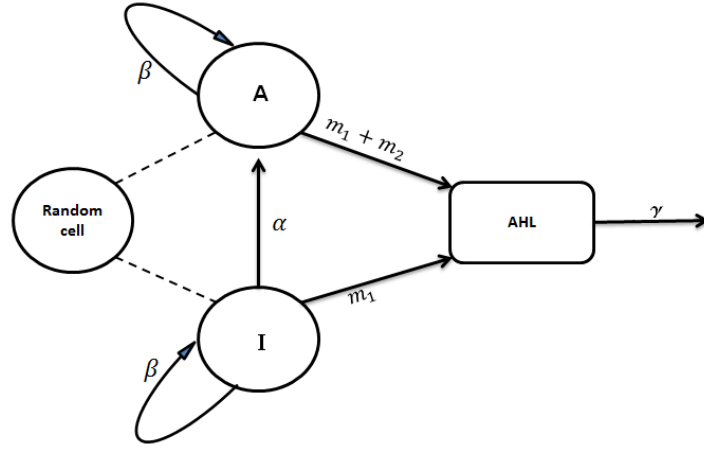


Figure 3.1: Possible states of one cell and their transition.

without the switch of the cell state is given by Equation (3.1).

$$\dot{z} = \begin{cases} m_1 - \gamma z, & \text{for cell state I} \\ (m_1 + m_2) - \gamma z, & \text{for cell state A.} \end{cases} \quad (3.1)$$

So, the AHL concentration at time t for the initial condition $z(0) = z_0$ reads

$$z(t) = \begin{cases} \frac{m_1}{\gamma} + (z_0 - \frac{m_1}{\gamma}) e^{-\gamma t}, & \text{for cell state I} \\ \frac{m_1 + m_2}{\gamma} + (z_0 - \frac{m_1 + m_2}{\gamma}) e^{-\gamma t}, & \text{for cell state A.} \end{cases} \quad (3.2)$$

While $t \rightarrow \infty$ we find that the maximum value of AHL concentration (z_{max}) for the inactive cell state is $z_{max}^- = \frac{m_1}{\gamma}$ and for the active cell state is $z_{max}^+ = \frac{m_1 + m_2}{\gamma}$. In Figure 3.2 the corresponding plot to Equation (3.2) can be found for the initial value $z_0 = 0$, i.e., assuming to have no AHL at time $t = 0$. The essential variables and parameters, which we need during the whole chapter, are given in Tables 3.1 and 3.2.

Our aim is to develop a model describing the AHL dependent distribution (in time) of inactive and active cells. Therefore, we define the probability density function (pdf) for a given AHL concentration at time t by $u(z, t, s)$, where s denotes the state of the cell, i.e. $s = I$ for the inactive state or $s = A$ for the active state. For simplification, we use the notation $u^- = u(z, t, I)$ and $u^+ = u(z, t, A)$. Here, for an arbitrary time point t_g , we have

$$\int_z (u^-(z, t_g) + u^+(z, t_g)) dz = 1.$$

We derive a PDE model, taking into account the change of AHL concentration continuously in time for both cell states given by Equation (3.1). Table 3.3 shows how the pdfs of

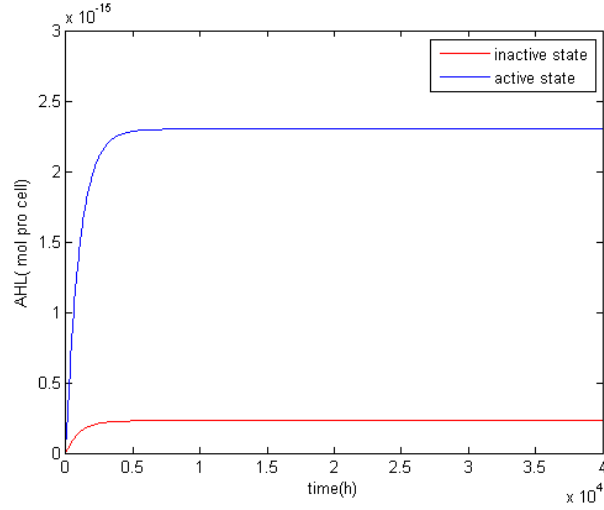


Figure 3.2: AHL concentration in active and inactive cell state. Equation (3.2) is plotted for the chosen parameter values from the Table 3.2.

inactive cells $u^-(z, t)$ and active cells $u^+(z, t)$ change in a small time step Δt correlated to the AHL concentration. Thus, we obtain the following system of equations

$$u^-(z + (m_1 - \gamma z)\Delta t, t + \Delta t) = u^-(z, t) + O(\Delta t),$$

and

$$u^+(z + (m_1 + m_2 - \gamma z)\Delta t, t + \Delta t) = u^+(z, t) + O(\Delta t),$$

where $O(\Delta t)$ is the first order correction term. This system of equations consists of the probability mass that leaves from u^- by activation, $-\alpha(z)u^-(z, t)$ and adds on the u^+ , $\alpha(z)u^-(z, t)$. Thus, we conclude

$$\begin{aligned} u^-(z + (m_1 - \gamma z)\Delta t, t + \Delta t) - u^-(z, t) &= (-\alpha(z)u^-(z, t))\Delta t + O(\Delta t^2) \\ \Leftrightarrow \frac{u^-(z + (m_1 - \gamma z)\Delta t, t + \Delta t) - u^-(z, t)}{\Delta t} &= -\alpha(z)u^-(z, t) + O(\Delta t) \end{aligned}$$

Table 3.1: Variables of the model developed in Chapter 3.

Variable	Description
z	AHL concentration
t	time
u^-	pdf for inactive cell state
u^+	pdf for active cell state

Table 3.2: Parameters of the model developed in Chapter 3.

Parameter	Description	Values	Reference
m_1	AHL production rate in inactive cells	$2.3 \times 10^{-19} \left[\frac{\text{mol}}{\text{cell.h}} \right]$	1
$m_1 + m_2$	AHL production rate in activated cells	$2.3 \times 10^{-18} \left[\frac{\text{mol}}{\text{cell.h}} \right]$	1
γ	AHL degradation rate	$0.001 \left[h^{-1} \right]$	2
α_c	activation rate of inactive cell	$0.1 \left[h^{-1} \right]$	3
β	division rate in both states	$0.13 \left[h^{-1} \right]$	3
A_{thresh}	activation threshold	$70 \times 10^{-9} \left[\frac{\text{mol}}{l} \right]$	1

¹ correspondent to [16].

² for a realistic PH value correspondent to [13].

³ roughly estimates of the experimental data correspondent to [38].

and obtain the model for a bacterium in the inactive state as $\Delta t \rightarrow 0$

$$\frac{\partial u^-(z, t)}{\partial t} + \frac{\partial((m_1 - \gamma z)u^-(z, t))}{\partial z} = -\alpha(z)u^-(z, t).$$

After a similar calculation for u^+ we have the following PDE model for the correspondent pdfs of the possible cell states, I and A

$$\frac{\partial u^-(z, t)}{\partial t} + \frac{\partial((m_1 - \gamma z)u^-(z, t))}{\partial z} = -\alpha(z)u^-(z, t), \quad (3.3)$$

$$\frac{\partial u^+(z, t)}{\partial t} + \frac{\partial((m_1 + m_2 - \gamma z)u^+(z, t))}{\partial z} = +\alpha(z)u^-(z, t). \quad (3.4)$$

We know that a probability distribution preserves mass, i.e., we have homogeneous Neumann boundary conditions [46]. Further, we assume to have the initial conditions, $u^-(z, 0) = u_0(z)$ for the inactive state and $u^+(z, 0) = 0$ for the active state, since we first want to describe the case starting with one inactive and no active cell. The system of PDEs need also boundary conditions. As an inactive cell activates in high AHL concentrations, we have $\lim_{z \rightarrow \infty} u^-(z, t) = 0$. According to the continuous AHL production within the cell,

Table 3.3: Change of AHL and pdf in time.

time	t	$t + \Delta t$
AHL concentration for cell state I	z	$z + (m_1 - \gamma z)\Delta t$
pdf for inactive state	$u^-(z, t)$	$u^-(z + (m_1 - \gamma z)\Delta t, t + \Delta t)$
AHL concentration for cell state A	z	$z + (m_1 + m_2 - \gamma z)\Delta t$
pdf for active state	$u^+(z, t)$	$u^+(z + (m_1 + m_2 - \gamma z)\Delta t, t + \Delta t)$

we suppose that the second boundary condition is given by $u^-(0, t) = 0$ for $t > 0$. Let us define the time dependent function for the inactive cell state:

$$u^-(t) = \int_0^{\infty} u^-(z, t) dz.$$

Taking the derivative of both sides of the equation with respect to t we have

$$\begin{aligned} \frac{d}{dt} u^-(t) &= \int_0^{\infty} \frac{\partial}{\partial t} u^-(z, t) dz \\ &= \int_0^{\infty} \left[-\frac{\partial}{\partial z} (m_1 - \gamma z) u^-(z, t) - \alpha(z) u^-(z, t) \right] dz \\ &= \int_0^{\infty} -\frac{\partial}{\partial z} ((m_1 - \gamma z) u^-(z, t)) dz - \int_0^{\infty} \alpha(z) u^-(z, t) dz, \end{aligned}$$

for a constant $\alpha(z) \equiv \alpha > 0$ we obtain

$$\begin{aligned} \frac{d}{dt} u^-(t) &= \int_0^{\infty} -\frac{\partial}{\partial z} ((m_1 - \gamma z) u^-(z, t)) dz - \alpha \int_0^{\infty} u^-(z, t) dz \\ &= \left[-(m_1 - \gamma z) u^-(z, t) \right]_0^{\infty} - \alpha u^-(t). \end{aligned} \quad (3.5)$$

As we have

$$\left[-(m_1 - \gamma z) u^-(z, t) \right] \Big|_0^{\infty} = 0,$$

according to the boundary conditions ($u^-(0, t) = 0$ and $\lim_{z \rightarrow \infty} u^-(z, t) = 0$), the Equation (3.5) reduces to a linear ODE

$$\frac{d}{dt} u^-(t) = -\alpha u^-(t),$$

or rather

$$u^-(t) = e^{-\alpha t} C,$$

where C is a constant. Due to the positivity condition, we acquire

$$u^- \equiv 0 \quad \text{for} \quad t \rightarrow \infty. \quad (3.6)$$

3.2.1 Stationary States

In this section, we examine the steady-state behavior of the Equation system (3.3)-(3.4). We assume here that the activation rate $\alpha(z) \equiv \alpha > 0$ is constant, i.e., does not depend on z .

We obtain two ODEs for the time independent state of the PDE system (3.3)-(3.4),

$$\begin{aligned} \frac{d}{dz}((m_1 - \gamma z)u^-(z)) &= -\alpha u^-(z), \\ \frac{d}{dz}((m_1 + m_2 - \gamma z)u^+(z)) &= +\alpha u^-(z), \end{aligned} \quad (3.7)$$

with boundary conditions $u^-(\frac{m_1}{\gamma}) = 0$ and $u^+(0) = 0$, which represent the probability density of being inactive at the maximum AHL concentration and the probability density of being active at the minimum AHL concentration, respectively. If $z \in [0, z_{max}]$, where $z_{max}^- = \frac{m_1}{\gamma}$ for inactive state and $z_{max}^+ = \frac{m_1+m_2}{\gamma}$ for active state, the Equation system (3.7) is equivalent to

$$\begin{aligned} (m_1 - \gamma z) \frac{du^-(z)}{dz} &= \gamma u^-(z) - \alpha u^-(z), \\ (m_1 + m_2 - \gamma z) \frac{du^+(z)}{dz} &= \gamma u^+(z) + \alpha u^-(z), \end{aligned} \quad (3.8)$$

where we suppose that $u^-(z) \equiv 0$ for $z > \frac{m_1}{\gamma}$ and $u^+(z) \equiv 0$ for $z > \frac{m_1+m_2}{\gamma}$. The system of Equations in (3.8) can be written in the form

$$\frac{du^-(z)}{dz} = \frac{\gamma}{m_1 - \gamma z} u^-(z) - \frac{\alpha}{m_1 - \gamma z} u^-(z), \quad (3.9)$$

$$\frac{du^+(z)}{dz} = \frac{\gamma}{m_1 + m_2 - \gamma z} u^+(z) + \frac{\alpha}{m_1 + m_2 - \gamma z} u^-(z). \quad (3.10)$$

The explicit solution of the ODE (3.9) for $z \in [0, z_{max}^-]$ reads

$$u^-(z) = (m_1 - \gamma z)^{-\frac{\gamma-\alpha}{\gamma}} C_1, \quad (3.11)$$

where C_1 is a constant and due to the boundary condition $C_1 = 0$. Additionally, we know from Equation (3.6) that u^- also vanishes for $t \rightarrow \infty$.

We now deal with the Equation (3.10) and solve it for a fixed z_0 , where $z_0 \in [0, \frac{m_1+m_2}{\gamma}]$. Since the Equation (3.9) includes the solution of Equation (3.11), we may keep it in mind by calculation that $u^-(z) \equiv 0$ for $t \rightarrow \infty$. Thus, the Equation (3.10) reduces to

$$\frac{d}{dz}((m_1 + m_2 - \gamma z) u^+(z)) = 0. \quad (3.12)$$

Definition 3.1 (*Viscosity solution*)[56]

We say that $u^+(z, t)$ is a viscosity solution of the equation

$$\frac{\partial}{\partial t} u^+(z, t) + \frac{\partial}{\partial z} f(u^+(z, t)) = 0,$$

if $u^+(z, t)$ can be obtained as the limit for $\epsilon > 0$

$$u^+(z, t) = \lim_{\epsilon \rightarrow 0^+} u_\epsilon^+(z, t),$$

of a solution of parabolic system of differential equations

$$\frac{\partial}{\partial t} u_\epsilon^+(z, t) + \frac{\partial}{\partial z} f(u_\epsilon^+(z, t)) = \epsilon A \frac{\partial^2}{\partial z^2} (u_\epsilon^+(z, t)),$$

for some positive definite matrix A .

The solution of Equation (3.12) is given by vanishing viscosity method as below where we first calculate for a small positive number ϵ and then let $\epsilon \rightarrow 0^+$:

$$\frac{d}{dz} ((m_1 + m_2 - \gamma z) u^+(z)) = \epsilon \frac{d^2}{dz^2} u^+(z) \quad (3.13)$$

Integrating both sides of the Equation (3.13) with respect to z we have

$$\frac{d}{dz} u^+(z) = \frac{1}{\epsilon} (m_1 + m_2 - \gamma z) u^+(z) + C_1$$

According to boundary conditions we have $C_1 = 0$. Thus, we obtain

$$\begin{aligned} \frac{d}{u^+(z)} u^+(z) &= \frac{1}{\epsilon} (m_1 + m_2 - \gamma z) dz \\ \ln(u^+(z)) &= \int_{z_0}^z \frac{1}{\epsilon} (m_1 + m_2 - \gamma z) dz + C_2(\epsilon) \end{aligned}$$

For letting $z_0 \rightarrow 0$, we have

$$u^+(z) = e^{\frac{1}{\epsilon}((m_1+m_2)z - \frac{1}{2}\gamma z^2)} e^{C_2(\epsilon)}$$

Since we have assumed $u^+(0) = 0$, we need

$$u^+(0) = e^{C_2(\epsilon)} = 0,$$

which implies $\lim_{C_2(\epsilon) \rightarrow -\infty} e^{C_2(\epsilon)} = 0$.

Let us denote the total probability density function $u(z) = u^-(z) + u^+(z)$. The properties on pdfs allow us to write $\int_0^{z_{max}} u(z) dz = 1$. Thus, we can calculate in the stationary state keeping in mind that $u^- \equiv 0$:

$$\begin{aligned} \int_0^{z_{max}} u(z) dz &= \int_0^{z_{max}^-} u^-(z) dz + \int_0^{z_{max}^+} u^+(z) dz \\ &= 0 + \int_0^{\frac{m_1+m_2}{\gamma}} \lim_{\epsilon \rightarrow 0} e^{\frac{1}{\epsilon}((m_1+m_2)z - \frac{1}{2}\gamma z^2)} e^{C_2(\epsilon)} dz \\ &= 1. \end{aligned}$$

We seek a suitable constant $C_2(\epsilon)$ which fulfills

$$\int_0^{\frac{m_1+m_2}{\gamma}} \lim_{\epsilon \rightarrow 0} e^{\frac{1}{\epsilon}((m_1+m_2)z - \frac{1}{2}\gamma z^2)} e^{C_2(\epsilon)} dz = 1. \quad (3.14)$$

Let us calculate the left hand side of the Equation (3.14)

$$\begin{aligned} & \int_0^{\frac{m_1+m_2}{\gamma}} \lim_{\epsilon \rightarrow 0} e^{\frac{1}{\epsilon}((m_1+m_2)z - \frac{1}{2}\gamma z^2)} e^{C_2(\epsilon)} dz \\ &= \lim_{\epsilon \rightarrow 0} e^{C_2(\epsilon)} \int_0^{\frac{m_1+m_2}{\gamma}} e^{\frac{1}{\epsilon}((m_1+m_2)z - \frac{1}{2}\gamma z^2)} dz \\ &= \lim_{\epsilon \rightarrow 0} e^{C_2(\epsilon)} \int_0^{\frac{m_1+m_2}{\gamma}} e^{-\frac{1}{2} \left(\frac{-2(m_1+m_2)}{\epsilon} z + \frac{\gamma}{\epsilon} z^2 \right)} dz \\ &= \lim_{\epsilon \rightarrow 0} e^{C_2(\epsilon)} e^{\frac{1}{2} \frac{(m_1+m_2)^2}{\epsilon \gamma}} \int_0^{\frac{m_1+m_2}{\gamma}} e^{-\frac{1}{2} \left(\frac{z - \frac{(m_1+m_2)}{\gamma}}{\sqrt{\epsilon/\gamma}} \right)^2} dz \\ &= \lim_{\epsilon \rightarrow 0} e^{C_2(\epsilon)} e^{\frac{1}{2} \frac{(m_1+m_2)^2}{\epsilon \gamma}} \frac{\sqrt{2\pi} \sqrt{\epsilon/\gamma}}{\sqrt{2\pi} \sqrt{\epsilon/\gamma}} \int_0^{\frac{m_1+m_2}{\gamma}} e^{-\frac{1}{2} \left(\frac{z - \frac{(m_1+m_2)}{\gamma}}{\sqrt{\epsilon/\gamma}} \right)^2} dz \\ &= \lim_{\epsilon \rightarrow 0} e^{C_2(\epsilon)} e^{\frac{1}{2} \frac{(m_1+m_2)^2}{\epsilon \gamma}} \sqrt{2\pi} \sqrt{\epsilon/\gamma} \left[\Phi(0) - \Phi \left(-\frac{(m_1+m_2)}{\gamma \sqrt{\epsilon/\gamma}} \right) \right], \end{aligned}$$

where Φ denotes the Gaussian error function. Choosing

$$C_2(\epsilon) = - \left(\frac{1}{2} \frac{(m_1+m_2)^2}{\epsilon \gamma} + \ln \left(\sqrt{2\pi} \sqrt{\epsilon/\gamma} \left[\Phi(0) - \Phi \left(-\frac{(m_1+m_2)}{\gamma \sqrt{\epsilon/\gamma}} \right) \right] \right) \right),$$

we achieve the Equation (3.14).

3.2.2 Exact Solution for the Single Cell Model

After analyzing the stationary states of the single cell model, we consider the time dependent PDE system for a single cell given by Equations (3.3)-(3.4), where $z, t \in \mathbb{R}$. Let us present the equivalent PDE system to the Equations (3.3)-(3.4):

$$\frac{\partial u^-(z, t)}{\partial t} + (m_1 - \gamma z) \frac{\partial u^-(z, t)}{\partial z} = (\gamma - \alpha(z)) u^-(z, t), \quad (3.15)$$

$$\frac{\partial u^+(z, t)}{\partial t} + (m_1 + m_2 - \gamma z) \frac{\partial u^+(z, t)}{\partial z} = \gamma u^+(z, t) + \alpha(z) u^-(z, t). \quad (3.16)$$

Since Equation (3.15) does not depend on $u^+(z, t)$, we first deal with the initial value problem for $u^-(z, t)$,

$$\frac{\partial u^-(z, t)}{\partial t} + (m_1 - \gamma z) \frac{\partial u^-(z, t)}{\partial z} = (\gamma - \alpha(z))u^-(z, t), \quad (3.17)$$

$$u^-(z, 0) = u_0(z). \quad (3.18)$$

Henceforth we will be able to use the corresponding solution in the second hyperbolic Equation (3.16).

The first order linear hyperbolic PDEs can be solved by the method of characteristics, which reduces a PDE into an appropriate system of ODE by changing from the current coordinate system (z, t) to a new coordinate system (z_0, s) , [15]. In general, any curve in the $z - t$ plane can be parametrized as $z(s)$ and $t(s)$, where s gives a measure of the distance along the curve. The set of these parametrized curves, i.e., $\{(z(s), t(s)) : 0 < s < \infty\}$ is called characteristic curves. Here, the variable s varies but the variable $z_0 = z(0)$ is constant along the characteristic curves and it only changes along the line $t = 0$ and can be interpreted as an index for the family of characteristics curves, denoted by the initial z -values, [37]. Since $u(z, t)$ is a function of two independent variables, the solution $u(z, t)$ is a surface on the plane $z - t$.

We consider the following system of ODEs via the new coordinate s

$$\begin{aligned} \frac{dt}{ds} &= 1, \\ \frac{dz}{ds} &= m_1 - \gamma z, \\ \frac{du^-}{ds} &= (\gamma - \alpha(z))u^-. \end{aligned}$$

Solving the first two equations of the ODE system we obtain a s -dependent relationship between z and t ,

$$\begin{aligned} t &= s + C_1, \\ z &= \frac{m_1 - C_2 e^{-\gamma s}}{\gamma}. \end{aligned}$$

For $s = 0$ and $z(0) = z_0^-$ we have $C_1 = 0$ and $C_2 = m_1 - \gamma z_0^-$. Thus, we obtain $t = s$ and $z = \frac{m_1 - (m_1 - \gamma z_0^-)e^{-\gamma t}}{\gamma}$, which represents the characteristic curves of the IVP (3.17)-(3.18) for several different values of z_0^- along the line $t = 0$. The corresponding graphs are shown in Figure 3.3 using the parameter values in the Table 3.2, where $0 \leq z_0^- \leq z_{max}^-$.

Hence the solution $u(z(t), t)$ is constant on characteristic curves, we substitute them in the third ODE. So, we convert the hyperbolic PDE (3.17) to the following ODE:

$$\frac{du^-(z(t), t)}{dt} = \left(\gamma - \alpha \left(\frac{m_1 - (m_1 - \gamma z_0^-)e^{-\gamma t}}{\gamma} \right) \right) u^-(z(t), t).$$

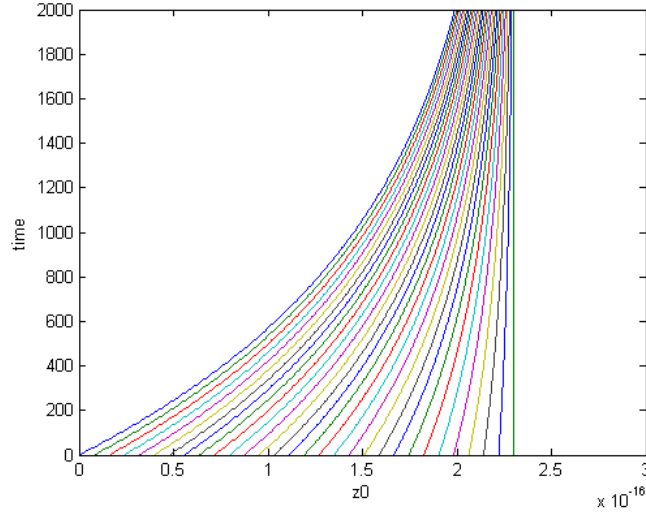


Figure 3.3: Characteristic curves of an inactive cell using the parameter values in Table 3.2.

The solution of this equation reads

$$u^-(z(t), t) = e^{\int_0^t \gamma - \alpha \left(\frac{m_1 - (m_1 - \gamma z_0^-) e^{-\gamma \rho}}{\gamma} \right) d\rho} C_3.$$

Using the initial conditions we find

$$u^-(z_0^-, 0) = C_3 = u_0^-(z_0^-),$$

and have

$$u^-(z(t), t) = e^{\int_0^t \gamma - \alpha \left(\frac{m_1 - (m_1 - \gamma z_0^-) e^{-\gamma \rho}}{\gamma} \right) d\rho} u_0^-(z_0^-),$$

which is transported on the characteristics, i.e., another choice of z_0^- gives another curve of $z(t)$ and the solution $u^-(z(t), t)$ is determined along this curve. Finally, we acquire the solution $u^-(z, t)$ to IVP (3.17)-(3.18) replacing z_0^- by $z_0^- = \frac{m_1 - (m_1 - \gamma z) e^{\gamma t}}{\gamma}$, i.e., we obtain the pdf of inactive cell state for one cell

$$u^-(z, t) = u_0 \left(\frac{m_1 - (m_1 - \gamma z) e^{\gamma t}}{\gamma} \right) e^{\int_0^t \gamma - \alpha \left(\frac{m_1 - (m_1 - \gamma z) e^{\gamma(t-\rho)}}{\gamma} \right) d\rho}. \quad (3.19)$$

Thereby, we are able to determine the pdf (3.19) of inactive cell state for one cell, explicitly. As we have assumed to start with one inactive cell, we have $u^-(z, 0) = u^-(z)$. According to the boundary conditions, we choose an appropriate Beta distribution as an initial function in the interval $0 \leq z \leq \frac{m_1}{\gamma}$, with the adequate shape parameters. This initial function reaches its maximum value at the low amount of AHL, decreases monotonely and vanishes for the maximum value of AHL. It is also possible to choose other

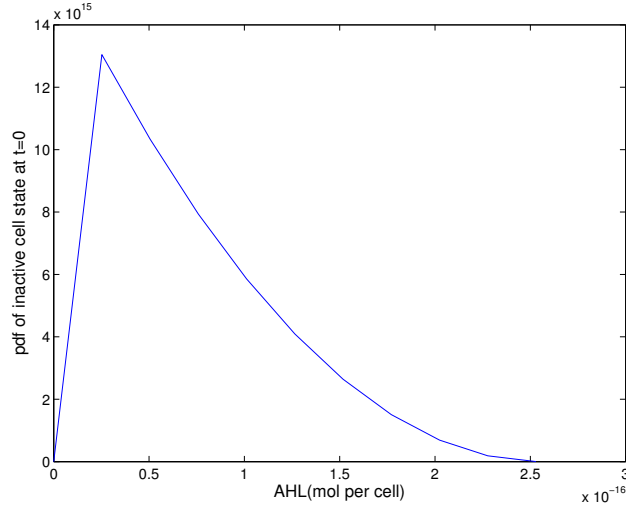


Figure 3.4: Suitable initial distribution for $u^-(z, 0)$ given by Equation 3.20 where $z_1 = 2.53 \times 10^{-17}$ and $M = 5.155 \times 10^{32}$

initial distributions which have a shape similar to our expectation. For example, Gaussian distribution $u_0^-(z_0^-) = \frac{\sqrt{2}}{\sigma\sqrt{\pi}} e^{-\frac{(z_0^-)^2}{2\sigma^2}}$ for $z_0 > 0$ could be also one of the other options. Let us define the initial distribution

$$u^-(z, 0) = \begin{cases} Mz & , \text{ for } z \leq z_1 \\ \frac{1}{B(0, \frac{m_1}{\gamma}, p, q)} (z_0^- - 0)^{(p-1)} \left(\frac{m_1}{\gamma} - z_0^- \right)^{(q-1)} & , \text{ for } z > z_1 \end{cases} \quad (3.20)$$

defined on the interval $[0, \frac{m_1}{\gamma}]$ for suitable shape parameters $p, q > 0$, where the denominator denotes $B(0, \frac{m_1}{\gamma}, p, q) = \int_0^{\frac{m_1}{\gamma}} (w - 0)^{(p-1)} (\frac{m_1}{\gamma} - w)^{(q-1)} dw$. See Figure 3.4 for the corresponding graph of the shifted Beta distribution ($p = 1, q = 3$ and $u^-(0, 0) = 0$). The initial distribution is followed by the concentration-temporal simulation of the pdf for one inactive cell in Figure 3.5, accordingly to parameter values in Table 3.2.

By now, we start to examine the hyperbolic PDE for the pdf of one active cell given by the Equation (3.16). Since a cell can be either in an active state or in an inactive state (an interstate is ignored) and since we assumed that the cell is inactive at the beginning, the initial pdf for an active cell can be chosen as $u^+(z, 0) = 0$.

So, the IVP for one active cell reads

$$\frac{\partial u^+(z, t)}{\partial t} + (m_1 + m_2 - \gamma z) \frac{\partial u^+(z, t)}{\partial z} = \gamma u^+(z, t) + \alpha(z) u^-(z, t), \quad (3.21)$$

$$u^+(z, 0) = 0. \quad (3.22)$$

Similar to the previous case, we use the method of characteristics to solve the IVP given

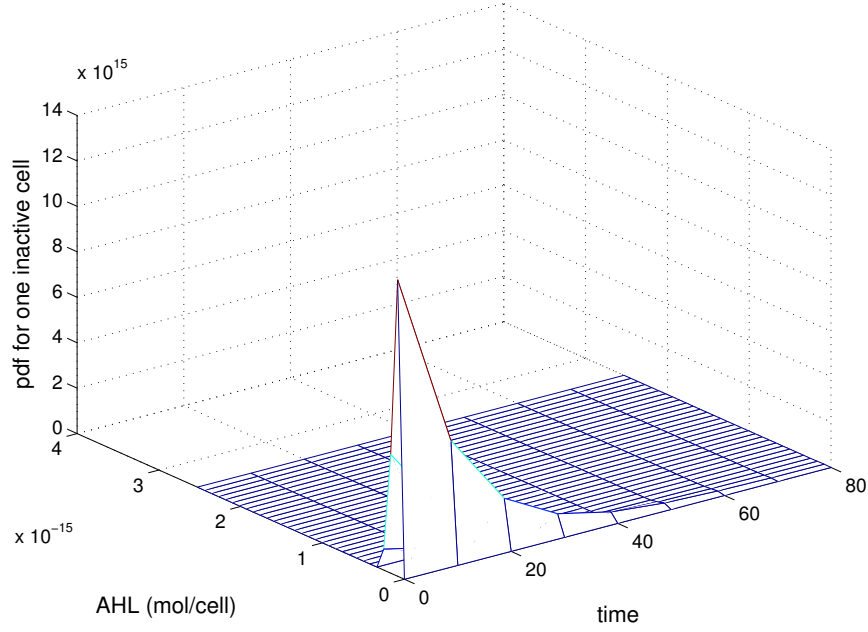


Figure 3.5: Simulation of one inactive cell.

by the equations (3.21)-(3.22). We consider the system of ODEs with the new coordinate s ,

$$\begin{aligned} \frac{dt}{ds} &= 1, \\ \frac{dz}{ds} &= m_1 + m_2 - \gamma z, \\ \frac{du^+}{ds} &= \gamma u^+ + \alpha(z)u^-, \end{aligned}$$

where $z, t \in \mathbb{R}$. Solving the first two equations of this ODE system we obtain

$$\begin{aligned} t &= s + C_1, \\ z &= \frac{(m_1 + m_2) - C_2 e^{-\gamma s}}{\gamma}. \end{aligned}$$

For $s = 0$ and $z(0) = z_0^+$ we have $C_1 = 0$, i.e., $t = s$ and $C_2 = (m_1 + m_2) - \gamma z_0^+$. The characteristic curves read $z = \frac{(m_1 + m_2) - ((m_1 + m_2) - \gamma z_0^+) e^{-\gamma t}}{\gamma}$ and they have the similar shape shown in Figure 3.3, but the interval of starting points changes because of the different maximum value of AHL in the active cell state, i.e., $z_0^+ \in [0, (m_1 + m_2)/\gamma]$. As the IVP given by the Equations (3.21)-(3.22) includes the pdf of inactive cell state, we substitute the

solution (3.19) in the third ODE of characterized system as below

$$\begin{aligned} \frac{du^+(z(t), t)}{dt} &= \gamma u^+(z(t), t) \\ &+ \alpha(z(t)) u_0 \left(\frac{m_1 - (m_1 - \gamma z(t)) e^{\gamma t}}{\gamma} \right) e^{\int_0^t \gamma - \alpha \left(\frac{m_1 - (m_1 - \gamma z(t)) e^{\gamma(t-\rho)}}{\gamma} \right) d\rho}. \end{aligned}$$

We seek a solution, which is transported on characteristic curves. Thereby, we write the characteristic curves instead of the $z(t)$

$$\begin{aligned} \frac{du^+(z(t), t)}{dt} - \gamma u^+(z(t), t) &= \alpha \left(\frac{(m_1 + m_2) - (m_1 + m_2 - \gamma z_0^+) e^{-\gamma t}}{\gamma} \right) \\ &\cdot u_0^- \left(\frac{m_1 + m_2 e^{\gamma t} - (m_1 + m_2 - \gamma z_0^+)}{\gamma} \right) \\ &\cdot e^{\int_0^t \gamma - \alpha \left(\frac{m_1 + m_2 e^{\gamma(t-\rho)} - (m_1 + m_2 - \gamma z_0^+) e^{-\gamma \rho}}{\gamma} \right) d\rho}. \end{aligned}$$

Using the variation of constants method the solution of this equation reads

$$\begin{aligned} u^+(z(t), t) &= e^{\gamma t} \left(\int_0^t e^{-\gamma \tau} \alpha \left(\frac{(m_1 + m_2) - (m_1 + m_2 - \gamma z_0^+) e^{-\gamma \tau}}{\gamma} \right) \right. \\ &\cdot u_0^- \left(\frac{m_1 + m_2 e^{\gamma \tau} - (m_1 + m_2 - \gamma z_0^+)}{\gamma} \right) \\ &\cdot e^{\int_0^{\tau} \gamma - \alpha \left(\frac{m_1 + m_2 e^{\gamma(\tau-\rho)} - (m_1 + m_2 - \gamma z_0^+) e^{-\gamma \rho}}{\gamma} \right) d\rho} d\tau + u^+(z_0^+) \Big). \end{aligned}$$

Due to initial condition (3.22), i.e., $u^+(z_0^+) = 0$ and replacing of z_0^+ by

$$z_0^+ = \frac{(m_1 + m_2) - ((m_1 + m_2) - \gamma z) e^{\gamma t}}{\gamma},$$

we require the solution of the IVP given by the Equations (3.21)-(3.22)

$$\begin{aligned} u^+(z, t) &= e^{\gamma t} \int_0^t e^{-\gamma \tau} \alpha \left(\frac{(m_1 + m_2) - (m_1 + m_2 - \gamma z) e^{\gamma(t-\tau)}}{\gamma} \right) \\ &\cdot u_0^- \left(\frac{m_1 + m_2 e^{\gamma \tau} - (m_1 + m_2 - \gamma z) e^{\gamma t}}{\gamma} \right) \\ &\cdot e^{\int_0^{\tau} \gamma - \alpha \left(\frac{m_1 + m_2 e^{\gamma(\tau-\rho)} - (m_1 + m_2 - \gamma z) e^{\gamma(t-\rho)}}{\gamma} \right) d\rho} d\tau. \end{aligned}$$

Thus, we obtain the pdf for one active cell explicitly, which is dependent on the pdf of one inactive cell. Here, it is important to take care of the characteristics of an inactive cell and an active cell, separately, while we simulate the pdf for one active cell. The corresponding simulation can be found in Figure 3.6. Additionally, we will explain the computing ideas of this recursive simulation in Section 3.4.

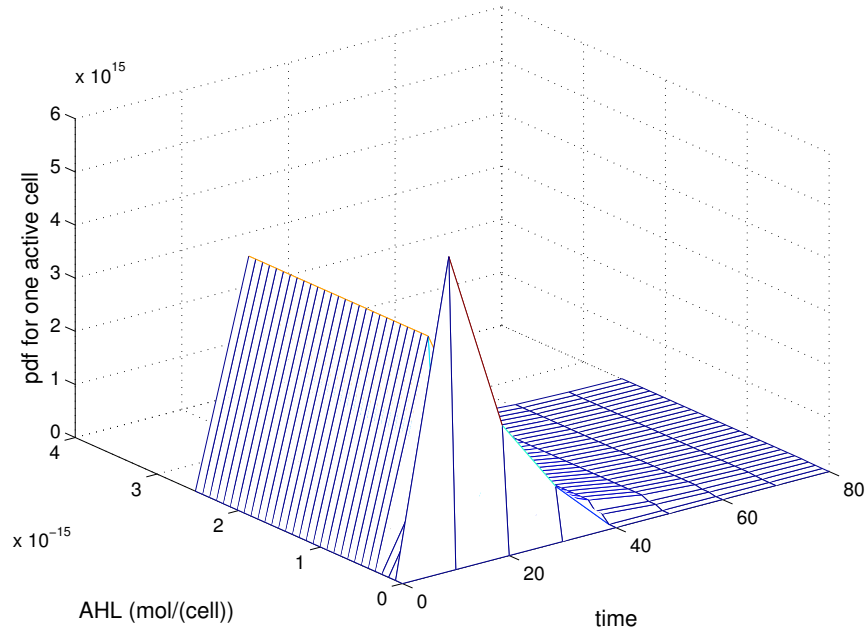


Figure 3.6: Simulation of one active cell.

3.3 A Population Model

In this section we evaluate a model for a population of finite size $N(t)$ based on the model declared in the previous Section 3.2 for one cell. We assume to have $k(t)$ inactive and $l(t)$ active cells at a given time and we denote the corresponding pdf by $u^{k,l}(z, t)$. As we supposed in the previous Section 3.2: a single cell can only perform one independent action in a time step, i.e., an inactive cell may either divide or activate and an active cell may only divide in a time step. It is assumed that an active cell never deactivates. Furthermore, in case that we have a population of finite size N , we state that only one cell of the population is allowed to perform an action in each time step, i.e., a single cell either divides or activates whereas the other cells in the populations preserve their current state. Keeping in mind that deactivation does not occur, we draw the following scheme in Figure 3.7, which shows all possible cell states in a population of finite size N .

The scheme given in Figure 3.7 leads us to derive the complete model for a population of finite size N with all their transitions between states. We first recall the model for one inactive/active cell given by Equations (3.3)-(3.4) which were constructed as described in Table 3.3. The same idea is also valid here and gives us the left hand side of the hyperbolic PDE given by the Equation (3.23). Moreover, having more than one cell forces us to take the division possibility into account in addition to the activation possibility. Thereby, we es-

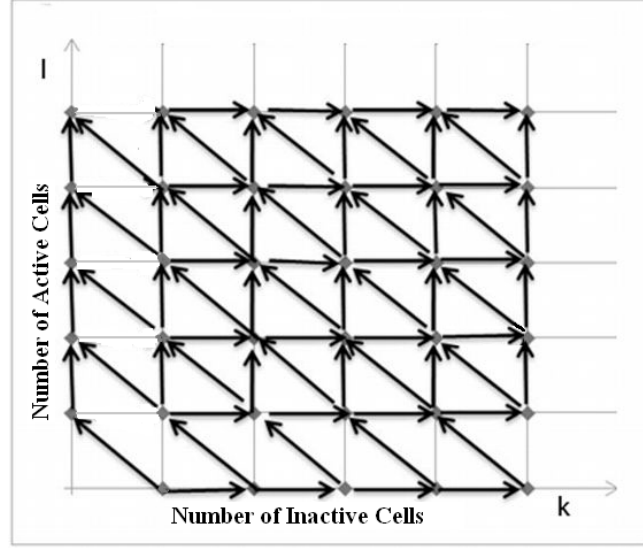


Figure 3.7: Structure of transition of cell states by cell division and activation.

establish the cell transitions shown in Figure 3.7 on the right hand side of the Equation (3.23), where β represents the division rate given also in the Table 3.2 as the other parameters.

$$\begin{aligned} \frac{\partial}{\partial t} u^{(k,l)}(z,t) + \frac{\partial}{\partial z} \left((m_1 k + (m_1 + m_2) l - \gamma z) u^{(k,l)}(z,t) \right) = & \quad (3.23) \\ & \beta(k-1) u^{(k-1,l)}(z,t) + \beta(l-1) u^{(k,l-1)}(z,t) - \beta(k+l) u^{(k,l)}(z,t) \\ & + \alpha(z)(k+1) u^{(k+1,l-1)}(z,t) - \alpha(z) k u^{(k,l)}(z,t). \end{aligned}$$

We have studied the model of one inactive cell and one active cell in Section 3.2 and defined the pdf for inactive cell state by $u^-(z,t)$ and pdf for active cell state by $u^+(z,t)$. Each of these two cases can be acquired from Equation (3.23), with the new notations $u^{(1,0)}(z,t)$ and $u^{(0,1)}(z,t)$ instead of previous ones $u^-(z,t)$ and $u^+(z,t)$, respectively.

3.3.1 Exact Solution for the Population Model

We construct the population model as a generalization of the one cell case. Since we have a system of hyperbolic PDEs given by the Equation (3.23), we will use again the method of characteristic to obtain explicit solutions for the population model. First, we will start by investigating the solutions of merely inactive cells,

$$\left\{ u^{(1,0)}(z,t), u^{(2,0)}(z,t), u^{(3,0)}(z,t), \dots, u^{(k,0)}(z,t) \right\},$$

from the corresponding hyperbolic PDE system. Afterwards, we will generalize this idea for k inactive and l active cells with the similar structure of characteristic curves.

Let us rewrite the population model given by the Equation (3.23) for k inactive cells, distinctly.

$$\begin{aligned}
 \frac{\partial}{\partial t} u^{(1,0)}(z, t) + (m_1 - \gamma z) \frac{\partial}{\partial z} u^{(1,0)}(z, t) &= (\gamma - \beta - \alpha(z)) u^{(1,0)}(z, t), \\
 \frac{\partial}{\partial t} u^{(2,0)}(z, t) + (2m_1 - \gamma z) \frac{\partial}{\partial z} u^{(2,0)}(z, t) &= (\gamma - 2\beta - 2\alpha(z)) u^{(2,0)}(z, t) + \beta u^{(1,0)}(z, t), \\
 \frac{\partial}{\partial t} u^{(3,0)}(z, t) + (3m_1 - \gamma z) \frac{\partial}{\partial z} u^{(3,0)}(z, t) &= (\gamma - 3\beta - 3\alpha(z)) u^{(3,0)}(z, t) + 2\beta u^{(2,0)}(z, t), \\
 &\vdots \\
 \frac{\partial}{\partial t} u^{(k,0)}(z, t) + (km_1 - \gamma z) \frac{\partial}{\partial z} u^{(k,0)}(z, t) &= (\gamma - k(\beta + \alpha(z))) u^{(k,0)}(z, t) + (k - 1)\beta u^{(k-1,0)}(z, t).
 \end{aligned}$$

Hence we have already calculated the characteristic curves for IVP given by Equations (3.17)-(3.18), we extend these related to the recursive PDE system:

$$\begin{aligned}
 z^{(1,0)} &= \frac{m_1 - (m_1 - \gamma z_0^{(1,0)})e^{-\gamma t}}{\gamma}, \\
 z^{(2,0)} &= \frac{2m_1 - (2m_1 - \gamma z_0^{(2,0)})e^{-\gamma t}}{\gamma}, \\
 z^{(3,0)} &= \frac{3m_1 - (3m_1 - \gamma z_0^{(3,0)})e^{-\gamma t}}{\gamma}, \\
 &\vdots \\
 z^{(k,0)} &= \frac{km_1 - (km_1 - \gamma z_0^{(k,0)})e^{-\gamma t}}{\gamma},
 \end{aligned} \tag{3.24}$$

where the initial values for each characteristic curve appear

$$z_0^{(k,0)} = \frac{k m_1 - (k m_1 - \gamma z^{(k,0)})e^{\gamma t}}{\gamma}.$$

Using the pdf of one inactive cell given by the Equation (3.19) and according to the characteristic curves we have represented by Equations (3.24), the exact solutions to the system

of PDEs for k inactive cells can be given as below:

$$\begin{aligned}
 u^{(1,0)}(z, t) &= u_0 \left(\frac{m_1 - (m_1 - \gamma z)e^{\gamma t}}{\gamma} \right) e^{\int_0^t \gamma - \beta - \alpha \left(\frac{m_1 - (m_1 - \gamma z)e^{\gamma(t-\rho)}}{\gamma} \right) d\rho}, \\
 u^{(2,0)}(z, t) &= e^{\int_0^t \gamma - 2\beta - 2\alpha \left(\frac{2m_1 - (2m_1 - \gamma z)e^{\gamma(t-\rho)}}{\gamma} \right) d\rho} \\
 &\quad \cdot \left(\int_0^t e^{-\int_0^\tau \gamma - 2\beta - 2\alpha \left(\frac{2m_1 - (2m_1 - \gamma z)e^{\gamma(t-\rho)}}{\gamma} \right) d\rho} e^{\int_0^\tau \gamma - \beta - \alpha \left(\frac{m_1 + m_1 e^{\gamma(t-\rho)} - (2m_1 - \gamma z)e^{\gamma(t-\rho)}}{\gamma} \right) d\rho} \right. \\
 &\quad \cdot u_0 \left(\frac{m_1 + m_1 e^{\gamma t} - (2m_1 - \gamma z)e^{\gamma t}}{\gamma} \right) d\tau \Big), \\
 &\quad \vdots \\
 u^{(k,0)}(z, t) &= e^{\int_0^t \gamma - k\beta - k\alpha \left(\frac{km_1 - (km_1 - \gamma z)e^{\gamma(t-\rho)}}{\gamma} \right) d\rho} \\
 &\quad \cdot \left(\int_0^t e^{-\int_0^\tau \gamma - k\beta - k\alpha \left(\frac{km_1 - (km_1 - \gamma z)e^{\gamma(t-\rho)}}{\gamma} \right) d\rho} u^{((k-1),0)}(z^{(k,0)}(z_0^{(k,0)}), \tau) d\tau \right).
 \end{aligned}$$

So, we obtain the whole system of pdfs for k inactive cells, where each pdf is dependent on the previous one via its own characteristic curves. If we generalize this idea for k inactive and l active cells thanks to the concept shown in Figure 3.7, we have the characteristic curves

$$z^{(k,l)}(z_0, t) = \frac{km_1 + (m_1 + m_2)l - (km_1 + (m_1 + m_2)l - \gamma z_0^{(k,l)})e^{-\gamma t}}{\gamma}, \quad (3.25)$$

and the explicit solution of Equation (3.23) on the characteristic curves is

$$\begin{aligned}
 u^{(k,l)}(z, t) &= e^{\int_0^t \gamma - (k+l)\beta - k\alpha \left(\frac{km_1 + (m_1 + m_2)l - (km_1 + (m_1 + m_2)l - \gamma z)e^{\gamma(t-\rho)}}{\gamma} \right) d\rho} \\
 &\quad \cdot \left(\int_0^t e^{-\int_0^\tau \gamma - (k+l)\beta - (k+l)\alpha \left(\frac{km_1 + (m_1 + m_2)l - (km_1 + (m_1 + m_2)l - \gamma z)e^{\gamma(t-\rho)}}{\gamma} \right) d\rho} \right. \\
 &\quad \cdot \left(\beta(l-1)u^{(k,l-1)}(z^{(k,l)}, \tau) + \beta(k-1)u^{(k-1,l)}(z^{(k,l)}, \tau) \right. \\
 &\quad \left. \left. + \alpha(z^{(k,l)})(k+1)u^{(k,l-1)}(z^{(k,l)}, \tau) \right) d\tau \right).
 \end{aligned} \quad (3.26)$$

3.4 Implementation of the Explicit Solution for the Parameter Estimation

In this section we implement explicitly the pdfs of $N = k + l$ cells given by Equation (3.26) in a computer program using MATLAB [36] (R2012a, The MathWorks Inc.) and start

checking our method by applying it in to simulated data with known parameter values. In the next step we determine real parameter values for the experiments performed by the group of Prof. Dr. Rädler, LMU München, as explained in Section 2.2.

3.4.1 Implementation

We define the parameter vector $\theta = (m_1, m_2, \gamma, \beta, \alpha_c, A_{thresh})$ as a collection of parameters given in Table 3.2. For numerical simulations we suppose the transition function $\alpha(z)$ as a Hill function, i.e.,

$$\alpha(z) = \alpha_c \frac{\left(\frac{z}{V}\right)^s}{A_{thresh}^s + \left(\frac{z}{V}\right)^s},$$

with Hill coefficient $s = 2.5$ in accordance to [16]. Assuming the volume of one bacterium to be $V_B = 1 \times 10^{-15}l$, as in [40], V represents the volume of a bacterial colony with 5000 cells, i.e., $V = 5000 \times 10^{-15}l$.

We construct a four dimensional regular grid of time (t), AHL concentration (z) and the number of cells in inactive (k) or active (l) state, independently. In fact, however, z is in some sense dependent on the independent variables t, k, l and z_0 given by Equation (3.25). Therefore, we have to determine on which characteristic curve an arbitrary point of the grid is located. For example, the two dimensional illustration of the $(z - t)$ -grid shown in Figure 3.8 indicates that the chosen point $(z = 3, t = 3)$ of the grid might stay on two different characteristic curves $(z^{(0,1)}, z^{(1,0)})$, which are starting from initial values $(z_0^{(0,1)}, z_0^{(1,0)})$, respectively. Indeed, an arbitrary point of the $(z - t)$ -grid is located on $((k + 1) \times (l + 1) - 1)$ different characteristics for a colony of size $N = k + l$, dependent on the considered cell states.

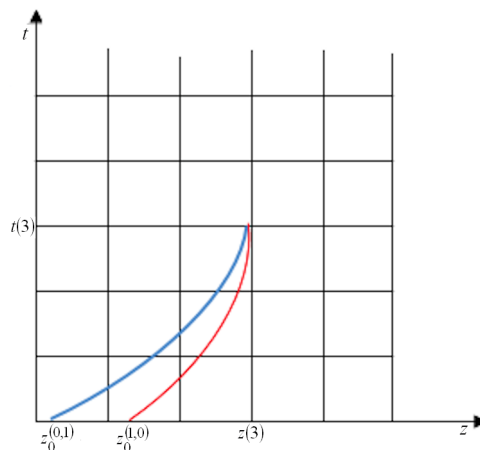


Figure 3.8: Characteristic curves on the $(z - t)$ -grid.

The characteristic curves appear in an interval changing up to the cell numbers, i.e., they exist in $[0, (k m_1 + l (m_1 + m_2)) / \gamma]$ for the starting values of $z^{(k,l)}(0) = z_0^{(k,l)}$. Outside of these intervals the corresponding characteristic curves are not relevant. Consequently, we adopt the starting values ($z_0^{(k,l)}$) of characteristics for each point (z, t) of the grid in order to see in which interval we might work. In other words, if

$$0 < z_0^{(k,l)} < (k m_1 + l (m_1 + m_2)) / \gamma,$$

then we establish the corresponding pdf $u(z, t, k, l)$ given by Equation (3.26) and store it by a matrix in a Matlab program. As the pdf $u(z, t, k, l)$ given by Equation (3.26) includes the previous pdfs, $u(z, t, k - 1, l)$ and $u(z, t, k, l - 1)$, we require the interpolation of the previous solutions on the current characteristics. Hence we collect all pdfs for $k + l$ cells. Next, we start to estimate appropriate parameters to the model given by Equation (3.25).

3.4.2 Parameter Estimation and Numerical Simulations

For a first validation of the algorithm given by Equation (3.25) we utilize some simulated data, created by Müller [43], to compare with the model. Let us built the grid for the model, i.e., time ($tgrid$), grid number of inactive cells ($kgrid$) and grid number of active cells ($lgrid$) and establish an algorithm for the model pdf $u(z, t, k, l)$. From the simulated data we have time ($tdata$), number of inactive cells ($kdata$) and number of active cells ($ldata$). However, in the mathematical model we have the pdf $u(z, t, k, l)$, which requires information on the AHL concentration z , but this is not provided from the data set. To get rid of this problem, we calculate the marginal function of the pdf $u(z, t, k, l)$ and reduce the pdf $u(z, t, k, l)$ to a z -independent function convenient to the data for the grid values:

$$u_M(t, k, l) = \int_z u(z, t, k, l) dz.$$

As we want to compare the marginal pdfs of the model and of the data, we generate the marginal pdf ($Marjdata$) for the simulated data, i.e., let us define the following vectors $\vec{t}data = (t_1, t_2, \dots, t_i, \dots, t_n)$, $\vec{k}data = (k_1, k_2, \dots, k_i, \dots, k_n)$ and $\vec{l}data = (l_1, l_2, \dots, l_i, \dots, l_n)$ where $i = 1, 2, \dots, n \in \mathcal{N}$. For any i we have

$$Marjdata(t, k, l) = \begin{cases} 1, & t = t(i) \text{ and } k = k(i) \text{ and } l = l(i), \\ 0, & \text{else.} \end{cases}$$

After this set out we are able to compare the marginal functions from model and from data, i.e., the model is available for parameter estimation.

There are two well-known methods of parameter estimation: least-square estimation (LSE) and maximum likelihood estimation (MLE). Both methods have some advantages

and it is difficult to say clearly that one of them is better than the other one. Since the LSE has minimum variance among all linear unbiased estimators, it is often called as best linear unbiased estimator [5]. LSE is a convenient method but MLE is preferred in the case where the distribution of errors are known. This is a more general and efficient approach and has better statistical properties than LSE. The mean difference between two methods are that the MLE requires a probability distribution unlike LSE [49]. As we do not use a standard pdf and do not know about the error function of the developed model we prefer to estimate the parameters by LSE.

LSE estimates parameter values by minimizing the sum of the m squared errors (SSE) between a value from the data set and the correspondent numerical simulation. In other words, the parameter vector to be estimated is $\theta_e = (\alpha_c, \beta, \gamma)$ and the observed data is given by y_i . So, we set

$$SSE(\theta_e) = \sum_{i=1}^m (y_i - model(\theta_e))^2. \quad (3.27)$$

Estimated values of θ_e can be found by minimizing the Equation (3.27)

$$\frac{\partial SSE}{\partial \theta_e} = 0 \quad \text{and} \quad \frac{\partial^2 SSE}{\partial^2 \theta_e} > 0.$$

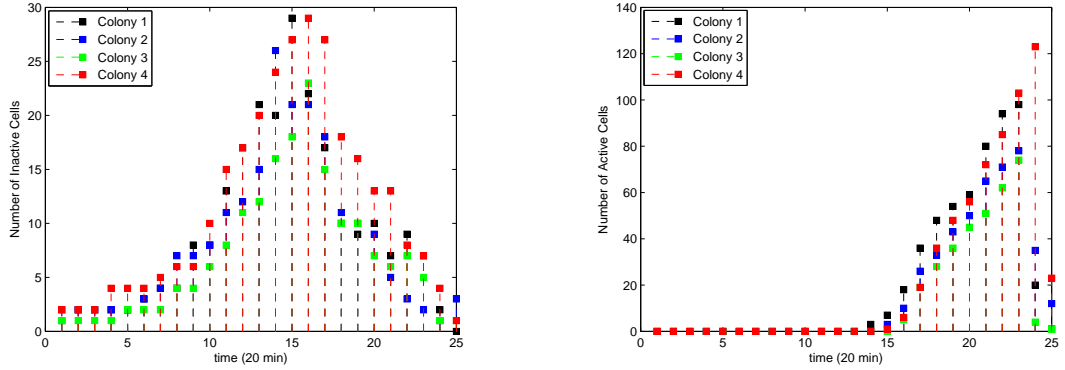
We reduced the parameter vector $\theta = (m_1, m_2, \gamma, \beta, \alpha_c, A_{thresh})$ to $\theta_e = (\alpha_c, \beta, \gamma)$, in case the parameters $\{m_1, m_2, A_{thresh}\}$ are conversant with [16]. In our case y_i is the set of $\{0, 1\}$ for each $tdata$ saved as (*Marjdata*) and $model(\theta_e)$ is the matrix of marginal distribution defined on grid points ($u_M(t, k, l)$). So, we achieve the SSE, by squaring the difference between (*Marjdata*) and ($u_M(t, k, l)$). We estimate parameters with the "fminsearch" tool of Matlab, which minimizes the SSE for a given initial value of parameter. The estimated parameters for a single simulation and for the mean value of ten different simulations are given in the Table 3.4.

Table 3.4: Comparison of start parameter values and the corresponding estimated parameter values, applied on simulated data.

Parameter	Start values	Estimation (1 Sim.)	Start values	Estimation (10 Sim.)
m_1	2.3 $\frac{10^{-7} \cdot pmol}{cell \cdot h}$	-	2.3 $\frac{10^{-7} \cdot pmol}{cell \cdot h}$	-
m_2	$9 \times 2.3 \frac{10^{-7} \cdot pmol}{cell \cdot h}$	-	$9 \times 2.3 \frac{10^{-7} \cdot pmol}{cell \cdot h}$	-
γ	0.001 h^{-1}	0.0042 h^{-1}	0.0042 h^{-1}	0.0073 h^{-1}
α_c	0.1 h^{-1}	0.0641 h^{-1}	0.0641 h^{-1}	0.0450 h^{-1}
β	0.13 h^{-1}	0.8916 h^{-1}	0.8916 h^{-1}	0.2362 h^{-1}
A_{thresh}	$70 \times 10^{10} \frac{10^{-7} \cdot pmol}{l}$	-	$70 \times 10^{10} \frac{10^{-7} \cdot pmol}{l}$	-

3.4 Implementation of the Explicit Solution for the Parameter Estimation

By now, we are interested in fitting the model with the experimental data, [40]. In Sub-section 2.2, we have mentioned how to convert the pictures of the experiment [40] to a set of numerical data, by [42]. Figure 3.9 shows the number of cells from the experiment under non-flow conditions and without adding external AHL in time steps of 20 minutes, each. We estimate parameters $\theta_e = \{\gamma, \beta, \alpha_c\}$ using the estimated parameters for the simulations



(a) Number of **inactive** cells counted from four different "Windows".

(b) Number of **active** cells counted from four different "Windows".

Figure 3.9: Number of cells without external AHL.

as start values. Then, we are able to calculate the expected values of cell numbers ($E(I)$ and $E(A)$), both for inactive and active cells whereby the marginal function $u_M(t, k, l)$ is needed. In Table 3.5 the model fitted to the mean value of real data via expected values of cells can be found, for the comparison with data see Figure 3.10.

Table 3.5: Find the start values in the Table 3.4.

Parameter	Start values	Estimation for real data
m_1	2.3 $\frac{10^{-7} \cdot pmol}{cell \cdot h}$	-
m_2	9×2.3 $\frac{10^{-7} \cdot pmol}{cell \cdot h}$	-
γ	$0.0073 h^{-1}$	$0.5339 h^{-1}$
α_c	$0.0450 h^{-1}$	$0.0402 h^{-1}$
β	$0.2362 h^{-1}$	$0.3028 h^{-1}$
A_{thresh}	70×10^{10} $\frac{10^{-7} \cdot pmol}{l}$	-

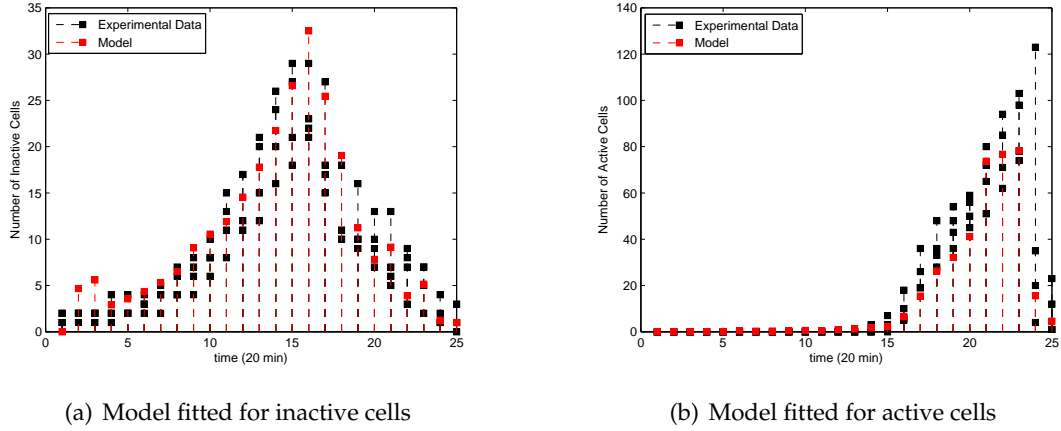


Figure 3.10: Model (3.26) fitted to experimental data

3.5 Conclusions

In this chapter, we developed an AHL mediated mathematical model for the QS of bacterial strain *P. putida* IsoF to describe the evolution (in time) of the population size of inactive and active cells, respectively. In a first approach, Equations (3.3)-(3.4), we combined a deterministic process (AHL production within the cell) with a stochastic one (transition from the inactive state to the active state for one cell) for a single cell. In the second model (3.23), we extended this idea to a population dynamics model in which we have considered each cell of the population with its own stochastic cellular dynamics. In both cases our model equations could be solved explicitly. We have provided the explicit unique analytical solution of the PDE and its numerical simulation. Furthermore, we have estimated the values for the parameters $(\gamma, \beta, \alpha_c)$ by mean of a data set of four colonies under non-flow conditions.

Our model was intended to describe the distribution in time of cellular states affected by signaling molecule concentration under non-flow conditions, without any external addition of AHL. We could fit the model to a given data set of the experiment for the QS strain *P. putida* IsoF, performed by the group of Prof. Dr. Rädler, LMU München (see Figure 3.10). We have estimated the division rate of the cells $\beta = 0.3028h^{-1}$ so that the correspondent doubling time is $T_d = \frac{\ln 2}{\beta} = 2.2891h^{-1}$ by the consideration of an exponential growth. Both these values are in accordance to previously reputed biological information, compare [40].

Nevertheless, the estimated degradation rate $\gamma = 0.5339h^{-1}$ is quite high, which might indicate that AHL accumulates on the surface of flow chamber. The long-chained AHLs

synthesized in the correspondent experiment, i.e., 3-oxo-C10-HSL and 3-oxo-C12-HSL (typical AHL molecules used in the experiment given in Section 2.2) are progressively less water-soluble molecules, [9, 40]. Moreover, AHL accumulation could be caused by the fact that the biofilm polymeric extracellular matrix, in which the bacteria are embedded, acts as a barrier to AHL diffusion, [40]. A model with an additional term for the adhesion process may give better results of the estimated degradation rate by inhibiting the accumulation.

The estimated activation rate of inactive cells $\alpha_c = 0.0402h^{-1}$ is also smaller than we expected. Since we have described a spatial structure (biofilms) by a non-spatial model, we could not conclude the exact locations of cells. If the cells lie close to the boundary of the biofilm, the activation of cells are less probable, considering the fast diffusion of AHL under the effect of the diffusion gradient. In our opinion, a spatial model could give a better estimation for the activation rate.

In a future work, the model could be extended by including the effect of flow. Moreover, addition of external AHL to the system can also be considered, there is already experimental data on this, [40]. With regard to improving the parameter estimation the fitting could be performed with a broader data range, i.e., for many more colonies. Alternatively, it may be beneficial to try different starting values for the fitting algorithm. Since the pdfs $u^{(k,l)}(z, t)$ representing our model include recursivity in their construction, the computational work of parameter estimation necessitates a long time period, e. g. the extensive interpolations which we absolutely needed seems to be quite costly. Another approach for the parameter estimation could be maximum likelihood estimation (MLE) and another choice of minimization function of Matlab might be a better alternative instead of "fmin-search", e.g., "lsqnonlin".

Consequently, we have developed an original modeling approach that fits good to experimental data and gives a future prediction of the cell state distribution for *P. putida* IsoF in the flow chamber. Additionally, we offer many different aspects to evolve the model and correspondent parameter estimation.

4 Spatial Structure of Cells and their Effect on the AHL Concentration

This chapter is devoted to understanding the QS system between cells where their locations and states are determined at the single cell level, even though the AHL concentration remains unknown. As a starting point we refer to the paper [45], which introduces a modeling approach for the description of the QS system of a bacterial population with their single cell dynamics, including a discussion of the regulatory network and its bistable behavior. The model consists of a system of non-linear ODEs and a linear parabolic PDE describing the AHL concentration within and outside of the cell, respectively. Even though an approximate solution (as an algebraic system) based on the single cell solution and superposition thereof was obtained, finding analytical solutions for the case of several cells was not possible. They avoid also numerical solutions which would need a quite fine discretization around each of the cells causing a high computational effort. Thus, the approach assuming the cells as shrinking objects to the size of points plays an important role to have a homogeneous equation for the signaling substance.

In contrast to [45] where the AHL production by single cells was described via intracellular ODEs and corresponding boundary conditions to the extracellular space, we assume here that cells are just characterized by locations in the whole space where AHL production takes place and AHL molecules move via free diffusion through the cell walls. We develop our model using reaction diffusion equations (RDEs), which explain the change of AHL substance within the cell and in the exterior, simultaneously. Moreover, these RDEs consist of the QS components managing the positive feedback loop and the interaction between cells. Assuming the cells as little spheres, we obtain an analytical solution for a single cell case thanks to the radially symmetric structure. Nevertheless, the scattered spatial structure of many cells frustrates finding analytical solutions. Numerical schemes are also not an ideal approach because the cells are supposed to be three dimensional objects which need fine discretization around each of them. Therefore, we aim to simplify the model. For that purpose, we let the cells shrink to a point conserving the behavior of the whole system with the appropriate scaling, which enables us to approach the RDEs point wise in the case of a homogeneous space.

4.1 Model Assumptions

We consider a model of N cells that communicate via AHL molecules and define each of them as a sphere by $\Omega_i := \{|x - x_i| \leq L \mid x \in \mathbb{R}^3, i = 1, \dots, N\}$ with radius L . The cells produce AHL but they do not only sense the self-produced signaling molecules but also those produced by other cells. Thus, it is indicated through a function f describing AHL production in terms of cell interaction, i.e. AHL production within the cell centered at x_i and its sense of AHL produced by others. The real valued function $u_i(x, t)$ denotes the AHL concentration of the cell centered at x_i , which can freely diffuse from the cell wall to the environment and come back into the cell. At this point, we prefer to use the notation $u_i(x, t)$ representing the substance concentration as usual in RDEs, instead of z describing the time dependent AHL concentration in the stochastic model derived in Chapter 3. Here, $x \in \mathbb{R}^3$ and t represent the spatial and temporal variable, respectively. The diffusion rate is constant and given by D in the sense of Fickian diffusion. γ denotes the abiotic AHL decay in whole domain and Δ denotes the Laplace operator which is defined by $\Delta = \sum_{j=1}^3 \frac{\partial^2}{\partial x_j^2}$.

Since we have an AHL production only within the cells and each cell senses the total concentration of AHL in themselves, χ represents the characteristic function for the source term. For N cells, we set the following general reaction diffusion model with an initial function $g(x)$ for $t = 0$

$$\frac{\partial u_i(x, t)}{\partial t} = D\Delta u_i(x, t) - \gamma u_i(x, t) + f \left(\sum_{\substack{j=1 \\ i \neq j}}^N u_j(x, t), u_i(x, t) \right) \chi_{|x-x_i| \leq L}, \quad (4.1)$$

$$u(x, 0) = g(x), \quad (4.2)$$

where $x \in \mathbb{R}^3, t \in [0, T), 0 \leq T < \infty$ and the characteristic function is

$$\chi_{|x-x_i| \leq L} = \begin{cases} 1, & \text{if } x \in \Omega_i, \\ 0, & \text{else.} \end{cases}$$

4.1.1 Pre-model: Line Shaped Single Cell in 1D

The first step to reach our goal is investigating the behavior of a one dimensional reaction diffusion model as a pre-model of our work. At the beginning, we consider a model in 1D with a constant production rate α of AHL within the cell. The AHL molecules are freely diffusible through the cell wall. Figure 4.1 represents the cell on the x -axis with a line shape and diameter L , i.e., $\Omega_1 = \{x \mid 0 \leq x \leq L\}$.



Figure 4.1: 1D cell on the x-axis.

Corresponding RDE for the pre-model reads

$$\begin{aligned}\frac{\partial u(x, t)}{\partial t} &= D\Delta u(x, t) + \alpha\chi_{\Omega_1}, \\ u(x, 0) &= g(x),\end{aligned}\tag{4.3}$$

where $x \in \mathbb{R}$ and χ_{Ω_1} is defined by

$$\chi_{\Omega_1} = \begin{cases} 1, & \text{if } 0 \leq x \leq L, \\ 0, & \text{else.} \end{cases}$$

We first want to check the validity of our idea in 1D, i.e., how does $u(x, t)$ behave as the diameter of cell, L tends to zero. Let us remind the fundamental solution of non-homogeneous parabolic equations with a reaction and diffusion term in an unbounded domain.

Definition 4.1 (*Diffusion equation and its fundamental solution*)[14]

We consider the diffusion equation in \mathbb{R}^n for $t > 0$

$$\frac{\partial u(x, t)}{\partial t} = D\Delta u(x, t)\tag{4.4}$$

The function

$$\Phi(x, t) = \begin{cases} \frac{1}{(4D\pi t)^{n/2}} e^{-|x|^2/4Dt}, & x \in \mathbb{R}^n, t > 0, \\ 0, & x \in \mathbb{R}^n, t < 0, \end{cases}$$

is called the Green's kernel or fundamental solution of the diffusion equation given by Equation (4.4).

Remark 4.2 Now, we consider the following IVP

$$\begin{aligned}\frac{\partial u(x, t)}{\partial t} &= D\Delta u(x, t), & x \in \mathbb{R}^n, t > 0, \\ u(x, 0) &= g(x), & x \in \mathbb{R}^n, t = 0.\end{aligned}\tag{4.5}$$

$\Phi(x-y, t)$ is a solution of the IVP (4.5) for all $y \in \mathbb{R}^n$ because of the translation invariance property of the diffusion equation, i.e., when x is replaced by $x-y$, the diffusion equation remains unchanged. By linearity and homogeneity of the diffusion equation (4.4) we may take a linear combination of solutions, e.g.,

$$u(x, t) = \int_{\mathbb{R}^n} \Phi(x-y, t)g(y)dy, \quad (4.6)$$

for a fixed $y \in \mathbb{R}^n$. The function $u(x, t)$ given by the Equation (4.6) is a solution of (4.4), in case the integral converges in an adequate manner.

Remark 4.3 The Green's Kernel $G(x, y, t) = \Phi(x-y, t)$ has the following properties

- (i) $G(x, y, t) \in C^\infty(\mathbb{R}^n \times \mathbb{R}^n \times (0, \infty))$,
- (ii) $(\frac{\partial}{\partial t} - \Delta)G(x, y, t) = 0, t > 0$,
- (iii) $G(x, y, t) > 0, t > 0$,
- (iv) $\int_{\mathbb{R}^3} G(x, y, t)dy = 1, t > 0$ and $x \in \mathbb{R}^n$,
- (v) for each fixed δ ,
 $\lim_{t \rightarrow 0} \int_{\mathbb{R}^n \setminus B_\delta(x)} G(x, y, t)dy = 0$.

Theorem 4.4 [14] Assume $g \in C(\mathbb{R}^n)$ and $\sup_{x \in \mathbb{R}^n} |g(x)| < \infty$. Then for $u(x, t)$ defined by Equation (4.6) we have

- (i) $u \in C^\infty(\mathbb{R}^n \times (0, \infty))$,
- (ii) $\lim_{\substack{(x,t) \rightarrow (x_0,0) \\ t > 0}} u(x, t) = g(x_0)$ for all $x_0 \in \mathbb{R}^n$,
- (iii) u is a solution of the IVP (4.5).

Definition 4.5 (Non-homogeneous RDE)[53]

We consider the following non-homogeneous IVP with a given source term f and given initial function g ,

$$\begin{aligned} \frac{\partial u(x, t)}{\partial t} &= D\Delta u(x, t) + f(x, t), & x \in \mathbb{R}^n, t > 0, \\ u(x, 0) &= g(x), & x \in \mathbb{R}^n, t = 0. \end{aligned} \quad (4.7)$$

We have already derived the solution of the diffusion equation (4.4) and we use it to define the function

$$u_h(x, t) = \int_{\mathbb{R}^n} \Phi(x-y, t)g(y)dy$$

satisfies the homogeneous part of the IVP in (4.7). Due to linearity, a linear combination of functions u_h and a particular solution u_p , e.g.,

$$u(x, t) = u_h(x, t) + u_p(x, t),$$

solves the IVP in (4.7). In order to find a solution to the non-homogeneous part of the IVP (4.7) u_p we use the so-called Duhamel's principle, which considers the non-homogeneous problem as a set of homogeneous problems. In this context, we define a family of functions $\tilde{u}(x, t; s)$ by introducing a parameter $s > 0$ as solutions to the following IVP

$$\begin{aligned} \frac{\partial \tilde{u}(x, t)}{\partial t} &= D\Delta \tilde{u}(x, t), & x \in \mathbb{R}^n, t > s, \\ \tilde{u}(x, s; s) &= f(x, s), & x \in \mathbb{R}^n, t = s. \end{aligned} \quad (4.8)$$

According to the Duhamel's principle, the particular solution to the non-homogeneous IVP (4.7) can be written as a sum of the solutions $\tilde{u}(x, t; s)$ over s , i.e.,

$$u_p(x, t) = \int_0^t \tilde{u}(x, t; s) ds. \quad (4.9)$$

By Theorem 4.4, we know that

$$\tilde{u}(x, t; s) = \int_{\mathbb{R}^n} \Phi(x - y, t - s) f(y, s) dy \quad (4.10)$$

is a solution of the IVP in (4.8). By combining the Equations (4.9) and (4.10)

$$u(x, t) = \int_{\mathbb{R}^3} \Phi(x - y, t) g(y) dy + \int_0^t \int_{\mathbb{R}^3} \Phi(x - y, t - s) f(y, s) dy ds. \quad (4.11)$$

Theorem 4.6 [14] *Assume that $f \in C_1^2(\mathbb{R}^n \times [0, \infty))$. Then for $u(x, t)$ defined as in (4.11) we have*

- (i) $u \in C_1^2(\mathbb{R}^n \times [0, \infty))$,
- (ii) $\lim_{\substack{(x,t) \rightarrow (x_0, 0^+) \\ t > 0}} u(x, t) = g(x_0)$ for all $x_0 \in \mathbb{R}^n$,
- (iii) u is a solution of the IVP in (4.7).

It is important to know how the reaction term f behaves, for the existence and uniqueness of the solution of Equation (4.7). Generally, small changes in the reaction term structure may lead to a completely different behavior. The reaction term might be linear or non-linear, i.e., the function f may depend on x, t and u as long as it is sufficiently smooth. The

theory describing the existence and uniqueness of solutions of these types of RDEs are well studied, at least locally in time, [35],[63]. The IVP (4.7) is known to be well posed in many Lebesgue spaces $L^p(\Omega)$ by assuming that the reaction term f is a Lipschitz continuous function. Thus, there exists for every given initial function $g \in B$ and for appropriate conditions on the reaction term f , a unique solution $u(x, t) \in B$ for all $t \in [0, T]$, where B is a Banach space.

We assume that the reaction term f is bounded and in C^∞ . Then the Cauchy problem can be solved and the solution $u(x, t)$ is unique, C^∞ smooth in $\mathbb{R}^n \times (0, \infty)$ and continuous in $\mathbb{R}^n \times [0, \infty)$, where the initial function $u(x, 0) = g(x)$ is bounded and continuous, [14].

We turn to the solution of the line-shaped model (4.3) which can be found in (4.11). Here we have to take into account that the AHL production is only possible within the cell. We substitute the Equation (4.11) for $x \in \mathbb{R}^3$ and $t > 0$ and replace Φ by Green's kernel G :

$$\begin{aligned}
 u(x, t) &= \int_{-\infty}^0 G(x-y, t)g(y)dy + \int_0^L G(x-y, t)g(y)dy + \int_L^\infty G(x-y, t)g(y)dy \\
 &+ \int_0^t \left(\int_{-\infty}^0 G(x-y, t-s)\alpha \chi_\Omega dy + \int_0^L G(x-y, t-s)\alpha \chi_\Omega dy \right. \\
 &\left. + \int_L^\infty G(x-y, t-s)\alpha \chi_\Omega dy \right) ds \\
 &= \int_{-\infty}^0 \frac{1}{2\sqrt{\pi Dt}} e^{-\frac{|x-y|^2}{4Dt}} g(y)dy + \int_0^L \frac{1}{2\sqrt{\pi Dt}} e^{-\frac{|x-y|^2}{4Dt}} g(y)dy \\
 &+ \int_L^\infty \frac{1}{2\sqrt{\pi Dt}} e^{-\frac{|x-y|^2}{4Dt}} g(y)dy \\
 &+ \int_0^t \left(\int_{-\infty}^0 0 dy + \alpha \int_0^L \frac{1}{2\sqrt{\pi D(t-s)}} e^{-\frac{|x-y|^2}{4D(t-s)}} g(y)dy + \int_L^\infty 0 dy \right) ds.
 \end{aligned}$$

Let us consider $L \rightarrow 0$, i.e., the cell is shrinking with a constant production rate α

$$\begin{aligned}
 \lim_{L \rightarrow 0} u(t, x) &= \int_{-\infty}^\infty \frac{1}{2\sqrt{\pi Dt}} e^{-\frac{|x-y|^2}{4Dt}} g(y)dy \\
 &+ \alpha \int_0^t \left[\lim_{L \rightarrow 0} \int_0^L \frac{1}{2\sqrt{\pi D(t-s)}} e^{-\frac{|x-y|^2}{4D(t-s)}} dy \right] ds \\
 &= \frac{1}{2\sqrt{\pi Dt}} \left[\int_{-\infty}^\infty e^{-\frac{|x-y|^2}{4Dt}} dy \right].
 \end{aligned}$$

Thus we find out that the AHL concentration $u(x, t)$ is independent of AHL production rate, i.e., for a constant α , the production vanishes completely. This means if we have a constant α , then the length of the cell does not play a role. Even for a very small cell we have the same equation for the AHL concentration. Further we assume that we have a source term $\alpha \chi_\Omega(L)$ which is dependent on cell length, then we get

$$\begin{aligned} \lim_{L \rightarrow 0} u(x, t) &= \frac{1}{2\sqrt{\pi Dt}} \left[\int_{-\infty}^{\infty} e^{-\frac{|x-y|^2}{4Dt}} g(y) dy \right] \\ &+ \int_0^t \left[\lim_{L \rightarrow 0} \int_0^L \frac{1}{2\sqrt{\pi D(t-s)}} \alpha(L) e^{-\frac{|x-y|^2}{4D(t-s)}} dy \right] ds. \end{aligned}$$

This means that if we let the cell length shrink then the source term has to produce the AHL with an appropriately scaled rate, so that the function of density does not disappear. We achieve the relationship between cell length and source term in the way of assuming the cell has a one dimensional shape. In order to ensure that the AHL concentration is positive, we have to choose an appropriate source term, which can be for example $\frac{1}{L}$.

The results of the pre-model will help to extend the main concept given by the Equations (4.1)-(4.2). Thus, we are able to examine the spatial behavior of a single sphere shaped cell in \mathbb{R}^3 and their suitable approximations. Through the analytical solutions to this model are not easy to find, we first simplify our model and start with the stationary state for a linear source term. We will derive some analytical results from this single cell model and extend them under suitable conditions to a N -cell model.

4.2 A Single Cell Model in \mathbb{R}^3 with a Linear Source Term

We first present a three-dimensional steady state model for a single cell with a special case of the AHL production within the cell, to capture the basic mathematical principles and the idea for a suitable scaling. The suitable scaling of the main model is interesting, because we do not only look into self produced molecules but also carried molecules through the cell membrane by diffusion.

4.2.1 Assumptions of the Single Cell Model with a Linear Source Term

We assume that we have a single cell centered at $x = 0$ with radius L in \mathbb{R}^3 and we suppose that we have only a constitutive AHL production with a rate a and a state-dependent decay $b u(x)$ of AHL within the cell, i.e., the reaction term reads $f(u(x)) = a - b u(x)$ for all $b > 0$. Note that the choice of the simplified linear reaction term contradicts the usual biologically meaningful assumption, but the decay $-b u(x)$ is justified by the need for bounded AHL production within the cell. Furthermore, we neglect the abiotic degradation rate γ (occurring over the whole domain) of AHL appearing in the main model (4.1), because it has no effect on the scaling concept.

Before we start to examine the model structure, we summarize all required variables for

this chapter in the Table 4.1 and the parameters that we need for the models with a linear reaction term in the Table 4.2, respectively.

Table 4.1: Variables used for the model 4.

Variable	Description
x	Position
t	Time
$u(x, t)$	AHL concentration in x at t

Table 4.2: Parameters used for the models with a linear reaction term in Sections 4.2 and 4.3.

Parameter	Description
D	Constant diffusion rate of AHL
a	AHL production rate within the cell
b	AHL degradation rate within the cell
α	Scaled AHL production rate
β	Scaled AHL degradation rate
γ	Abiotic AHL degradation rate in whole domain

Knowing that AHL production is highly dependent on the position of cell, we start with the stationary state assumption, which will also simplify to determine the suitable scaling factor.

$$-D\Delta u(x) = (a - bu(x)), \quad \text{if } |x| \leq L, \quad (4.12)$$

$$-D\Delta u(x) = 0, \quad \text{if } |x| > L. \quad (4.13)$$

We assume that $a, b > 0$, in case $b < 0$ there may appear a blow-up of the solution for $t \rightarrow \infty$ in the dynamical state. Suppose that the solution $u = u(r)$ is radially symmetric and recall the three-dimensional Laplacian in terms of spherical coordinates, $\Delta u(r) = \frac{d^2u}{dr^2} + \frac{2}{r} \frac{du}{dr}$. Expecting a delta-peak behavior from the solution $u(r)$ as $L \rightarrow 0$ brings us to define the Equation (4.14) in terms of radial coordinates:

$$u(r) = \frac{s(r)}{r}. \quad (4.14)$$

Then, we convert the model given by Equations (4.12)-(4.13) in the Cartesian coordinates to the spherical coordinates and obtain the following system of second order ODEs by

transforming it in terms of s

$$s''(r) - \frac{b}{D}s(r) + \frac{a}{D}r = 0, \quad \text{if } r \leq L, \quad (4.15)$$

$$\frac{s''(r)}{r} = 0, \quad \text{if } r > L. \quad (4.16)$$

Avoiding to have a pole at $r = 0$ we obtain the general solutions to the Equations given by (4.15)-(4.16)

$$s(r) = A e^{\sqrt{b/D}r} + B e^{-\sqrt{b/D}r} + \frac{a}{b}r, \quad \text{if } r \leq L,$$

$$s(r) = c_1 + c_2r, \quad \text{if } r > L,$$

where $A, B, c_1, c_2 \in \mathbb{R}$. Since the signaling molecule production is only possible within the cell, we know that $s(r)$ is not a monotone increasing/decreasing function in $r > L$. Thus, we set $c_2 = 0$ and have $s(r) = c_1$. In order to avoid a singularity at $r = 0$, we set $s(0) = 0$ which gives us $A = -B$. Furthermore, the necessity of the smoothness on the boundary imposes the boundary conditions where the solutions for $r \leq L$ and $r > L$ have to be equivalent at $r = L$, as well as the first derivatives thereof. The first derivatives of the solutions are

$$\begin{aligned} s'(L) &= A\sqrt{b/D}e^{\sqrt{b/D}L} - B\sqrt{b/D}e^{-\sqrt{b/D}L} + \frac{a}{b} \\ &= A\sqrt{b/D} \left(e^{\sqrt{b/D}L} + e^{-\sqrt{b/D}L} \right) + \frac{a}{b} \\ &= 2A\sqrt{b/D} \cosh(\sqrt{b/D}L) + \frac{a}{b}, \end{aligned}$$

for $r \leq L$ and

$$s'(L) = 0,$$

for $r > L$. By setting those equal at the boundary, we obtain the coefficients

$$\begin{aligned} A &= -\frac{a\sqrt{D}}{2b^{3/2}} \frac{1}{\cosh(\sqrt{b/D}L)}, \\ B &= \frac{a\sqrt{D}}{2b^{3/2}} \frac{1}{\cosh(\sqrt{b/D}L)}. \end{aligned}$$

Finally, let us determine the constant c_1 by avoiding any jumps at $r = L$,

$$\begin{aligned} c_1 &= \frac{a}{b}L - \frac{a\sqrt{D}}{b^{3/2}} \frac{\sinh(\sqrt{b/D}L)}{\cosh(\sqrt{b/D}L)} \\ \Rightarrow c_1 &= \frac{aL}{b} \left(1 - \sqrt{D/b} \frac{\tanh(\sqrt{b/D}L)}{L} \right). \end{aligned}$$

Here, c_1 should be independent of L in the exterior of cell, so we we have to scale the parameters a and b , appropriately.

After determining the coefficients, we obtain the explicit solution to the model given by Equations (4.12)-(4.13) in the following:

$$u(r) = \begin{cases} \frac{a}{b} - \frac{a\sqrt{D}}{b^{3/2}} \frac{\sinh(\sqrt{b/D}r)}{\cosh(\sqrt{b/D}L)}, & \text{if } r \leq L, \\ \frac{a}{b} L \left(1 - \sqrt{D/b} \frac{\tanh(\sqrt{b/D}L)}{L}\right) \frac{1}{r}, & \text{if } r > L. \end{cases} \quad (4.17)$$

Additionally, we want to ensure that this function has a finite limit for $b \rightarrow 0$ which restricts the infinite production ($\lim_{b \rightarrow 0} u(r) = \infty$) or extinction ($\lim_{b \rightarrow 0} u(r) = 0$) of AHL concentration within the cell. Here, we show that the $\lim_{b \rightarrow 0} u(r)$ tends to a constant value, which is not equal to zero:

$$\begin{aligned} \lim_{b \rightarrow 0} u(r) &= \lim_{b \rightarrow 0} \frac{a}{b} - \frac{a\sqrt{D}}{b^{3/2}} \frac{\sinh(\sqrt{b/D}r)}{r \cosh(\sqrt{b/D}L)} \\ &= \lim_{b \rightarrow 0} \frac{a}{b} - \frac{a\sqrt{D}}{b^{3/2}} \frac{\sqrt{b/D}r + (b/D)^{3/2} \frac{r^3}{3!} + \mathcal{O}(b^{5/2})}{1 + \frac{L^2 b}{2!D} + \mathcal{O}(b^2)} \\ &= \lim_{b \rightarrow 0} \frac{a}{b} - \frac{a\sqrt{D}}{r} \frac{\left(6b^{-3/2}\sqrt{b/D}r + r^3 D^{-3/2} + \mathcal{O}(b)\right)}{6\left(1 + \frac{L^2 b}{2!D} + \mathcal{O}(b^2)\right)} \\ &= \lim_{b \rightarrow 0} \frac{1}{\left(1 + \frac{L^2 b}{2!D} + \mathcal{O}(b^2)\right)} \left(\frac{a(1 + \frac{L^2 b}{2!D} + \mathcal{O}(b^2))}{b} - \frac{a}{b} - \frac{a r^2}{6D} + \mathcal{O}(b)\right) \\ &= \lim_{b \rightarrow 0} \frac{1}{\left(1 + \frac{L^2 b}{2!D} + \mathcal{O}(b^2)\right)} \left(\frac{a L^2}{2\sqrt{D}} - \frac{a r^2}{6D} + \mathcal{O}(b)\right) \\ &= \frac{a L^2}{2D} - \frac{a r^2}{6D}. \end{aligned}$$

Note that $b = 0$ causes an infinite AHL production within the cell, therefore we assume here $b \neq 0$.

4.2.2 Suitable Scaling for the Single Cell Model with a Linear Source Term

Since we ignore the sensing process for simplicity in the single cell model, we consider that the net AHL production is represented by the right hand side of the Equation (4.12). By integrating it over space, we determine the parameters a and b so that the total mass of

AHL in the first order within the cell is:

$$\begin{aligned}
 \int_{\mathbb{R}^3} (a - b u(x)) \chi_{|x| \leq L} dx &= \int_0^L a 4\pi r^2 dr - \int_0^L b u(r) 4\pi r^2 dr & (4.18) \\
 &= \frac{4}{3} \pi a L^3 - b \int_0^L u(r) 4\pi r^2 dr \\
 &= \frac{4}{3} \pi a L^3 - b T_L,
 \end{aligned}$$

where $T_L := \int_0^L u(r) 4\pi r^2 dr$ represents the total mass of AHL within the cell. Using the explicit solution given by Equation (4.17) we obtain T_L as below:

$$\begin{aligned}
 T_L &= \int_0^L u(r) 4\pi r^2 dr \\
 &= \int_0^L \left[\frac{a}{b} - \frac{a\sqrt{D}}{b^{3/2} \cosh(\sqrt{b/D}L)} \frac{\sinh(\sqrt{b/D}r)}{r} \right] 4\pi r^2 dr \\
 &= \frac{4\pi a}{3b} L^3 - \frac{4\pi a\sqrt{D}}{b^{3/2} \cosh(\sqrt{b/D}L)} \int_0^L \sinh(\sqrt{b/D}r) r dr.
 \end{aligned}$$

Though the integral is analytically solvable, we use a Taylor expansion in r for small L and we have

$$\begin{aligned}
 T_L &= \frac{4\pi a}{3b} L^3 - \frac{4\pi a\sqrt{D} \sqrt{b/D}}{b^{3/2} \cosh(\sqrt{b/D}L)} \\
 &\quad \cdot \int_0^L \left(r + (b/D) \frac{r^3}{3!} + (b/D)^2 \frac{r^5}{5!} + (b/D)^3 \frac{r^7}{7!} + \mathcal{O}(r^9) \right) r dr \\
 &= \frac{4\pi a}{3b} L^3 - \frac{4\pi a}{b \cosh(\sqrt{b/D}L)} \\
 &\quad \cdot \left(\frac{L^3}{3} + \frac{b}{D} \frac{L^5}{5 \cdot 3!} + \left(\frac{b}{D}\right)^2 \frac{L^7}{7 \cdot 5!} + \left(\frac{b}{D}\right)^3 \frac{L^9}{9 \cdot 7!} + \mathcal{O}(L^{11}) \right) \\
 &= \frac{4\pi a}{3b} L^3 - \frac{4\pi a}{b} \frac{L^3}{3} \left(1 + \frac{b}{D} \frac{3L^2}{5 \cdot 3!} + \left(\frac{b}{D}\right)^2 \frac{3L^4}{7 \cdot 5!} + \left(\frac{b}{D}\right)^3 \frac{3L^6}{9 \cdot 7!} + \mathcal{O}(L^8) \right) \\
 &\quad \cdot \left(1 - \left(\frac{b}{D}\right) \frac{L^2}{2!} + \left(\frac{b}{D}\right)^2 \frac{5L^4}{4!} - \left(\frac{b}{D}\right)^3 \frac{61L^6}{6!} + \mathcal{O}(L^8) \right),
 \end{aligned}$$

Hence we only need the order of L to reach a suitable scaling, we do not need all coefficients accurately. Therefore, the real numbers $\{\mu_1, \mu_2, \mu_3, \mu_4, \mu_5, \mu_6, \mu_7, \mu_8, \mu_9\}$ embody the real coefficients family for the product term

$$(1 + b\mu_1 L^2 + b^2\mu_2 L^4 + b^3\mu_3 L^6 + \mathcal{O}(L^8)) (1 - b\mu_4 L^2 + b^2\mu_5 L^4 - b^4\mu_6 L^6 + \mathcal{O}(L^8)) = (1 - \mu_7 bL^2 + \mu_8 b^2 L^4 + \mu_9 b^3 L^6 + \mathcal{O}(L^8)).$$

We come back to the calculation of T_L ,

$$\begin{aligned} T_L &= \frac{4\pi a L^3}{3b} - \frac{4\pi a L^3}{3b} (1 - \mu_7 bL^2 + \mu_8 b^2 L^4 + \mu_9 b^3 L^6 + \mathcal{O}(L^8)) \\ &= \frac{4\pi}{3} \mu_7 a L^5 - \frac{4\pi}{3} \mu_8 a b L^7 + \mathcal{O}(L^9). \end{aligned}$$

Then, we insert this Taylor expansion of T_L into the integral in (4.18)

$$\begin{aligned} \int_{\mathbb{R}^3} (a - bu(x)) \chi_{|x| \leq L} dx &= \frac{4}{3} \pi a L^3 - b T_L \\ &= \frac{4}{3} \pi a L^3 - b \left(\frac{4\pi}{3} \mu_7 a L^5 - \frac{4\pi}{3} \mu_8 b L^7 + \mathcal{O}(L^8) \right) \\ &= \frac{4}{3} \pi a L^3 - \frac{4\pi}{3} \mu_7 a b L^5 - \frac{4\pi}{3} \mu_8 a b^2 L^7 + \mathcal{O}(L^8). \end{aligned}$$

Choosing the parameters $a = \alpha L^{-3}$ and $b = \beta L^{-2}$ makes all terms in zero order. So, we achieve the scaled model for a single cell

$$-D\Delta u(x) = \left(\frac{\alpha}{L^3} - \frac{\beta}{L^2} u(x) \right) \chi_{|x| \leq L}.$$

The radial symmetric solution for the scaled model reads

$$u(r) = \begin{cases} \frac{\alpha L^{-1}}{\beta} \left(1 - \frac{1}{\sqrt{\beta/D} \cosh(\sqrt{\beta/D})} \frac{\sinh(\sqrt{\beta/D} \frac{r}{L})}{\frac{r}{L}} \right), & \text{if } r \leq L, \\ \frac{\alpha}{\beta} \left(1 - \sqrt{D/\beta} \tanh(\sqrt{\beta/D}) \right) \frac{1}{r}, & \text{if } r > L. \end{cases}$$

After determining the suitable scaling of parameters, we check the positivity of the solution as $r \rightarrow 0$:

$$\begin{aligned} \lim_{r \rightarrow 0} u(r) &= \frac{\alpha L^{-1}}{\beta} \left(1 - \frac{1}{\sqrt{\beta/D} \cosh(\sqrt{\beta/D})} \lim_{r \rightarrow 0} \frac{\sinh(\sqrt{\beta/D} \frac{r}{L})}{\frac{r}{L}} \right) \\ &= \frac{\alpha L^{-1}}{\beta} \left(1 - \frac{1}{\sqrt{\beta/D} \cosh(\sqrt{\beta/D})} \sqrt{\beta/D} \right) \\ &= \frac{\alpha L^{-1}}{\beta} \left(1 - \frac{1}{\cosh(\sqrt{\beta/D})} \right). \end{aligned}$$

As being $0 < \frac{1}{\cosh(\sqrt{\beta/D})} < 1$, $u(r)$ fulfills the positivity condition.

4.2.3 Single Cell Model with Abiotic AHL Degradation

By now, we add a general decay term γ to our model which preserves the previous scaling. Thus, the model reads

$$-D\Delta u(x) + \gamma u(x) = \left(\frac{\alpha}{L^3} - \frac{\beta}{L^2} u(x) \right), \quad \text{if } |x| \leq L, \quad (4.19)$$

$$-D\Delta u(x) + \gamma u(x) = 0, \quad \text{if } |x| > L. \quad (4.20)$$

We can convert this model to the system of second order ODEs because of the radial symmetry for the assumption $u(r) = \frac{s(r)}{r}$, so we have

$$s''(r) - \left(\frac{\beta L^{-2} + \gamma}{D} \right) s(r) + \frac{\alpha L^{-3}}{D} r = 0, \quad \text{if } r \leq L, \quad (4.21)$$

$$s''(r) - \frac{\gamma}{D} s(r) = 0, \quad \text{if } r > L. \quad (4.22)$$

The general solution to the system of ODEs (4.21)-(4.22) is

$$s(r) = \begin{cases} A e^{\sqrt{(\beta L^{-2} + \gamma)/Dr}} + B e^{-\sqrt{(\beta L^{-2} + \gamma)/Dr}} + \frac{\alpha L^{-3}}{\beta L^{-2} + \gamma} r, & \text{if } r \leq L, \\ c_1 e^{\sqrt{\gamma/Dr}} + c_2 e^{-\sqrt{\gamma/Dr}}, & \text{if } r > L. \end{cases} \quad (4.23)$$

As we have no pole at $r = 0$, we set $s(0) = 0$ in the solution for $r \leq L$ and obtain $A = -B$. Since $s(r)$ given by the solution for $r > L$ has to be bounded for a large r , we necessarily have $c_1 = 0$. So, we obtain

$$s(r) = \begin{cases} A \left(e^{\sqrt{(\beta L^{-2} + \gamma)/Dr}} - e^{-\sqrt{(\beta L^{-2} + \gamma)/Dr}} \right) + \frac{\alpha L^{-3}}{\beta L^{-2} + \gamma} r, & \text{if } r \leq L, \\ C e^{-\sqrt{\gamma/Dr}}, & \text{if } r > L. \end{cases}$$

We substitute the constants A and C though $u(L) = u_0$ by avoiding any jump of the solutions on the boundary and we enforce the first derivatives of $s(r)$ at $r = L$ to be equal for the smoothness. Thus, the radially symmetric solution to the model given by the Equations (4.19) and (4.20) is

$$u(r) = \begin{cases} \left(u_0 - \frac{\alpha L^{-1}}{\gamma L^2 + \beta} \right) \frac{L}{\sinh\left(\sqrt{(\gamma L^2 + \beta)/D}\right)} \frac{\sinh\left(\sqrt{(\gamma L^2 + \beta)/D} \frac{r}{L}\right)}{r} + \frac{\alpha L^{-1}}{\gamma L^2 + \beta}, & \text{if } r \leq L, \\ u_0 L e^{\sqrt{\gamma/D} L} \frac{e^{-\sqrt{\gamma/D} r}}{r}, & \text{if } r > L, \end{cases} \quad (4.24)$$

where

$$u_0 = \frac{\alpha L^{-1}}{\gamma L^2 + \beta} \left(\frac{\sqrt{(\gamma L^2 + \beta)/D} \coth\left(\sqrt{(\gamma L^2 + \beta)/D}\right) - 1}{\sqrt{(\gamma L^2 + \beta)/D} \coth\left(\sqrt{(\gamma L^2 + \beta)/D}\right) + L\sqrt{\gamma/D}} \right).$$

Since the decay term γ suppresses the infinite AHL production within the cell, we take $\beta = 0$. Next, our goal is to seek an optimal approximate model for a single cell in \mathbb{R}^3 , which aims to minimize the error between the explicit solution of the real model given by the Equation (4.24) and the solution of the approximate model.

4.2.4 A suitable Approximate Model for a Single Cell in \mathbb{R}^3 with a Linear Source Term

As we expect a delta peak behavior from the source term while $L \rightarrow 0$, we describe an approximate model essentially similar to the rescaled model given by Equations (4.19)-(4.20)

$$-D\Delta v(x) + \gamma v(x) = M(L)\delta_0(x), \quad (4.25)$$

where $v(x)$ denotes the approximate concentration of AHL and δ_0 is the dirac delta distribution in radial coordinates, which makes a peak at the center of the cell, i.e., at $r = 0$. Here, $M(L)$ is the total amount of AHL production within the cell. So, the solution of the approximate model (4.25) yields

$$v(x) = \frac{M(L)}{4\pi D |x|} e^{-\sqrt{\gamma/D}|x|},$$

where $M(L)$ is given by

$$\begin{aligned} M(L) &= \int_{\mathbb{R}^3} \left(\frac{\alpha}{L^3} - \frac{\beta}{L^2} u(x) \right) \chi_{|x| \leq L} dx \\ &= \int_0^L \left(\frac{\alpha}{L^3} - \frac{\beta}{L^2} u(r) \right) 4\pi r^2 dr \\ &= \frac{4\pi\alpha}{3} - \frac{\beta}{L^2} \int_0^L u(r) 4\pi r^2 dr \\ &= \frac{4\pi\alpha}{3} - \frac{\beta}{L^2} D_L, \end{aligned} \quad (4.26)$$

where $D_L := \int_0^L u(r) 4\pi r^2 dr$ represents the total amount of AHL within the cell. We compute D_L using the exact solution of the single cell model given by the Equation (4.24)

$$\begin{aligned} D_L &= \int_0^L u(r) 4\pi r^2 dr \\ &= \int_0^L \left(\left(u_0 - \frac{\alpha L^{-1}}{\gamma L^2 + \beta} \right) \frac{L \sinh \left(\frac{\sqrt{(\gamma L^2 + \beta)/D} r}{L} \right)}{\sinh \left(\frac{\sqrt{(\gamma L^2 + \beta)/D}}{L} \right)} + \frac{\alpha L^{-1}}{\gamma L^2 + \beta} \right) 4\pi r^2 dr \\ &= \frac{4\pi}{3} \frac{\alpha L^{-1}}{\gamma L^2 + \beta} L^3 + \left(u_0 - \frac{\alpha L^{-1}}{\gamma L^2 + \beta} \right) \frac{4\pi L}{\sinh \left(\frac{\sqrt{(\gamma L^2 + \beta)/D}}{L} \right)} \end{aligned}$$

$$\begin{aligned}
 & \cdot \int_0^L \sinh\left(\sqrt{(\gamma L^2 + \beta)/D} \frac{r}{L}\right) r dr \\
 &= \frac{4\pi}{3} \frac{\alpha L^2}{\gamma L^2 + \beta} + \left(u_0 - \frac{\alpha L^{-1}}{\gamma L^2 + \beta}\right) 4\pi L \frac{DL^2}{\gamma L^2 + \beta} \\
 & \cdot \left(\sqrt{(\gamma L^2 + \beta)/D} \coth\left(\sqrt{(\gamma L^2 + \beta)/D}\right) - 1\right).
 \end{aligned}$$

Substituting D_L in Equation (4.26), we have

$$\begin{aligned}
 M(L) &= \frac{4\pi\alpha}{3} - \frac{\beta}{L^2} D_L \\
 &= \frac{4\pi\alpha}{3} \left(1 - \frac{\beta}{\gamma L^2 + \beta}\right) \\
 &+ \frac{4\pi D\alpha\beta}{(\gamma L^2 + \beta)^2} \frac{\left(1 + L\sqrt{\gamma/D}\right) \left(\left(\sqrt{(\gamma L^2 + \beta)/D}\right) \coth\left(\sqrt{(\gamma L^2 + \beta)/D}\right) - 1\right)}{\left(\sqrt{(\gamma L^2 + \beta)/D}\right) \coth\left(\sqrt{(\gamma L^2 + \beta)/D}\right) + L\sqrt{\gamma/D}}.
 \end{aligned}$$

Further, $\lim_{L \rightarrow 0} M(L)$ is a constant and equal to

$$M = \frac{4\pi\alpha}{\beta/D} \left(1 - \sqrt{D/\beta} \tanh(\sqrt{\beta/D})\right).$$

So far, we have established the explicit solution to the rescaled single cell model u and its possible approximation v . In the following we want to show that we have attained the optimal approximate model for the single cell case. Therefore, we define $w := u - v$ as a difference between original and approximate solutions. We will show that this difference is sufficiently small, i.e., it is possible to take the approximate model instead of the original one for small L . We substitute $u = w + v$ in Equation (4.19) and find

$$\begin{aligned}
 & -D\Delta(w(x) + v(x)) + \gamma(w(x) + v(x)) = \left(\frac{\alpha}{L^3} - \frac{\beta}{L^2}(w(x) + v(x))\right) \chi_{|x| \leq L} \\
 \Leftrightarrow & -D\Delta w(x) - D\Delta v(x) + \gamma w(x) + \gamma v(x) = \left(\frac{\alpha}{L^3} - \frac{\beta}{L^2}w(x) - \frac{\beta}{L^2}v(x)\right) \chi_{|x| \leq L} \\
 \Leftrightarrow & -D\Delta w(x) + \gamma w(x) + M(L)\delta_0(x) = -\frac{\beta}{L^2}w(x)\chi_{|x| \leq L} + \left(\frac{\alpha}{L^3} - \frac{\beta}{L^2}v(x)\right) \chi_{|x| \leq L} \\
 \Leftrightarrow & -D\Delta w(x) + \gamma w(x) + \frac{\beta}{L^2}w(x)\chi_{|x| \leq L} = \left(\frac{\alpha}{L^3} - \frac{\beta}{L^2}v(x)\right) \chi_{|x| \leq L} - M(L)\delta_0(x).
 \end{aligned}$$

Thereby, we achieved a PDE in the form $Aw(x) = f(x)$, where A is an elliptic operator and $f(x) = \left(\frac{\alpha}{L^3} - \frac{\beta}{L^2}v(x)\right) \chi_{|x| \leq L} - M(L)\delta_0(x)$. For this elliptic equation we are looking for a weak convergence of $w(x) \in H_0^1(\mathbb{R}^3)$, where $\phi(x)$ is a test function, i.e., $\phi(x) \in C_0^\infty(\mathbb{R}^3)$.

Thus we have

$$\begin{aligned} \int_{\mathbb{R}^3} w(x)\phi(x)dx &= \int_{\mathbb{R}^3} (u(x) - v(x))\phi(x)dx \\ &= \int_{|x|\leq L} (u(x) - v(x))\phi(x)dx + \int_{|x|>L} (u(x) - v(x))\phi(x)dx, \end{aligned}$$

and we aim to achieve $\lim_{L\rightarrow 0} w(x) = \mathcal{O}(L)$.

Let us estimate first $\int_{|x|\leq L} (u(x) - v(x))\phi(x)dx$ for small L ,

$$\begin{aligned} \int_{|x|\leq L} (u(x) - v(x))\phi(x)dx &= \int_{|x|\leq L} u(x)\phi(x)dx - \int_{|x|\leq L} v(x)\phi(x)dx \tag{4.27} \\ &= \int_{|x|\leq L} u(x)(\phi(0) + \mathcal{O}(|x|))dx - \int_{|x|\leq L} v(x)(\phi(0) + \mathcal{O}(|x|))dx \\ &= \int_{|x|\leq L} u(x)\phi(0)dx - \int_{|x|\leq L} v(x)\phi(0)dx \\ &\quad + \int_{|x|\leq L} u(x)\mathcal{O}(|x|)dx - \int_{|x|\leq L} v(x)\mathcal{O}(|x|)dx. \end{aligned}$$

Using the previous calculation given by (4.26) we have

$$\begin{aligned} \int_{|x|\leq L} u(x)\phi(0)dx &= \int_0^L u(r)4\pi r^2\phi(0)dr \\ &= D_L\phi(0) \\ &= L^2 \frac{4\pi\alpha}{3} - \frac{M}{\beta} \phi(0) \leq \mathcal{O}(L^2). \end{aligned}$$

Analogously, we obtain the error term while for a small L

$$\begin{aligned} \int_{|x|\leq L} v(x)\phi(0)dx &= \int_0^L v(r)\phi(0)4\pi r^2dr \\ &= \int_0^L \frac{M}{4\pi D r} e^{-\sqrt{\gamma/D}r} 4\pi r^2\phi(0)dr \\ &= \frac{M}{D}\phi(0) \int_0^L r \left(1 - \sqrt{\gamma/D}r + \mathcal{O}(r^2)\right) dr \\ &= \frac{M}{D} \frac{L^2}{2} (1 - 2\sqrt{\gamma/D}L + \mathcal{O}(L^2))\phi(0) \leq \mathcal{O}(L^2). \end{aligned}$$

On the other hand, we need to show that $\int_{|x| \leq L} u(x) \mathcal{O}(|x|) dx \rightarrow 0$ as $L \rightarrow 0$ and similarly, $\int_{|x| \leq L} v(x) \mathcal{O}(|x|) dx \rightarrow 0$ as $L \rightarrow 0$. Recall that

$$\left| \int_{|x| \leq L} u(x) \mathcal{O}(|x|) dx \right| \leq \int_{|x| \leq L} |u(x)| |\mathcal{O}(|x|)| dx$$

and we have $|\mathcal{O}(|x|)| \leq KL$ due to $|x| \leq L$, where K is a constant. Thus we obtain

$$\int_{|x| \leq L} u(x) \mathcal{O}(|x|) dx \leq KLO(L^2).$$

Correspondingly, we achieve $\int_{|x| \leq L} v(x) \mathcal{O}(|x|) dx \leq KLO(L^2)$.

Substituting these estimates in Equation (4.27) we find that

$$\int_{|x| \leq L} (u(x) - v(x)) \phi(x) dx \rightarrow 0, \quad (4.28)$$

as $L \rightarrow 0$.

Next, we deal with the weak convergence of the difference between the original and approximate solutions for $L > r$, i.e., $\int_{|x| > L} (u(x) - v(x)) \phi(x) dx$. Knowing that $w \in L^2(\mathbb{R}^3)$, we estimate

$$\begin{aligned} |u(x) - v(x)|^2 &= \left| u_0 \frac{L}{|x|} e^{-\sqrt{\gamma/D}(|x|-L)} - \frac{M}{|x|} e^{-\sqrt{\gamma/D}|x|} \right|^2 \\ &= \left(\frac{1}{|x|} e^{-\sqrt{\gamma/D}|x|} \left(u_0 L e^{\sqrt{\gamma/D}L} - M \right) \right)^2 \\ &= \left(\frac{1}{|x|} e^{-\sqrt{\gamma/D}|x|} \right)^2 L^2 e^{2\sqrt{\gamma/D}L} \left(u_0 - \frac{M}{L} e^{-\sqrt{\gamma/D}L} \right)^2 \\ &\leq C \left(\frac{1}{|x|} e^{-\sqrt{\gamma/D}|x|} \right)^2 L^2 \mathcal{O}(1) L^2 \\ &\leq C \left(\frac{1}{|x|} e^{-\sqrt{\gamma/D}|x|} \right)^2 L^4. \end{aligned}$$

We integrate both sides of the inequality over $|x| > L$,

$$\begin{aligned}
 \int_{|x|>L} |u(x) - v(x)|^2 dx &\leq \int_{|x|>L} C \left(\frac{1}{|x|} e^{-\sqrt{\gamma/D}|x|} \right)^2 L^4 dx \\
 &= CL^4 \frac{L}{L^2} \int_{|x|>L} e^{-2\sqrt{\gamma/D} \frac{|x|L}{L}} \frac{L^2}{|x|^2} \frac{dx}{L} \\
 &= CL^3 \int_1^\infty e^{-2\sqrt{\gamma/D}\theta L} \frac{1}{\theta^2} d\theta \\
 &\leq CL^3 \int_1^\infty e^{-2\sqrt{\gamma/D}\theta L} \frac{1}{\theta} d\theta \\
 &= CL^3 \int_L^\infty e^{-2\sqrt{\gamma/D}s} \frac{1}{s} ds \\
 &= CL^3 \left(\int_L^1 e^{-2\sqrt{\gamma/D}s} \frac{1}{s} ds + \int_1^\infty e^{-2\sqrt{\gamma/D}s} \frac{1}{s} ds \right) \\
 &= CL^3 \int_L^1 \frac{1 - 2\sqrt{\gamma/D}s + \mathcal{O}(s^2)}{s} ds \\
 &= CL^3 \left(-2\sqrt{\gamma/D} + \left(2\sqrt{\gamma/D}L - \ln L \right) + \mathcal{O}(L^2) \right) \\
 &\leq CL^3 (-\ln L).
 \end{aligned}$$

So, we find for $|x| > L$ the following estimation

$$\begin{aligned}
 \int_{|x|>L} |u(x) - v(x)| \phi(x) dx &\leq \|u(x) - v(x)\|_{L_2(|x|>L)} \|\phi(x)\|_{L_2(|x|>L)} \\
 &= \mathcal{O}\left(L^2 \sqrt{\ln(L)}\right),
 \end{aligned}$$

analogously we have

$$\int_{|x|>L} (u(x) - v(x)) \phi(x) dx \rightarrow 0, \tag{4.29}$$

as $L \rightarrow 0$.

The Equations (4.28)-(4.29) explain that the difference between the solutions of the original model and the approximate model for a single cell is sufficiently small and vanishes for $L \rightarrow 0$, so that we can utilize the approximate model instead of the original model.

4.3 A Population Model in \mathbb{R}^3 with a Linear Source Term and a suitable Approximate Model

In this section we generalize the model in Subsection 4.2.3 for a single cell to the case of the population model of N cells. For a first approach, we introduce a simple model which is reduced to a population consisting of two identical cells, centered at the positions x_1 and x_2 with radius L . In the following, we present this two cells model analogously to the scaled model given by the Equations (4.19) and (4.20),

$$-D\Delta u_1(x) + \gamma u_1(x) = (\alpha_1 L^{-3} - \beta_1 L^{-2} (u_1(x) + u_2(x))) \chi_{|x-x_1| \leq L}, \quad (4.30)$$

$$-D\Delta u_2(x) + \gamma u_2(x) = (\alpha_2 L^{-3} - \beta_2 L^{-2} (u_2(x) + u_1(x))) \chi_{|x-x_2| \leq L}, \quad (4.31)$$

where $u_1(x)$ and $u_2(x)$ denote the AHL concentrations of the corresponding cells, respectively. We consider that the new approximate model should be similar to the single cell model, which we examined in Subsection 4.2.3. Thus, we reformulate the model (4.19) with suitable choice of coefficients for two cells,

$$-D\Delta \tilde{u}_1(x) + \gamma \tilde{u}_1(x) = ((C_1 + LF_1) L^{-3} - B_1 L^{-2} (\tilde{u}_1(x))) \chi_{|x-x_1| \leq L}, \quad (4.32)$$

$$-D\Delta \tilde{u}_2(x) + \gamma \tilde{u}_2(x) = ((C_2 + LF_2) L^{-3} - B_2 L^{-2} (\tilde{u}_2(x))) \chi_{|x-x_2| \leq L}, \quad (4.33)$$

where $\tilde{u}_1(x)$ and $\tilde{u}_2(x)$ represent the approximate AHL concentrations to the corresponding cells, respectively. We expect to have an insight about the typical interactions considering the model from the side of the cell centered at x_1 . So, the related solution to the approximate model (4.32) reads

$$\tilde{u}_1(r) = \begin{cases} \left(\tilde{u}_0 - \frac{(C_1 + LF_1) L^{-1}}{\gamma L^2 + B_1} \right) \frac{L \sinh\left(\frac{\sqrt{(\gamma L^2 + B_1)/D} r}{L}\right)}{r \sinh\left(\frac{\sqrt{(\gamma L^2 + B_1)/D}}{L}\right)} + \frac{(C_1 + LF_1) L^{-1}}{\gamma L^2 + B_1}, & \text{if } r \leq L, \\ \tilde{u}_0 L e^{\sqrt{\gamma/D} L} \frac{e^{-\sqrt{\gamma/D} r}}{r}, & \text{if } r > L, \end{cases} \quad (4.34)$$

where \tilde{u}_0 is given by

$$\tilde{u}_0 = \frac{(C_1 + LF_1) L^{-1}}{\gamma L^2 + B_1} \left(\frac{\sqrt{(\gamma L^2 + B_1)/D} \coth\left(\frac{\sqrt{(\gamma L^2 + B_1)/D}}{L}\right) - 1}{\sqrt{(\gamma L^2 + B_1)/D} \coth\left(\frac{\sqrt{(\gamma L^2 + B_1)/D}}{L}\right) + L\sqrt{\gamma/D}} \right).$$

In order to find the suitable coefficients for the approximate solution, we define the difference between the original solution and approximate solution for two cells by $w_1 := u_1 - \tilde{u}_1$ and $w_2 := u_2 - \tilde{u}_2$. Then, we substitute $u_1 = w_1 + \tilde{u}_1$ and $u_2 = w_2 + \tilde{u}_2$ in the model given by Equation (4.30) and obtain

$$\begin{aligned} & -D\Delta (w_1(x) + \tilde{u}_1(x)) + \gamma (w_1(x) + \tilde{u}_1(x)) \\ & = (\alpha_1 L^{-3} - \beta_1 L^{-2} (w_1(x) + \tilde{u}_1(x) + w_2(x) + \tilde{u}_2(x))) \chi_{|x-x_1| \leq L}. \end{aligned}$$

So, we have the following elliptic PDE for the cell located at x_1

$$\begin{aligned} & -D\Delta w_1(x) + \gamma w_1(x) + \beta_1 L^{-2} (w_1(x) + w_2(x)) \\ & = (\alpha_1 L^{-3} - \beta_1 L^{-2} (\tilde{u}_1(x) + \tilde{u}_2(x))) \chi_{|x-x_1| < L} - ((C_1 + LF_1) L^{-3} - B_1 L^{-2} \tilde{u}_1(x)) \chi_{|x-x_1| \leq L}. \end{aligned} \quad (4.35)$$

Considering $Aw(x) = f_L(x)$ represents the Equation (4.35), where A is an elliptic operator, we define the associated bilinear form of the operator A by B and recall the Lax-Milgram Theorem 4.7 below:

Theorem 4.7 (Lax-Milgram Theorem)[4]

Let H be a Hilbert space and consider a bilinear functional $B : H \times H \rightarrow \mathbb{R}$. If there exist $C < \infty$ and $\alpha > 0$ such that

$$\begin{aligned} |B(w, v)| &\leq C \|w\| \|v\|, & \text{for all } (w, v) \in H \times H, \\ |B(w, w)| &\geq \alpha \|w\|^2, & \text{for all } w \in H, \end{aligned}$$

then for every $f \in H^{-1}$ (the dual space of H), the equation

$$B(w, v) = (f, v)_{H^{-1}, H^1}$$

has a unique solution

$$w \in H.$$

Remark 4.8 According to the Lax Milgram Theorem we have

$$\begin{aligned} \alpha \|w\|_{H^1}^2 &\leq B(w, w) = (f, w) \\ \Leftrightarrow \alpha \|w\|_{H^1}^2 &\leq \|f\|_{H^{-1}} \|w\|_{H^1}. \end{aligned}$$

So, we obtain for every $\alpha > 0$,

$$\alpha \|w\|_{H^1} \leq \|f\|_{H^{-1}}.$$

Therefore, we claim that a suitable estimation for $\|f\|_{H^{-1}}$ lead us to the conclusion

$$w = |u - v| \rightarrow 0$$

as $L \rightarrow 0$.

The following theorem shows that we can find a suitable estimation for $\|f\|_{H^{-1}}$ under special circumstances.

Theorem 4.9 Let $L > 0$ and $f_L(x) \in L^2(\mathbb{R}^3) \cap L^\infty(\mathbb{R}^3)$ such that there are constants $C_1, C_2 > 0$ and $\alpha \in (0, 1)$ with

1. $\text{supp}(f_L) \subseteq \{|x| < L\}$

$$2. \left| L^{-3} \int_{\mathbb{R}^3} f_L(x) dx \right| \leq C_1 L^{-1/2-\alpha}$$

$$3. \text{ess inf}_{x \in \mathbb{R}^3} |f_L(x)| \leq C_2 L^{-3/2-\alpha}$$

then

$$\|f_L\|_{H^{-1}} = O(L^{1-\alpha}).$$

Proof 4.10 We use the H^{-1} -norm of f_L , as defined by

$$\|f_L\|_{H^{-1}} = \sup_{\phi \in H^1, \|\phi\|_{H^1} \leq 1} |(f_L, \phi)|,$$

with the inner product (\cdot, \cdot) on \mathbb{R}^3 , [62]. Let us fix $\phi \in C^1 \cap H^1$ and assume that $\|\phi\|_{H^1} \leq 1$. For a fixed $y \in \mathbb{R}^3$, $|y| < L$, we find

$$\begin{aligned} |(f_L, \phi)| &= \left| \int_{\mathbb{R}^3} f_L(x) \phi(x) dx \right| \\ &= \left| \int_{|x| < L} f_L(\rho) (\phi(\rho) - \phi(y) + \phi(y)) d\rho \right| \\ &= \left| \int_{|x| < L} f_L(\rho) (\phi(\rho) - \phi(y)) d\rho + \int_{|x| < L} f_L(\rho) \phi(y) d\rho \right| \\ &= \left| \int_{|x| < L} f_L(\rho) (\phi(\rho) - \phi(y)) d\rho + \phi(y) \int_{|x| < L} f_L(\rho) d\rho \right| \\ &\leq \left| \int_{|x| < L} f_L(\rho) (\phi(\rho) - \phi(y)) d\rho \right| + \left| \phi(y) \int_{|x| < L} f_L(\rho) dx \right| \\ &\leq \|f_L\|_{\infty} \int_{|x| < L} |\phi(x\rho) - \phi(y)| d\rho + |\phi(y)| \left| \int_{|x| < L} f_L(\rho) d\rho \right| \\ &\leq C_2 L^{-3/2-\alpha} \int_{|x| < L} |\phi(\rho) - \phi(y)| d\rho + C_1 L^{5/2-\alpha} |\phi(y)|, \end{aligned}$$

according to the assumptions 1 and 2 of the Theorem 4.9.

Now we integrate both sides of the inequality with respect to τ over the region $\{|y| < L\}$ and divide

both sides by $4\pi L^3/3$. So, we have

$$\left| \int_{\mathbb{R}^3} f_L(x)\phi(x) dx \right| \leq C_3 \left(L^{-9/2-\alpha} \int_{|y|<L} \int_{|x|<L} |\phi(\rho) - \phi(\tau)| d\rho d\tau + L^{-1/2-\alpha} \int_{|y|<L} |\phi(\rho)| d\rho \right).$$

The second term on the right hand side of the inequality can be estimated by using the Hölder's inequality and the assumption $\|\phi\| \leq 1$ as follows:

$$\begin{aligned} L^{-1/2-\alpha} \int_{|y|<L} |\phi(\tau)| d\tau &= L^{-1/2-\alpha} \int_{|y|<L} |\phi(\tau)| 1 d\tau \\ &\leq L^{-1/2-\alpha} \left(\int_{|y|<L} |\phi(\tau)|^2 d\tau \right)^{1/2} \left(\int_{|y|<L} 1 d\tau \right)^{1/2} \\ &\leq C_4 L^{-1/2-\alpha} \|\phi\|_{L^2} L^{3/2} \\ &\leq C_4 \|\phi\|_{H^1} L^{1-\alpha} \\ &\leq C_4 L^{1-\alpha}. \end{aligned}$$

Then, we estimate the first term:

$$\begin{aligned} &L^{-9/2-\alpha} \int_{|y|<L} \int_{|x|<L} |\phi(\rho) - \phi(\tau)| d\rho d\tau \\ &= L^{-9/2-\alpha} \int_{|y|<L} \int_{|x|<L} \left| \int_0^1 \frac{d}{d\theta} \phi(\rho + \theta(\tau - \rho)) d\theta \right| d\rho d\tau \\ &\leq L^{-9/2-\alpha} \int_0^1 \int_{|y|<L} \int_{|x|<L} \left| \frac{d}{d\theta} \phi(\rho + \theta(\tau - \rho)) \right| d\rho d\tau d\theta \\ &= L^{-9/2-\alpha} \int_0^1 \int_{|y|<L} \int_{|x|<L} |\nabla_\theta \phi(\rho + \theta(\tau - \rho)) (\rho - \tau)| d\rho d\tau d\theta \\ &\leq L^{-9/2-\alpha} \int_0^1 \int_{|y|<L} \int_{|x|<L} |\nabla_\theta \phi(\rho + \theta(\tau - \rho))| |\rho - \tau| d\rho d\tau d\theta \\ &\leq 2L^{-7/2-\alpha} \int_0^1 \int_{|y|<L} \int_{|x|<L} |\nabla_\theta \phi(\rho + \theta(\tau - \rho))| d\rho d\tau d\theta \end{aligned}$$

$$\begin{aligned}
&\leq 2L^{-7/2-\alpha} \int_0^1 \int_{|y|<L} \left(\int_{|x|<L} |\nabla_\theta \phi(\rho + \theta(\tau - \rho))|^2 d\rho \right)^{1/2} \left(\int_{|x|<L} 1 d\rho \right)^{1/2} d\tau d\theta \\
&\leq CL^{-2-\alpha} \int_0^1 \int_{|y|<L} \left(\int_{\mathbb{R}^3} |\nabla_\theta \phi(\rho + \theta(\tau - \rho))|^2 d\rho \right)^{1/2} d\tau d\theta \\
&\leq CL^{-2-\alpha} \int_0^1 \int_{|y|<L} \left(\int_{\mathbb{R}^3} |\nabla_\theta \phi(\tilde{\rho})|^2 d\tilde{\rho} (1-\theta)^{-1} \right)^{1/2} d\tau d\theta \\
&\leq CL^{-2-\alpha} \|\phi\|_{H^1} \int_0^1 \int_{|y|<L} (1-\theta)^{-1/2} d\tau d\theta \\
&\leq CL^{1-\alpha} \|\phi\|_{H^1}.
\end{aligned}$$

According to the assumptions, $\phi \in C^1 \cap H^1$ and $\|\phi\|_{H^1} \leq 1$, we find

$$\sup_{\phi \in C^1 \cap H^1, \|\phi\|_{H^1} \leq 1} |(f_L, \phi)| \leq CL^{1-\alpha}.$$

As $C^1 \cap H^1$ is dense in H^1 , this inequality carries over to all $\phi \in H^1$, $\|\phi\|_{H^1} \leq 1$ and thereby we achieve

$$\|f_L\|_{H^{-1}} = O(L^{1-\alpha}).$$

□

Corollary 4.11 *If we choose $\alpha = 1/2$ in Theorem 4.9, we find in particular that*

1. $\text{supp}(f_L) \subseteq \{|x| < L\}$
2. $|L^{-3} \int_{\mathbb{R}^3} f_L(x) dx| \leq C_1 L^{-1}$
3. $\text{ess inf}_{x \in \mathbb{R}^3} |f_L(x)| \leq C_2 L^{-2}$

which imply

$$\|f_L\|_{H^{-1}} = O(\sqrt{L}).$$

Thanks to the Corollary 4.11 we will achieve the estimation $\|f_L\|_{H^{-1}} = O(\sqrt{L})$ to our case, where we defined

$$f_L(x) = ((\alpha_1 - C_1 - L F_1) L^{-3} - (\beta_1 - B_1) \tilde{u}_1(x) L^{-2} - \beta_1 \tilde{u}_2(x) L^{-2}) \chi_{|x-x_1|<L}.$$

In the following we show that f_L fulfills the assumptions in Corollary 4.11:

4 Spatial Structure of Cells and their Effect on the AHL Concentration

1. $f_L(x)$ is defined with the characteristic function $\chi_{|x-x_1|<L}$, which enforce $f_L(x)$ to have its support in the same domain, i.e.,

$$\text{supp}(f_L(x)) \subset \{|x - x_1| < L\}.$$

2. Let us estimate the error of the integral $\int_{\mathbb{R}^3} f_L(x) dx$ below:

$$\begin{aligned} \int_{\mathbb{R}^3} f_L(x) dx &= \int_0^L ((\alpha_1 - C_1 - L F_1) L^{-3} - (\beta_1 - B_1) \tilde{u}_1(r) L^{-2} - \beta_1 \tilde{u}_2(r) L^{-2}) 4\pi r^2 dr \\ &= (\alpha_1 - C_1 - L F_1) L^{-3} \frac{4\pi L^3}{3} - (\beta_1 - B_1) L^{-2} \int_0^L \tilde{u}_1(r) 4\pi r^2 dr \\ &\quad - \beta_1 L^{-2} \int_0^L \tilde{u}_2(r) 4\pi r^2 dr \\ &= (\alpha_1 - C_1 - L F_1) \frac{4\pi}{3} - (\beta_1 - B_1) L^{-2} I_1(L) - \beta_1 L^{-2} I_2(L), \end{aligned}$$

where $I_1(L) := \int_0^L \tilde{u}_1(r) 4\pi r^2 dr$ and $I_2(L) := \int_0^L \tilde{u}_2(r) 4\pi r^2 dr$. Here, we evaluate the integrals, $I_1(L)$ and $I_2(L)$ using the explicit solutions of the approximate model given by the Equation (4.34), respectively.

$$\begin{aligned} I_1(L) &= 4\pi \int_0^L \left(\left(\tilde{u}_0 - \frac{(C_1 + L F_1) L^{-1}}{\gamma L^2 + B_1} \right) \left(\frac{L \sinh \left(\frac{\sqrt{(\gamma L^2 + B_1) D} r}{L} \right)}{r \sinh \left(\frac{\sqrt{(\gamma L^2 + B_1) D}}{D} \right)} \right) \right. \\ &\quad \left. + \frac{(C_1 + L F_1) L^{-1}}{\gamma L^2 + B_1} \right) r^2 dr \\ &= 4\pi \left(\tilde{u}_0 - \frac{(C_1 + L F_1) L^{-1}}{\gamma L^2 + B_1} \right) \frac{L}{\sinh \left(\frac{\sqrt{(\gamma L^2 + B_1) D}}{D} \right)} \\ &\quad \cdot \int_0^L \frac{\sinh \left(\frac{\sqrt{(\gamma L^2 + B_1) D} r}{L} \right)}{r} r^2 dr + 4\pi \frac{(C_1 + L F_1) L^{-1} L^3}{\gamma L^2 + B_1} \frac{1}{3} \\ &= 4\pi \left(\tilde{u}_0 - \frac{(C_1 + L F_1) L^{-1}}{\gamma L^2 + B_1} \right) \frac{L}{\sinh \left(\frac{\sqrt{(\gamma L^2 + B_1) D}}{D} \right)} \frac{L^2 D}{\gamma L^2 + B_1} \\ &\quad \cdot \int_0^{\frac{\sqrt{\gamma L^2 + B_1}}{D}} \sinh(r) r dr + \frac{4\pi (C_1 + L F_1) L^2}{3 \gamma L^2 + B_1} \end{aligned}$$

$$\begin{aligned}
&= \frac{4\pi L^3 D}{\gamma L^2 + B_1} \frac{(C_1 + LF_1) L^{-1}}{\gamma L^2 + B_1} \\
&\quad \cdot \left(\frac{\sqrt{(\gamma L^2 + B_1)/D} \coth\left(\sqrt{(\gamma L^2 + B_1)/D}\right) - 1}{\sqrt{(\gamma L^2 + B_1)/D} \coth\left(\sqrt{(\gamma L^2 + B_1)/D}\right) - L\sqrt{\gamma/D}} - 1 \right) \\
&\quad \cdot \left(\sqrt{(\gamma L^2 + B_1)/D} \coth\left(\sqrt{(\gamma L^2 + B_1)/D}\right) - 1 \right) + \frac{4\pi}{3} \frac{(C_1 + LF_1) L^2}{\gamma L^2 + B_1} \\
&= -4\pi \frac{(C_1 + LF_1) DL^2}{(\gamma L^2 + B_1)^2} \left(1 + L\sqrt{\gamma/D} \right) \\
&\quad \cdot \frac{\sqrt{(\gamma L^2 + B_1)/D} \coth\left(\sqrt{(\gamma L^2 + B_1)/D}\right) - 1}{\sqrt{(\gamma L^2 + B_1)/D} \coth\left(\sqrt{(\gamma L^2 + B_1)/D}\right) + L\sqrt{\gamma/D}} + \frac{4\pi}{3} \frac{(C_1 + LF_1) L^2}{\gamma L^2 + B_1},
\end{aligned}$$

and then,

$$\begin{aligned}
I_2(L) &= \frac{4\pi L^3}{3} \tilde{u}_2(x_1) + \mathcal{O}(L^4) \\
&= \frac{4\pi L^3}{3} \tilde{u}_0(x) \frac{L}{|x_1 - x_2|} e^{-\sqrt{\gamma/D}(|x_1 - x_2| - L)} \\
&= \frac{4\pi L^3}{3} \frac{(C_2 + LF_2) L^{-1}}{\gamma L^2 + B_2} \left(\frac{\sqrt{(\gamma L^2 + B_2)/D} \coth\left(\sqrt{(\gamma L^2 + B_2)/D}\right) - 1}{\sqrt{(\gamma L^2 + B_2)/D} \coth\left(\sqrt{(\gamma L^2 + B_2)/D}\right) + L\sqrt{\gamma/D}} \right) \\
&\quad \cdot \frac{L}{|x_1 - x_2|} e^{-\sqrt{\gamma/D}(|x_1 - x_2| - L)} \\
&= \frac{4\pi}{3} \frac{(C_2 + LF_2) L^2}{\gamma L^2 + B_2} \left(\frac{\sqrt{(\gamma L^2 + B_2)/D} \coth\left(\sqrt{(\gamma L^2 + B_2)/D}\right) - 1}{\sqrt{(\gamma L^2 + B_2)/D} \coth\left(\sqrt{(\gamma L^2 + B_2)/D}\right) + L\sqrt{\gamma/D}} \right) \\
&\quad \cdot \frac{L}{|x_1 - x_2|} e^{-\sqrt{\gamma/D}(|x_1 - x_2| - L)}.
\end{aligned}$$

As a result, the boundedness of $\left(\frac{\sqrt{(\gamma L^2 + B_2)/D} \coth\left(\sqrt{(\gamma L^2 + B_2)/D}\right) - 1}{\sqrt{(\gamma L^2 + B_2)/D} \coth\left(\sqrt{(\gamma L^2 + B_2)/D}\right) + L\sqrt{\gamma/D}} \right)$ as $L \rightarrow 0$ leads the error estimations $I_1(L) < \mathcal{O}(L^2)$ and $I_2(L) < \mathcal{O}(L^3)$. Choosing $\beta_1 = B_1$ and analogously $\beta_2 = B_2$, we have

$$\left| \int_{\mathbb{R}^3} f_L(x) dx \right| = (\alpha_1 - C_1 - LF_1) \frac{4\pi}{3} - \beta_1 L^{-2} I_2(L).$$

Further, we take $\alpha_1 = C_1$ and then we find

$$\left| \int_{\mathbb{R}^3} f_L(x) dx \right| = LF_1 \frac{4\pi}{3} + \beta_1 L^{-2} I_2(L).$$

Thus, $F_1 = -\frac{3}{4\pi}\beta_1 L^{-2}I_2(L)$ appears and the second assumption of the Theorem 4.9 is satisfied, i.e.,

$$\left| \int_{\mathbb{R}^3} f_L(x) dx \right| \leq CL^2.$$

3. Here we estimate the error term for $\text{ess inf}_{x \in \mathbb{R}^3} |f_L(x)|$ according to the chosen constants. We have

$$\begin{aligned} f_L(x) &= F_1 L^{-2} \\ &- \beta_1 \frac{(C_2 + F_2 L) L^{-3}}{\gamma L^2 + B_2} \left(\frac{\sqrt{(\gamma L^2 + B_2)/D} \coth\left(\sqrt{(\gamma L^2 + B_2)/D}\right) - 1}{\sqrt{(\gamma L^2 + B_2)/D} \coth\left(\sqrt{(\gamma L^2 + B_2)/D}\right) + L\sqrt{\gamma/D}} \right) \\ &\cdot \frac{L}{r} e^{-\sqrt{\gamma/D}(r-L)}. \end{aligned}$$

$\left(\frac{\sqrt{(\gamma L^2 + B_2)/D} \coth\left(\sqrt{(\gamma L^2 + B_2)/D}\right) - 1}{\sqrt{(\gamma L^2 + B_2)/D} \coth\left(\sqrt{(\gamma L^2 + B_2)/D}\right) + L\sqrt{\gamma/D}} \right)$ is bounded for $L \rightarrow 0$ and so we obtain

$$\begin{aligned} |f_L(x)| &\leq F_1 L^{-2} + \beta_1 \frac{(C_2 + F_2 L) L^{-2}}{\gamma L^2 + B_2} \\ &\cdot \frac{1}{r} e^{-\sqrt{\gamma/D}r} \left(1 + L\sqrt{\gamma/D} + \mathcal{O}(L^2) \right). \end{aligned}$$

Eventually, we have

$$\text{ess inf}_{x \in \mathbb{R}^3} |f_L(x)| < \mathcal{O}(L^2),$$

which fulfills the third hypothesis of the Theorem 4.9.

Since the three assumptions of the Theorem 4.9 are fulfilled, we conclude

$$\|f_L\|_{H^{-1}} = \mathcal{O}(\sqrt{L}),$$

as in Remark 4.11. Moreover, according to Remark 4.8 we acquire

$$\|w\| \leq \mathcal{O}(\sqrt{L}).$$

So, we have determined that the difference between approximate and original solutions tends to zero when $L \rightarrow 0$, i.e., we have found a suitable approximate solution to our model. If we extend the idea of the two cells model to a population model with N cells we obtain the following model and its corresponding approximation:

$$\begin{aligned} -D\Delta u_i(x) + \gamma u_i(x) &= \left(\alpha_i L^{-3} - \beta_i L^{-3} \left(\sum_{\substack{j=1 \\ j \neq i}}^N u_j(x) \right) \right) \chi_{|x-x_i| \leq L}, \\ -D\Delta \tilde{u}_i(x) + \gamma \tilde{u}_i(x) &= ((\alpha_i + LF_i) L^{-3} - \beta_i L^{-3} \tilde{u}_i(x)) \chi_{|x-x_i| \leq L}, \end{aligned}$$

where $F_i = -\beta_i \frac{4\pi}{3} \frac{\alpha_j}{\beta_j} \left(\frac{\sqrt{\beta_j/D} \coth(\sqrt{\beta_j/D}) - 1}{\sqrt{\beta_j/D} \coth(\sqrt{\beta_j/D})} \right) \frac{e^{-(\sqrt{\gamma/D}|x_i-x_j|)}}{|x_i-x_j|}$. The approximate solution to the model reads analogously to the case with two cells:

$$\tilde{u}_i(r) = \begin{cases} \left(\tilde{u}_{i0} - \frac{(\alpha_i + LF_i)L^{-1}}{\gamma L^2 + \beta_i} \right) \left(\frac{L \sinh(\sqrt{(\gamma L^2 + \beta_i)/D} \frac{r}{L})}{r \sinh(\sqrt{(\gamma L^2 + \beta_i)/D})} \right) + \frac{(\alpha_i + LF_i)L^{-1}}{\gamma L^2 + \beta_i}, & r \leq L, \\ \tilde{u}_{i0} \frac{L}{r} e^{-\sqrt{\gamma/D}(r-L)}, & r > L, \end{cases} \quad (4.36)$$

where \tilde{u}_{i0} is given by

$$\tilde{u}_{i0} = \frac{(\alpha_i + LF_i)L^{-1}}{\gamma L^2 + \beta_i} \left(\frac{\sqrt{(\gamma L^2 + \beta_i)/D} \coth(\sqrt{(\gamma L^2 + \beta_i)/D}) - 1}{\sqrt{(\gamma L^2 + \beta_i)/D} \coth(\sqrt{(\gamma L^2 + \beta_i)/D}) + L\sqrt{\gamma/D}} \right).$$

4.4 A Single Cell Model in \mathbb{R}^3 with a Lipschitz Continuous Source Term

In this section we generalize the model which includes a linear source term given by Equations (4.19)-(4.20) into a model with a non-linear source term (see Equations (4.38)-(4.39)). In Table 4.3 the parameters which we need during the Sections 4.4 and 4.5 can be found.

Table 4.3: Parameters used for the models with a Lipschitz continuous source term in Sections 4.4 and 4.5.

Parameter	Description
D	Constant diffusion rate of AHL
a	Constitutive AHL production rate within the cell
b	(Positive) feed-back correlated AHL production rate within the cell
α	Scaled AHL production rate
β	Scaled (positive) feed-back correlated AHL production rate within the cell
γ	Abiotic AHL degradation rate in whole domain
A_{thresh}	(Scaled) threshold of AHL concentration for the start of positive feed-back within the cell

We aim that this new model satisfies the essential biological expectations, therefore we describe the source term with a simple Hill function,

$$f(\bar{u}_L) = a + b \frac{\bar{u}_L}{A_{thresh} + \bar{u}_L},$$

which fits to the transcriptional regulation in the QS system, [45]. This non-linear source term characterizes the finite production of AHL via a positive feedback loop, where a represents the constitutive production rate and b corresponds to the production parameter due to the positive feedback loop. A_{thresh} determines the activation threshold of a cell. As the cells are tiny organisms, we take the mean value of AHL concentration in the cell \bar{u}_L instead of the position dependent (spatially described) AHL concentration $u(x)$. Assuming that the single cell is located at $x = 0$ we define the mean value of AHL concentration by

$$u_L := \frac{1}{\frac{4\pi}{3}L^3} \int_{|x|<L} u(x)dx. \quad (4.37)$$

Thus, we present the following model with a non-linear source term for a single cell centered at $x = 0$:

$$-D\Delta u(x) + \gamma u(x) = \left(a + b \frac{\bar{u}_L}{A_{thresh} + \bar{u}_L} \right), \quad |x| \leq L, \quad (4.38)$$

$$-D\Delta u(x) + \gamma u(x) = 0, \quad |x| > L. \quad (4.39)$$

The mathematical structure of this model is exactly the same as we have already discussed for the previous model (4.19)-(4.20), when we suppose that the scaled value of b , i.e., $\beta = 0$. The Lipschitz continuity of the source term guarantees the existence of solutions to the Equations (4.38)-(4.39), [14]. Thereby, we obtained the radially symmetric solutions to the model assuming to have a constant \bar{u}_L

$$u(r) = \begin{cases} \left(u_0 - \frac{1}{\gamma} \left(a + b \frac{\bar{u}_L}{A_{thresh} + \bar{u}_L} \right) \right) \frac{L \sinh(\sqrt{\gamma/D}r)}{r \sinh(\sqrt{\gamma/D}L)} + \frac{1}{\gamma} \left(a + b \frac{\bar{u}_L}{A_{thresh} + \bar{u}_L} \right), & r \leq L, \\ u_0 L e^{\sqrt{\gamma/D}L} \frac{e^{-\sqrt{\gamma/D}r}}{L}, & r > L, \end{cases}$$

where

$$u_0 = \frac{1}{\gamma} \left(a + b \frac{\bar{u}_L}{A_{thresh} + \bar{u}_L} \right) \left(\frac{L \sqrt{\gamma/D} \coth(\sqrt{\gamma/D}L) - 1}{L \sqrt{\gamma/D} \coth(\sqrt{\gamma/D}L) + L \sqrt{\gamma/D}} \right).$$

Using the solution $u(r)$, we can compute a new \bar{u}_L given by Equation 4.37. Thus, we are looking for a fixed point \bar{u}_L . For a small cell radius L , we can apply contraction principle and thereby, we have such a fixed point \bar{u}_L . So, we can use it for the radially symmetric solution $U(r)$. The biological assumption $0 < \sqrt{\gamma/D} < 1$ is sufficient to preserve the positivity of solutions.

4.4.1 Suitable Scaling for the Single Cell Model with a Nonlinear Source Term

We seek the appropriate scaling for the parameters a, b, A_{thresh} and further, for the mean value of AHL concentration \bar{u}_L , which is supposed in this context to be a parameter. Taking

into account the boundedness of the Hill function, i.e.,

$$0 \leq \frac{\bar{u}_L}{A_{thresh} + \bar{u}_L} \leq 1,$$

we assume that it has no effect on the scaling of the parameters a and b . Let us evaluate the total production of AHL within the cell:

$$\int_0^L \left(a + b \frac{\bar{u}_L}{A_{thresh} + \bar{u}_L} \right) 4\pi r^2 dr = \left(a + b \frac{\bar{u}_L}{A_{thresh} + \bar{u}_L} \right) \frac{4\pi}{3} L^3.$$

Thus, suitable scaling for a and b yields $a = \alpha L^{-3}$ and $b = \beta L^{-3}$. Further, we scale the mean value of AHL concentration \bar{u}_L appropriately,

$$\begin{aligned} & \frac{1}{\frac{4\pi}{3} L^3} \int_0^L u(r) 4\pi r^2 dr & (4.40) \\ &= 3 L^{-3} \left(u_0 - \frac{1}{\gamma} \left(a + b \frac{\bar{u}_L}{A_{thresh} + \bar{u}_L} \right) \right) \left(\frac{L}{\sinh(\sqrt{\gamma/D} L)} \right) \\ & \quad \cdot \int_0^L \sinh(\sqrt{\gamma/D} r) r dr + \frac{1}{\gamma} \left(a + b \frac{\bar{u}_L}{A_{thresh} + \bar{u}_L} \right) \\ &= 3 L^{-3} \frac{1}{\gamma} \left(a + b \frac{\bar{u}_L}{A_{thresh} + \bar{u}_L} \right) \left(\frac{1 + \sqrt{\gamma/D} L}{\sqrt{\gamma/D} L \coth(\sqrt{\gamma/D} L) + \sqrt{\gamma/D} L} \right) \\ & \quad \cdot \frac{L}{\sinh \sqrt{\gamma/D} L} \left(\frac{\sqrt{\gamma/D}}{3} L^3 + \frac{(\sqrt{\gamma/D})^3}{5 \cdot 3!} L^5 + \mathcal{O}(L^7) \right) + \frac{1}{\gamma} \left(a + b \frac{\bar{u}_L}{A_{thresh} + \bar{u}_L} \right) \\ &= 3 L^{-3} \frac{1}{\gamma} \left(a + b \frac{\bar{u}_L}{A_{thresh} + \bar{u}_L} \right) \left(\frac{1 + \sqrt{\gamma/D} L}{\sqrt{\gamma/D} (\cosh(\sqrt{\gamma/D} L) + \sinh(\sqrt{\gamma/D} L))} \right) \\ & \quad \cdot \frac{\sqrt{\gamma/D}}{3} L^3 \left(1 + \frac{3\gamma/D}{5 \cdot 3!} L^2 + \mathcal{O}(L^4) \right) + \frac{1}{\gamma} \left(a + b \frac{\bar{u}_L}{A_{thresh} + \bar{u}_L} \right) \\ &= -\frac{1}{\gamma} \left(a + b \frac{\bar{u}_L}{A_{thresh} + \bar{u}_L} \right) \left(1 + \sqrt{\gamma/D} L \right) e^{-\sqrt{\gamma/D} L} \left(1 + \frac{\gamma/D}{10} L^2 + \mathcal{O}(L^4) \right) \\ & \quad + \frac{1}{\gamma} \left(a + b \frac{\bar{u}_L}{A_{thresh} + \bar{u}_L} \right) \end{aligned}$$

$$\begin{aligned}
 &= \frac{1}{\gamma} \left(a + b \frac{\bar{u}_L}{A_{thresh} + \bar{u}_L} \right) \\
 &\quad \cdot \left(1 - \left(1 + \sqrt{\gamma/D} L \right) \left(1 - \sqrt{\gamma/D} L + \frac{\gamma}{D} \frac{L^2}{2!} - \left(\sqrt{\gamma/D} \right)^3 \frac{L^3}{3!} + \mathcal{O}(L^4) \right) \right. \\
 &\quad \left. \cdot \left(1 + \frac{\gamma/D}{10} L^2 + \mathcal{O}(L^4) \right) \right) \\
 &= \frac{1}{\gamma} \left(a + b \frac{\bar{u}_L}{A_{thresh} + \bar{u}_L} \right) \\
 &\quad \cdot \left(1 - \left(1 + \sqrt{\gamma/D} L \right) \left(1 - \sqrt{\gamma/D} L + \frac{6\gamma/D}{10} L^2 - \frac{8 \left(\sqrt{\gamma/D} \right)^3}{30} L^3 + \mathcal{O}(L^4) \right) \right) \\
 &= \frac{1}{\gamma} \left(a + b \frac{\bar{u}_L}{A_{thresh} + \bar{u}_L} \right) \left(1 - \left(1 - \frac{2\gamma/D}{5} L^2 + \frac{(\gamma/D)^{1/3}}{3} L^3 + \mathcal{O}(L^4) \right) \right) \\
 &= \frac{1}{\gamma} \left(a + b \frac{\bar{u}_L}{A_{thresh} + \bar{u}_L} \right) \left(\frac{2\gamma/D}{5} L^2 - \frac{(\gamma/D)^{1/3}}{3} L^3 + \mathcal{O}(L^4) \right).
 \end{aligned}$$

Substituting the appropriate scaling for $a = \alpha L^{-3}$ and $b = \beta L^{-3}$ enforces to scale \bar{u}_L by L . For simplicity, we do not change the notation for scaled $\bar{u}_L L$. Thus, the scaled model for a single cell located at $x = 0$ reads

$$-D\Delta u(x) + \gamma u(x) = L^{-3} \left(\alpha + \beta \frac{L \bar{u}_L}{A_{thresh} + L \bar{u}_L} \right), \quad |x| \leq L, \quad (4.41)$$

$$-D\Delta u(x) + \gamma u(x) = 0, \quad |x| > L. \quad (4.42)$$

Moreover, the radially symmetric solution to the scaled model is

$$u(r) = \begin{cases} \left(u_0 - \frac{1}{\gamma} L^{-3} \left(\alpha + \beta \frac{L \bar{u}_L}{A_{thresh} + L \bar{u}_L} \right) \right) \frac{L \sinh(\sqrt{\gamma/D} r)}{r \sinh(\sqrt{\gamma/D} L)} \\ \quad + \frac{1}{\gamma} L^{-3} \left(\alpha + \beta \frac{L \bar{u}_L}{A_{thresh} + L \bar{u}_L} \right), & r \leq L, \\ u_0 L e^{\sqrt{\gamma/D} L} \frac{e^{-\sqrt{\gamma/D} r}}{r}, & r > L, \end{cases} \quad (4.43)$$

where

$$u_0 = \frac{1}{\gamma} L^{-3} \left(\alpha + \beta \frac{L \bar{u}_L}{A_{thresh} + L \bar{u}_L} \right) \left(\frac{L \sqrt{\gamma/D} \coth(\sqrt{\gamma/D} L) - 1}{L \sqrt{\gamma/D} \coth(\sqrt{\gamma/D} L) + L \sqrt{\gamma/D}} \right).$$

4.4.2 A Suitable Approximate Model for a Single Cell with a Lipschitz Continuous Source Term

The approximate equation for the AHL concentration reads

$$-D\Delta v(x) + \gamma v(x) = L^{-3}M\chi_{|x|\leq L}$$

where we are interested in the appropriate M . The explicit solution to the approximate model is calculated as the solution of the original model Equation (4.43),

$$v(r) = \begin{cases} \left(v_0 - \frac{1}{\gamma}L^{-3}M\right) \frac{L \sinh(\sqrt{\gamma/D}r)}{r \sinh(\sqrt{\gamma/D}L)} + \frac{1}{\gamma}L^{-3}M, & r \leq L, \\ v_0 L e^{\sqrt{\gamma/D}L} \frac{e^{-\sqrt{\gamma/D}r}}{r}, & r > L, \end{cases} \quad (4.44)$$

where

$$v_0 = \frac{1}{\gamma}L^{-3}M \left(\frac{L \sqrt{\gamma/D} \coth(\sqrt{\gamma/D}L) - 1}{L \sqrt{\gamma/D} \coth(\sqrt{\gamma/D}L) + L \sqrt{\gamma/D}} \right).$$

Analogously to the original model we define the mean value of the approximate AHL concentration by $\bar{v}_L = \frac{1}{\frac{4\pi}{3}L^3} \int_{\mathbb{R}^3} v(x)dx$. Further, we scale it by L , which enables to have a first order error term of L through Taylor expansion, i.e., according to the calculation in Equation (4.40), we have

$$\begin{aligned} L\bar{v}_L &= \frac{L}{\frac{4\pi}{3}L^3} \int_{\mathbb{R}^3} v(x)dx \\ &= 3L^{-2} \int_0^L v(r)r^2 dr \\ &= 3L^{-2} \int_0^L \left(\left(v_0 - \frac{1}{\gamma}L^{-3}M\right) \frac{L \sinh(\sqrt{\gamma/D}r)}{r \sinh(\sqrt{\gamma/D}L)} + \frac{1}{\gamma}L^{-3}M \right) r^2 dr \\ &= \frac{M}{\gamma}L^{-2} \left(\frac{2\gamma/D}{5}L^2 - \frac{(\gamma/D)^{1/3}}{3}L^3 + \mathcal{O}(L^4) \right) \\ &= M(\mu_1 + \mu_2L + \mathcal{O}(L^2)), \end{aligned} \quad (4.45)$$

where the coefficients are $\mu_1 = \frac{2}{5D}$ and $\mu_2 = -\frac{1}{3\gamma^{2/3}D^{1/3}}$.

Let us define a difference function between original and approximate solutions $w := u - v$ and its correspondent mean values $\bar{w}_L := \bar{u}_L - \bar{v}_L$. Substituting $u = w + v$ and $\bar{u}_L := \bar{w}_L + \bar{v}_L$ in the Equation (4.41) we obtain

$$-D\Delta w(x) + \gamma w(x) = \left(L^{-3} \left(\alpha + \beta \frac{L(\bar{w}_L + \bar{v}_L)}{A_{thresh} + L(\bar{w}_L + \bar{v}_L)} \right) - L^{-3}M \right) \chi_{|x|\leq L}. \quad (4.46)$$

Integrating Equation (4.46) over \mathbb{R}^3 we achieve

$$\begin{aligned} \int_{\mathbb{R}^3} (-D\Delta w(x) + \gamma w(x)) dx &= \int_0^L \left(L^{-3} \left(\alpha + \beta \frac{L(\bar{w}_L + \bar{v}_L)}{A_{thresh} + L(\bar{w}_L + \bar{v}_L)} \right) - L^{-3}M \right) 4\pi r^2 dr \\ &= \frac{4\pi}{3} \left(\alpha + \beta \frac{L(\bar{w}_L + \bar{v}_L)}{A_{thresh} + L(\bar{w}_L + \bar{v}_L)} - M \right). \end{aligned}$$

Choosing $\bar{w}_L = 0$, we gain $\|w(x)\|_{L^2} \rightarrow 0$ while $L \rightarrow 0$ where $M = \alpha + \beta \frac{M(\mu_1 + \mu_2 L + \mathcal{O}(L^2))}{A_{thresh} + M(\mu_1 + \mu_2 L + \mathcal{O}(L^2))}$ accordingly to the Equation (4.45). To be precise, we claim that there exists an approximate \tilde{M} which satisfies

$$|M - \tilde{M}| < \mathcal{O}(L).$$

In the following, we show that $\tilde{M} = \alpha + \beta \frac{\tilde{M}(\mu_1 + \mu_2 L)}{A_{thresh} + \tilde{M}(\mu_1 + \mu_2 L)}$ is a suitable approximation for M :

$$\begin{aligned} |M - \tilde{M}| &= \left| \alpha + \beta \frac{M(\mu_1 + \mu_2 L + \mathcal{O}(L^2))}{A_{thresh} + M(\mu_1 + \mu_2 L + \mathcal{O}(L^2))} - \alpha - \beta \frac{\tilde{M}(\mu_1 + \mu_2 L)}{A_{thresh} + \tilde{M}(\mu_1 + \mu_2 L)} \right| \\ &= \left| \beta \left(\frac{M(\mu_1 + \mu_2 L + \mathcal{O}(L^2))}{A_{thresh} + M(\mu_1 + \mu_2 L + \mathcal{O}(L^2))} - \frac{\tilde{M}(\mu_1 + \mu_2 L)}{A_{thresh} + \tilde{M}(\mu_1 + \mu_2 L)} \right) \right| \\ &= \left| \beta \frac{A_{thresh}(\mu_1 M + \mu_2 ML + \mathcal{O}(L^2)) - A_{thresh}(\mu_1 \tilde{M} + \mu_2 \tilde{M}L)}{(A_{thresh} + M(\mu_1 + \mu_2 L + \mathcal{O}(L^2)))(A_{thresh} + \tilde{M}(\mu_1 + \mu_2 L))} \right| \\ &\leq \left| \beta \frac{A_{thresh}(\mu_1 M + \mu_2 ML + \mathcal{O}(L^2)) - A_{thresh}(\mu_1 \tilde{M} + \mu_2 \tilde{M}L)}{A_{thresh}^2} \right| \\ &= \left| \beta \frac{\mu_1(M - \tilde{M}) + \mu_2(M - \tilde{M})L + \mathcal{O}(L^2)}{A_{thresh}} \right| \\ &\leq \beta \frac{|\mu_1| |M - \tilde{M}| + |\mu_2| |M - \tilde{M}| L + \mathcal{O}(L^2)}{A_{thresh}}. \end{aligned}$$

Consequently, we find

$$|M - \tilde{M}| - \frac{\beta |\mu_2|}{A_{thresh} - \beta |\mu_1|} |M - \tilde{M}| L + \mathcal{O}(L^2) \leq 0,$$

for $(A_{thresh} - \beta |\mu_1|) > 0$, i.e., we achieve the desired estimate

$$|M - \tilde{M}| \leq \mathcal{O}(L).$$

Thereby, we have seen that $\tilde{M} = \alpha + \beta \frac{\tilde{M}(\mu_1 + \mu_2 L)}{A_{thresh} + \tilde{M}(\mu_1 + \mu_2 L)}$ is a suitable approximation for M and we can replace M by \tilde{M} in the approximative solution (4.44). Let us determine the

explicit value of \widetilde{M}

$$\widetilde{M} = \frac{-d \pm \sqrt{d^2 + 4\alpha A_{thresh} (\mu_1 + \mu_2 L)}}{2(\mu_1 + \mu_2 L)}, \quad (4.47)$$

where $d = (A_{thresh} - \alpha(\mu_1 + \mu_2 L) - \beta(\mu_1 + \mu_2 L))$.

4.4.3 Numerical Simulations for a Single Cell

All parameters we need for the simulations in Chapter 4 can be found in Table 4.4. Since we originally have the AHL production rates α and β per cell, we need to convert them to production per volume. So, we supposed to have a volume per cell which is directly 'accessible' for the AHL production, i.e., a typical 'free space' around the cells (very roughly estimated from [40]). Therefore, we assume to have the volume of 100 cells that is reasonable for some biofilm-volume around the cells.

Numerical simulations in Figures 4.2, 4.3, 4.4 and 4.5 show an application of the approximate solution (4.44) of a single cell for a unique value of approximate AHL production \widetilde{M} computed by (4.47). Here, the single cell is assumed to be located at $x = 0$ and has the cell radius $L = 0.6203 \mu m$ correspondent to a single cell volume given in Table 4.4. The red asterisks in Figures 4.2 and 4.3 represent the original cell radius and the black dotted lines in Figures 4.2 refer to the 'shrinking' cell radius L that assumed to manage the approximate AHL concentration accordingly to the approximate solution (4.44). In Figure 4.2 can be seen the AHL concentrations for a 'shrinking' cell, i.e., the approximate AHL concentrations are simulated as the cell radius $L \rightarrow 0$. We observe that reducing the cell radius to a point administrates a larger concentration of AHL within the cell. This is necessary, as the smaller cell volume should still have the same influence on the extracellular space. Therefore, choosing a cell as a point source does not cause any loss of AHL concentration which supports our approximative approach given in Subsection 4.4.2. Furthermore, Figure 4.3 includes plots for four different size of L together for an expanded interval of the radial coordinate r to remark the changing scale of AHL concentration within the 'shrinking' cell and its vanishing behavior in the medium. A zoom in of this figure is shown in Figure 4.4 in an interval of $r \in [30, 50]$ to understand better that the outer AHL concentration of a single cell converges to zero while $r \rightarrow \infty$. Since the approximate AHL concentration on the boundary between intra-extracellular space of a cell is given by $v(L) = v_0(L)$ we show the behavior of $v_0(L)$ which can be found in Figure 4.5 in a logarithmic plot.

Table 4.4: Parameters used for numerical simulations in Chapter 4.

Parameter	Description	Values	Reference
α	Basal AHL production rate	$2.3 \times 10^{-12} \frac{nmol}{\mu m^3 \times h}$	1
β	Induced AHL production rate	$2.3 \times 10^{-11} \frac{nmol}{\mu m^3 \times h}$	1
D	Diffusion rate of AHL	$3232542 \frac{\mu m^2}{h}$	2
V	Volume of a single cell	$1 \times 10^{-15} [l]$	3
A_{thresh}	Induction threshold of AHL	$70 \times 10^{-15} \frac{nmol}{\mu m^3}$	1

¹ correspondent to [16].

² diffusion rate in water correspondent to [24].

³ correspondent to [40].

4.5 A Population Model in \mathbb{R}^3 with a Lipschitz Continuous Source Term

From now on we aim to generalize the single cell model to a population model of N cells. We first consider the case of two cells so that the source term does not only include the self produced AHL but also the AHL which is produced by the other cell. We assume that these two identical cells have the radius L and they are located at $x_1, x_2 \in \mathbb{R}^3$, respectively. Furthermore, we suppose that their AHL concentrations are given by u_1 and u_2 . In the Hill-type source term, \bar{u}_{1,L,x_1} refers to the mean value of AHL concentration which is produced by the cell located at x_1 whereas \bar{u}_{2,L,x_1} represents the mean value of AHL concentration which is produced by the cell located at x_2 but transported by diffusion into the cell located at x_1 . More general, we say \bar{u}_{i,L,x_j} describes the mean value of the self produced AHL concentration within the cell for $i = j$ and the mean value of the AHL concentration produced by the other cells for $i \neq j$. Under these assumptions, the model of two cells reads

$$-D\Delta u_1(x) + \gamma u_1(x) = L^{-3} \left(\alpha + \beta \frac{L(\bar{u}_{1,L,x_1} + \bar{u}_{2,L,x_1})}{A_{thresh} + L(\bar{u}_{1,L,x_1} + \bar{u}_{2,L,x_1})} \right) \chi_{|x-x_1| \leq L}, \quad (4.48)$$

$$-D\Delta u_2(x) + \gamma u_2(x) = L^{-3} \left(\alpha + \beta \frac{L(\bar{u}_{2,L,x_2} + \bar{u}_{1,L,x_2})}{A_{thresh} + L(\bar{u}_{2,L,x_2} + \bar{u}_{1,L,x_2})} \right) \chi_{|x-x_2| \leq L} \quad (4.49)$$

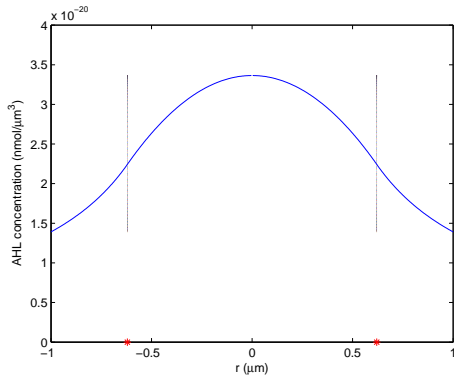
We consider the approximate model which has to be similar to the single cell model, i.e.,

$$-D\Delta v_1(x) + \gamma v_1(x) = L^{-3} M_1 \chi_{|x-x_1| \leq L}, \quad (4.50)$$

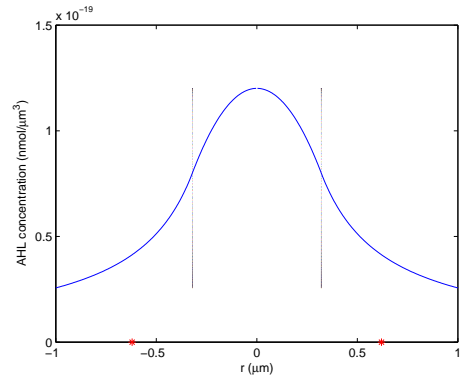
$$-D\Delta v_2(x) + \gamma v_2(x) = L^{-3} M_2 \chi_{|x-x_2| \leq L}.$$

Using again the previous idea for the current case, we define a difference function by $w_1 := u_1 - v_1$ and substitute $u_1 = w_1 + v_1$ into Equation (4.48). Similarly, we define

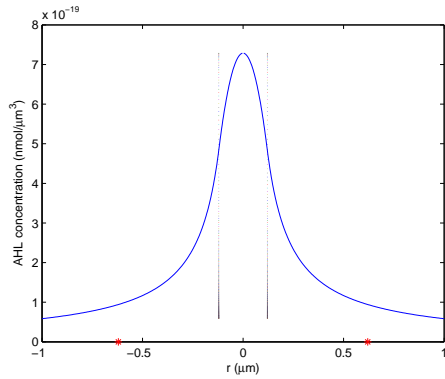
4.5 A Population Model in \mathbb{R}^3 with a Lipschitz Continuous Source Term



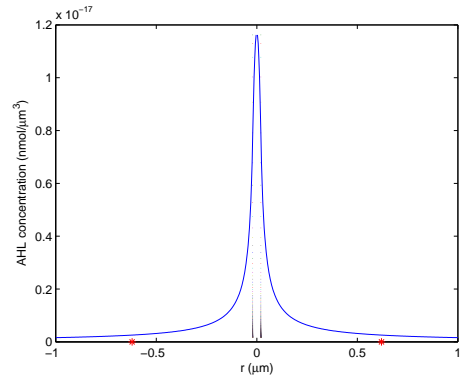
(a) $L = 0.6203 \mu m$



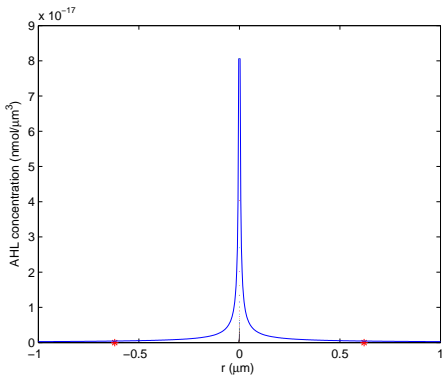
(b) $L = 0.3203 \mu m$



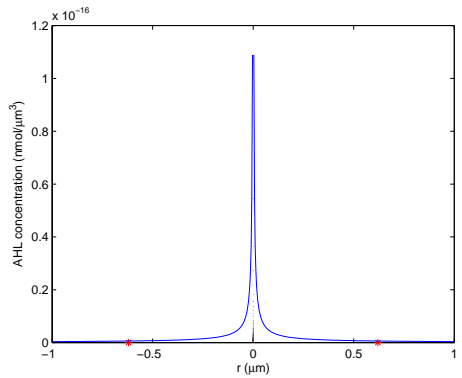
(c) $L = 0.1203 \mu m$



(d) $L = 0.0203 \mu m$



(e) $L = 0.0010 \mu m$



(f) $L = 0.0005 \mu m$

Figure 4.2: Numerical simulation of the approximate solution for a single 'shrinking' cell: initial cell radius $L = 0.6203 \mu m$, [40]. As $L \rightarrow 0$, the AHL concentration makes a peak at the center of the cell.

4 Spatial Structure of Cells and their Effect on the AHL Concentration

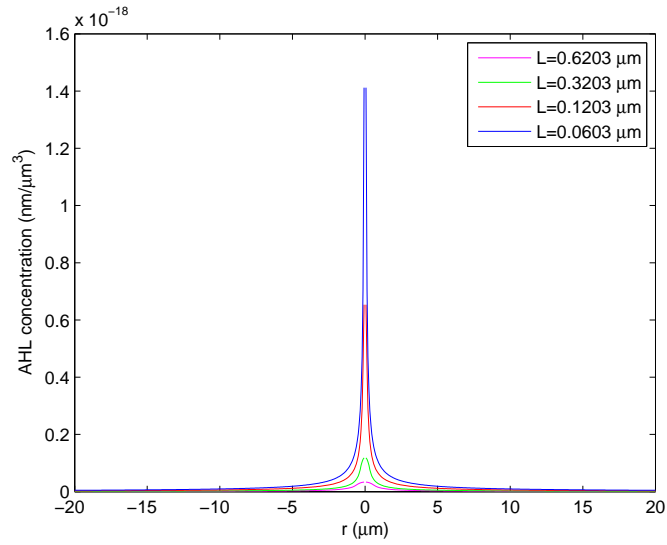


Figure 4.3: Numerical simulation of the changing scale of AHL concentration within the 'shrinking' cell and its extracellular behavior.

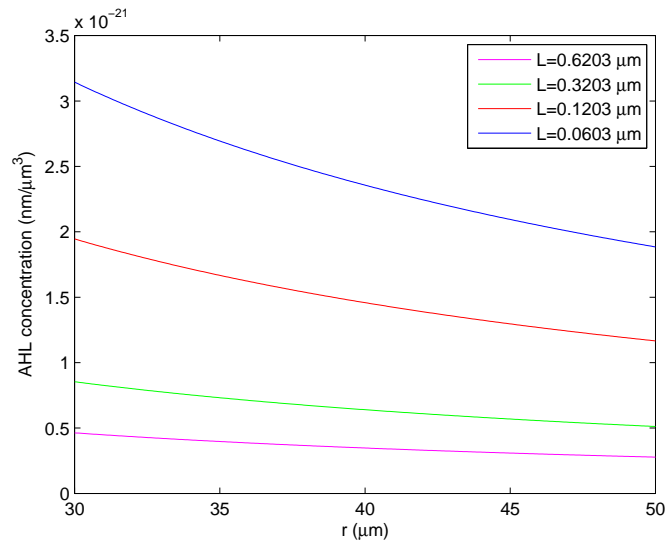


Figure 4.4: Numerical simulation of the vanishing extracellular AHL concentration for a single cell as $r \rightarrow \infty$. This figure is the zoom in of the Figure 4.3.

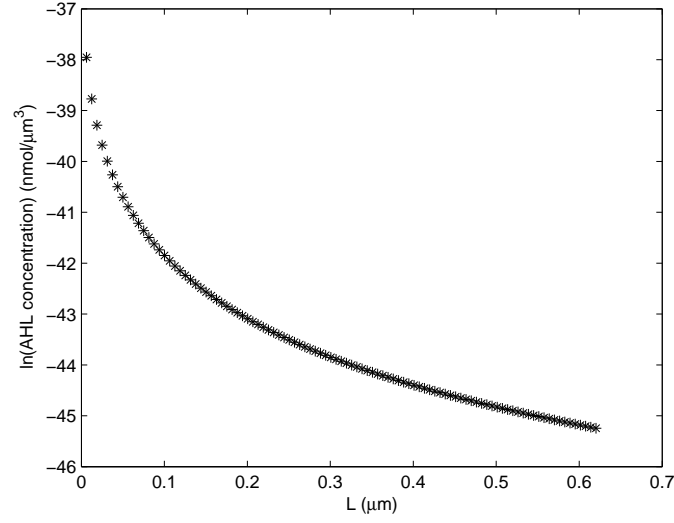


Figure 4.5: Numerical simulation of the AHL concentration on the boundary between the intra-extra cellular spaces for different values of L in the interval of $(0, 0.6203]\mu m$ as a logarithmic plot.

$\bar{w}_{1,L,x_1} := \bar{u}_{1,L,x_1} - \bar{v}_{1,L,x_1}$ and $\bar{w}_{2,L,x_1} := \bar{u}_{2,L,x_1} - \bar{v}_{2,L,x_1}$. Thus, we achieve the following equation which explains the model from the side of the cell located at x_1 ,

$$\begin{aligned} & -D\Delta w_1(x) + \gamma w_1(x) \\ & = L^{-3} \left(\alpha + \beta \frac{L(\bar{w}_{1,L,x_1} + \bar{w}_{2,L,x_1} + \bar{v}_{1,L,x_1} + \bar{v}_{2,L,x_1})}{A_{thresh} + L(\bar{w}_{1,L,x_1} + \bar{w}_{2,L,x_1} + \bar{v}_{1,L,x_1} + \bar{v}_{2,L,x_1})} - M_1 \right) \chi_{|x-x_1| \leq L}. \end{aligned} \quad (4.51)$$

Recall that we have defined before the approximate production within the cell by

$$\bar{v}_{1,L,x_1} = \frac{1}{\frac{4\pi}{3}L^3} \int_{|x-x_1| < L} v_1(r) 4\pi r^2 dr,$$

further the scaled form is

$$L\bar{v}_{1,L} = M_1 (\mu_1 + \mu_2 L + \mathcal{O}(L^2)).$$

Since the cell located at x_1 sense the AHL production of the cell located at x_2 via diffusion, we describe it by the approximate solution outside of the cell

$$\bar{v}_{2,L,x_1} = \frac{1}{\frac{4\pi}{3}L^3} \int_{|x-x_1| < L} v_2(x_1) 4\pi r^2 dr = v_2(x_1) + \mathcal{O}(L).$$

Let us determine the scaled form of the outer production, i.e.,

$$\begin{aligned}
 L\bar{v}_{2,L,x_1} &= L(v_2(x_1) + \mathcal{O}(L)) \\
 &= L \left(v_0 L e^{\sqrt{\gamma/D}L} \frac{e^{-\sqrt{\gamma/D}|x_1-x_2|}}{|x_1-x_2|} + \mathcal{O}(L) \right) \\
 &= L \left(\frac{1}{\gamma} L^{-3} M_2 \left(\frac{L \sqrt{\gamma/D} \coth(\sqrt{\gamma/D}L) - 1}{L \sqrt{\gamma/D} \coth(\sqrt{\gamma/D}L) + L \sqrt{\gamma/D}} \right) L e^{\sqrt{\gamma/D}L} \frac{e^{-\sqrt{\gamma/D}|x_1-x_2|}}{|x_1-x_2|} + \mathcal{O}(L) \right) \\
 &= \frac{1}{\gamma} L^{-2} M_2 \frac{L \sqrt{\gamma/D} \cosh(\sqrt{\gamma/D}L) - \sinh(\sqrt{\gamma/D}L)}{L \sqrt{\gamma/D} (\cosh(\sqrt{\gamma/D}L) + \sinh(\sqrt{\gamma/D}L))} L e^{\sqrt{\gamma/D}L} \frac{e^{-\sqrt{\gamma/D}|x_1-x_2|}}{|x_1-x_2|} + \mathcal{O}(L) \\
 &= \frac{1}{\gamma} L^{-2} M_2 \frac{L \sqrt{\gamma/D} \cosh(\sqrt{\gamma/D}L) - \sinh(\sqrt{\gamma/D}L)}{\sqrt{\gamma/D}} \frac{e^{-\sqrt{\gamma/D}|x_1-x_2|}}{|x_1-x_2|} + \mathcal{O}(L) \\
 &= \frac{1}{\gamma} L^{-2} M_2 \frac{1}{\sqrt{\gamma/D}} \frac{e^{-\sqrt{\gamma/D}|x_1-x_2|}}{|x_1-x_2|} \\
 &\quad \cdot \left(\frac{(L \sqrt{\gamma/D})^3}{2} + \frac{(L \sqrt{\gamma/D})^5}{4!} - \frac{(L \sqrt{\gamma/D})^3}{3!} - \frac{(L \sqrt{\gamma/D})^5}{5!} + \mathcal{O}(L^7) \right) \\
 &= \frac{1}{\gamma} L^{-2} M_2 \frac{1}{\sqrt{\gamma/D}} \frac{e^{-\sqrt{\gamma/D}|x_1-x_2|}}{|x_1-x_2|} \frac{(L \sqrt{\gamma/D})^3}{3} \left(1 + \frac{(L \sqrt{\gamma/D})^2}{10} \mathcal{O}(L^4) \right) \\
 &= M_2 \left(\frac{1}{3D} \frac{e^{-\sqrt{\gamma/D}|x_1-x_2|}}{|x_1-x_2|} \right) L + \mathcal{O}(L^2) \\
 &= M_2 \mu_3 L + \mathcal{O}(L^2),
 \end{aligned}$$

where $\mu_3 = \left(\frac{1}{3D} \frac{e^{-\sqrt{\gamma/D}|x_1-x_2|}}{|x_1-x_2|} \right)$ consist of the distance between two cells.

Thus, the right hand side of the Equation (4.51) is interpreted for two unknown variables and written more general as below

$$\begin{aligned}
 A \vec{w} &= F(\bar{w}_{1,L,x_1}, \bar{w}_{2,L,x_1}) \\
 &= f(\bar{w}_{1,L,x_1}, \bar{w}_{2,L,x_1}) \chi_{|x-x_1| < L}
 \end{aligned} \tag{4.52}$$

where A is an elliptic operator and F is a function represents the right hand side of the Equation (4.51), i.e.,

$$\begin{aligned}
 F : \mathbb{R}^2 &\rightarrow L^2, \\
 \vec{h} &= \begin{pmatrix} \bar{w}_{1,L,x_1} \\ \bar{w}_{2,L,x_1} \end{pmatrix} \mapsto f(\vec{h}) \chi_{|x-x_1| < L}.
 \end{aligned}$$

Let us define the function

$$\begin{aligned} \Phi : L^2 &\rightarrow \mathbb{R}^2, \\ \vec{g} = \begin{pmatrix} w_1 \\ w_2 \end{pmatrix} &\mapsto \vec{h} = \begin{pmatrix} \bar{w}_{1,L,x_1} \\ \bar{w}_{2,L,x_1} \end{pmatrix}. \end{aligned}$$

Thereby, we have the composition of functions $(F \circ \Phi)(\vec{g}) = F(\Phi(\vec{g}))$. The solution operator A^{-1} to the Equation (4.51) denotes

$$\begin{aligned} A^{-1} : L^2(\mathbb{R}^3) &\rightarrow H_0^1(\mathbb{R}^3), \\ A^{-1}(F(\Phi(\vec{g}))) &= \vec{w}. \end{aligned}$$

Banach's fixed point Theorem 4.12 guarantees the existence and uniqueness of fixed points to the self-map

$$\begin{aligned} T : L_+^2(\mathbb{R}^3) \subset L^2(\mathbb{R}^3) &\rightarrow L^2(\mathbb{R}^3) \\ T &= A^{-1}(F(\Phi(\vec{g}))). \end{aligned}$$

Theorem 4.12 (Banach Fixed Point Theorem)[4]

Let K be a complete metric space in which the distance between two points P and Q is denoted by $d(P, Q)$. Let $T : K \rightarrow K$ be a contraction; i.e., there exists a constant $C \in (0, 1)$ such that for all $P, Q \in K$, then

$$d(T(P), T(Q)) \leq C d(P, Q).$$

T has a unique fixed point, i.e., there exists a unique $x^* \in K$ such that $T(x^*) = x^*$.

According to Theorem 4.12, we write

$$\begin{aligned} \|T(\vec{g}_1) - T(\vec{g}_2)\|_{L^2} &= \|A^{-1}(F(\Phi(\vec{g}_1))) - A^{-1}(F(\Phi(\vec{g}_2)))\|_{L^2} \\ &= \|A^{-1}(F(\Phi(\vec{g}_1)) - F(\Phi(\vec{g}_2)))\|_{L^2} \\ &\leq \|F(\Phi(\vec{g}_1)) - F(\Phi(\vec{g}_2))\|_{H^{-1}} \\ &= \left\| \left(f(\vec{h}_1) - f(\vec{h}_2) \right) \chi_{|x-x_1| \leq L} \right\|_{H^{-1}} \\ &\leq \left| f(\vec{h}_1) - f(\vec{h}_2) \right| \left\| \chi_{|x-x_1| \leq L} \right\|_{H^{-1}} \end{aligned}$$

where $\vec{h}_1 = \begin{pmatrix} \bar{w}_{1,1,L,x_1} \\ \bar{w}_{2,1,L,x_1} \end{pmatrix}$ and $\vec{h}_2 = \begin{pmatrix} \bar{w}_{1,2,L,x_1} \\ \bar{w}_{2,2,L,x_1} \end{pmatrix}$. Recall that $\bar{w}_{L,x_1} = \frac{1}{\frac{4\pi}{3}L^3} \int_{|x-x_1| \leq L} w(x) dx$. Assuming $x_1 = 0$ for simplicity, we have $\bar{w}_L = \frac{1}{\frac{4\pi}{3}L^3} \int_{|x| \leq L} w(x) dx$. Since f is a globally Lipschitz continuous, bounded function on \mathbb{R}_+ we have

$$\left| f(\vec{h}_1) - f(\vec{h}_2) \right| \leq C \left| \vec{h}_1 - \vec{h}_2 \right|.$$

Thereby, we find

$$\begin{aligned}
 & \|T(\vec{g}_1) - T(\vec{g}_2)\|_{L^2} \\
 & \leq C \|\chi_{|x|\leq L}\|_{H^{-1}} (|\bar{w}_{1,1,L} - \bar{w}_{1,2,L}| + |\bar{w}_{2,1,L} - \bar{w}_{2,2,L}|) \\
 & = C \|\chi_{|x|\leq L}\|_{H^{-1}} \left(\frac{1}{\frac{4\pi}{3}L^3} \left| \int_{|x|<L} (w_{1,1}(x) - w_{1,2}(x)) dx \right| + \frac{1}{\frac{4\pi}{3}L^3} \left| \int_{|x|<L} (w_{2,1}(x) - w_{2,2}(x)) dx \right| \right) \\
 & \leq C \|\chi_{|x|<L}\|_{H^{-1}} \left(\frac{1}{\frac{4\pi}{3}L^3} \int_{|x|<L} |w_{1,1}(x) - w_{1,2}(x)| dx + \frac{1}{\frac{4\pi}{3}L^3} \int_{|x|<L} |w_{2,1}(x) - w_{2,2}(x)| dx \right) \\
 & \leq C \|\chi_{|x|<L}\|_{H^{-1}} \frac{1}{\frac{4\pi}{3}L^3} \left(\int_{|x|<L} 1 dx \right)^{1/2} \left(\left(\int_{|x|<L} (|w_{1,1}(x) - w_{1,2}(x)|)^2 dx \right)^{1/2} \right. \\
 & \quad \left. + \left(\int_{|x|<L} (|w_{2,1}(x) - w_{2,2}(x)|)^2 dx \right)^{1/2} \right) \\
 & \leq C \|\chi_{|x|\leq L}\|_{H^{-1}} L^{-3/2} (\|w_{1,1}(x) - w_{1,2}(x)\|_{L^2} + \|w_{2,1}(x) - w_{2,2}(x)\|_{L^2}) \\
 & = C \|\chi_{|x|\leq L}\|_{H^{-1}} L^{-3/2} \|\vec{g}_1 - \vec{g}_2\|_{L^2}.
 \end{aligned}$$

We then state and prove the following theorem which gives an estimate to $\|\chi_{|x|\leq L}\|_{H^{-1}}$.

Theorem 4.13

Let $\phi(x) \in C_0^\infty$ be a test function with the H^{-1} norm (as given in [62]), then we have the following estimate

$$\|\phi(x)\|_{H^{-1}} \leq 4L^{5/2} \|\phi\|_{H^1}.$$

Proof 4.14 According to the definition of the H^{-1} norm (as given in [62]) we have

$$\|\phi(x)\|_{H^{-1}} = \sup_{\phi \in H^1(\mathbb{R}^3), \|\phi\|_{H^1} \leq 1} \left| \int_{|x|<L} \phi(x) dx \right|.$$

Using the divergence theorem

$$\begin{aligned}
 \left| \int_{|x| \leq L} \phi(x) dx \right| &= \left| \int_{|x| \leq L} (\nabla_{x_1})(e_1 \phi(x)) dx \right| \\
 &= \left| \int_{|x|=L} x_1 e_1 \phi(x) d\vec{o} - \int_{|x| < L} x_1 \nabla_{x_1}(e_1 \phi(x)) dx \right| \\
 &\leq \left| \int_{|x|=L} x_1 e_1 \phi(x) d\vec{o} \right| + \left| \int_{|x| < L} x_1 \nabla_{x_1}(e_1 \phi(x)) dx \right| \\
 &\leq \left| L \int_{|x|=L} \phi(x) d\vec{o} \right| + \int_{|x| < L} |x_1| |\nabla_{x_1}(e_1 \phi(x))| dx \\
 &\leq \left| L \int_{|x| < L} \operatorname{div} \phi(x) dx \right| + L \int_{|x| < L} |\partial_{x_1} \phi(x)| dx
 \end{aligned}$$

Using Hölder inequality

$$\begin{aligned}
 \int_{|x| < L} \partial_{x_1} \phi(x) dx &\leq \left(\int_{|x| < L} 1 \right)^{1/2} \left(\int_{|x| < L} (\partial_{x_1} \phi(x))^2 dx \right)^{1/2} \\
 &\leq L^{3/2} \|\partial_{x_1} \phi(x)\|_{L^2} \\
 &\leq L^{3/2} \|\phi(x)\|_{H^1}
 \end{aligned}$$

then

$$\begin{aligned}
 \left| \int_{|x| < L} \operatorname{div} \phi(x) dx \right| &= \left| \int_{|x| < L} \partial_{x_1} \phi(x) dx + \int_{|x| < L} \partial_{x_2} \phi(x) dx + \int_{|x| < L} \partial_{x_3} \phi(x) dx \right| \\
 &\leq 3L^{3/2} \|\phi\|_{H^1}
 \end{aligned}$$

So, we can write

$$\begin{aligned}
 \left| \int_{|x| < L} \phi(x) dx \right| &= \left| \int_{|x| < L} (\nabla_{x_1})(e_1 \phi(x)) dx \right| \\
 &\leq \left| L \int_{|x| < L} \operatorname{div} \phi(x) dx \right| + L \int_{|x| < L} |\partial_{x_1} \phi(x)| dx
 \end{aligned}$$

$$\begin{aligned} &\leq 3L^{5/2} \|\phi\|_{H^1} + L^{5/2} \|\phi\|_{H^1} \\ &= 4L^{5/2} \|\phi\|_{H^1} \end{aligned}$$

□

Thus, we conclude

$$\begin{aligned} \|T(\vec{g}_1) - T(\vec{g}_2)\|_{L^2} &\leq 4L^{5/2} \|\phi\|_{H^1} L^{-3/2} \|\vec{g}_1 - \vec{g}_2\|_{L^2} \\ &= 4L \|\phi\|_{H^1} C \|\vec{g}_1 - \vec{g}_2\|_{L^2} \end{aligned}$$

and it shows that the operator T is a contraction. According to the Banach's fixed point theorem 4.12 there exists an unique solution \vec{w} to (4.52). Moreover, it is a fixed point $T(\vec{w}) = \vec{w}$.

Choosing $\bar{w}_{1,L} = \bar{w}_{2,L} = 0$ gives us the appropriate M_1 , i.e.,

$$\begin{aligned} M_1 &= \alpha + \beta \frac{L(\bar{v}_{1,L,x_1} + \bar{v}_{2,L,x_1})}{A_{thresh} + L(\bar{v}_{1,L,x_1} + \bar{v}_{2,L,x_1})} \\ &= \alpha + \beta \frac{(\mu_1 M_1 + \mu_2 M_1 L + \mu_3 M_2 L + \mathcal{O}(L^2))}{A_{thresh} + (\mu_1 M_1 + \mu_2 M_1 L + \mu_3 M_2 L + \mathcal{O}(L^2))}. \end{aligned}$$

Similarly, M_2 reads

$$\begin{aligned} M_2 &= \alpha + \beta \frac{L(\bar{v}_{2,L,x_2} + \bar{v}_{1,L,x_2})}{A_{thresh} + L(\bar{v}_{2,L,x_2} + \bar{v}_{1,L,x_2})} \\ &= \alpha + \beta \frac{(\mu_1 M_2 + \mu_2 M_2 L + \mu_3 M_1 L + \mathcal{O}(L^2))}{A_{thresh} + (\mu_1 M_2 + \mu_2 M_2 L + \mu_3 M_1 L + \mathcal{O}(L^2))}. \end{aligned}$$

Let us define an approximate $\widetilde{M}_1 = \alpha + \beta \frac{(\mu_1 \widetilde{M}_1 + \mu_2 \widetilde{M}_1 L + \mu_3 \widetilde{M}_2 L)}{A_{thresh} + (\mu_1 \widetilde{M}_1 + \mu_2 \widetilde{M}_1 L + \mu_3 \widetilde{M}_2 L)}$ and estimate the error function for $|M_1 - \widetilde{M}_1|$. So,

$$\begin{aligned} &|M_1 - \widetilde{M}_1| \\ &= \left| \beta \frac{(\mu_1 M_1 + \mu_2 M_1 L + \mu_3 M_2 L + \mathcal{O}(L^2))}{A_{thresh} + (\mu_1 M_1 + \mu_2 M_1 L + \mu_3 M_2 L + \mathcal{O}(L^2))} - \beta \frac{(\mu_1 \widetilde{M}_1 + \mu_2 \widetilde{M}_1 L + \mu_3 \widetilde{M}_2 L)}{A_{thresh} + (\mu_1 \widetilde{M}_1 + \mu_2 \widetilde{M}_1 L + \mu_3 \widetilde{M}_2 L)} \right| \\ &= \left| \beta \frac{A_{thresh} (\mu_1 (M_1 - \widetilde{M}_1) + \mu_2 (M_1 - \widetilde{M}_1) L + \mu_3 (M_2 - \widetilde{M}_2) L + \mathcal{O}(L^2))}{(A_{thresh} + \mu_1 M_1 + \mu_2 M_1 L + \mu_3 M_2 L + \mathcal{O}(L^2)) (A_{thresh} + \mu_1 \widetilde{M}_1 + \mu_2 \widetilde{M}_1 L + \mu_3 \widetilde{M}_2 L)} \right| \\ &\leq \beta \frac{\mu_1 |M_1 - \widetilde{M}_1| + \mu_2 |M_1 - \widetilde{M}_1| L + \mu_3 |M_2 - \widetilde{M}_2| L + \mathcal{O}(L^2)}{A_{thresh}}. \end{aligned}$$

Thus we find

$$\left| M_1 - \widetilde{M}_1 \right| - \frac{\beta \mu_2}{A_{thresh} - \beta \mu_1} |M_1 - \widetilde{M}_1| L - \frac{\beta \mu_3}{A_{thresh} - \beta \mu_1} |M_2 - \widetilde{M}_2| L + \mathcal{O}(L^2) \leq 0$$

where $A_{thresh} > \beta\mu_1$. Analogously, we have

$$\left| M_2 - \widetilde{M}_2 \right| - \frac{\beta\mu_2}{A_{thresh} - \beta\mu_1} \left| M_2 - \widetilde{M}_2 \right| L - \frac{\beta\mu_3}{A_{thresh} - \beta\mu_1} \left| M_1 - \widetilde{M}_1 \right| L + \mathcal{O}(L^2) \leq 0.$$

Thus, we achieve the error estimates $\left| M_1 - \widetilde{M}_1 \right| \leq \mathcal{O}(L)$ and $\left| M_2 - \widetilde{M}_2 \right| \leq \mathcal{O}(L)$. Hence we showed that \widetilde{M}_1 is a suitable approximate for M_1 , as well as \widetilde{M}_2 for M_2 . Finally, we have the following nonlinear algebraic equation system

$$\begin{aligned} \widetilde{M}_1 &= \alpha + \beta \frac{\mu_1 \widetilde{M}_1 + \mu_2 \widetilde{M}_1 L + \mu_3 \widetilde{M}_2 L}{A_{thresh} + \mu_1 \widetilde{M}_1 + \mu_2 \widetilde{M}_1 L + \mu_3 \widetilde{M}_2 L}, \\ \widetilde{M}_2 &= \alpha + \beta \frac{\mu_1 \widetilde{M}_2 + \mu_2 \widetilde{M}_2 L + \mu_3 \widetilde{M}_1 L}{A_{thresh} + \mu_1 \widetilde{M}_2 + \mu_2 \widetilde{M}_2 L + \mu_3 \widetilde{M}_1 L}. \end{aligned}$$

The auxiliary results for the case of two cells can be extended for a population of N cells. So, the model of N cells reads

$$-D\Delta u_i(x) + \gamma u_i(x) = L^{-3} \left(\alpha + \beta \frac{L \sum_{\substack{j=1 \\ i \neq j}}^N \bar{u}_{j,L,x_i}}{A_{thresh} + L \sum_{\substack{j=1 \\ i \neq j}}^N \bar{u}_{j,L,x_i}} \right) \chi_{|x-x_i| \leq L},$$

where the approximate model has to be similar to the model of two cells, i.e.,

$$-D\Delta v_i(x) + \gamma v_i(x) = L^{-3} \widetilde{M}_i \chi_{|x-x_i| \leq L}. \quad (4.53)$$

Further, the nonlinear algebraic equation system for a population of N cells can be written as

$$\widetilde{M}_i = \alpha + \beta \frac{\mu_1 \widetilde{M}_i + \mu_2 \widetilde{M}_i L + L \sum_{\substack{j=1 \\ i \neq j}}^N \mu_d(j) \widetilde{M}_j}{A_{thresh} + \mu_1 \widetilde{M}_i + \mu_2 \widetilde{M}_i L + L \sum_{\substack{j=1 \\ i \neq j}}^N \mu_d(j) \widetilde{M}_j}. \quad (4.54)$$

where $\mu_d = \left(\frac{1}{3D} \frac{e^{-\sqrt{\gamma/D}|x_i-x_j|}}{|x_i-x_j|} \right)$ is dependent on the distance between two cells. The implicit function form of \widetilde{M}_i yields

$$F_i(\widetilde{M}_1, \widetilde{M}_2, \dots, \widetilde{M}_N, L) = 0.$$

Thanks to the implicit function theorem the above nonlinear algebraic equation system may be solved for \widetilde{M}_i , [25]. Thus, the solution to the approximate model (4.53) for suitable

\widetilde{M}_i reads

$$v_i(r) = \begin{cases} \left(v_{0,i} - \frac{1}{\gamma} L^{-3} \widetilde{M}_i \right) \frac{L \sinh(\sqrt{\gamma/D} r)}{r \sinh(\sqrt{\gamma/D} L)} + \frac{1}{\gamma} L^{-3} \widetilde{M}_i, & r \leq L, \\ v_{0,i} L e^{\sqrt{\gamma/D} L} \frac{e^{-\sqrt{\gamma/D} r}}{r}, & r > L, \end{cases} \quad (4.55)$$

where

$$v_{0,i} = \frac{1}{\gamma} L^{-3} \widetilde{M}_i \left(\frac{L \sqrt{\gamma/D} \coth(\sqrt{\gamma/D} L) - 1}{L \sqrt{\gamma/D} \coth(\sqrt{\gamma/D} L) + L \sqrt{\gamma/D}} \right).$$

Similar to the approximate solution of a single cell (4.44) we determine here that the radial direction r starts with the center of i -th cell for each cell, repeatedly.

4.5.1 Numerical simulations for N cells

We present the numerical simulations for the results of Chapter 4.5. All simulations are based on the approximate solution (4.55) with the explicit values of \widetilde{M}_i given by the Equation (4.54). We find all \widetilde{M}_i via the Symbolic Math Toolbox of Matlab [36] for the algebraic equations system (4.54). All parameters we need for the simulations are taken as in Subsection 4.4.3 and we use the cell radius $L = 0.6203 \mu m$ for each plot. Recall the simulations for a single cell where the AHL concentration for one cell with radius $L = 0.6203 \mu m$ was $4 \times 10^{-20} nmol/\mu m^3$. (See Figure 4.2 for the single cell case.)

First, we assumed to have two cells in the system and one of them was supposed to have a fixed location. We consider the change of the approximate AHL production within the 'fixed' cell, i.e. M , as the other one is assumed to getting closer. Figure 4.6 shows how the interaction between two cells is dependent on the distance, i.e., the closer the cells are, the higher the AHL production there is.

The simulations for AHL concentrations of 5, 10, 25, 50, 75 cells can be found in Figure 4.7. Here, we aim to plot the approximate AHL concentration in a random cell distribution; for that we generate normally distributed random numbers for the cell positions in x and y (a vector of size 75). As our model distinguishes between the AHL concentration produced by cells 1, 2, \dots , N , we sum up these 'single' AHL concentration to get the final total AHL concentration. Please note the different scales of AHL concentration in each simulation.

- The exemplary simulations of AHL concentration for 5 and 10 cells are almost equal to the single cell concentration $4 \times 10^{-20} nmol/\mu m^3$ and far away from the induction threshold of AHL $70 \times 10^{-15} nmol/\mu m^3$.
- While the AHL concentration of 25 cells in the given spatial distribution approaches to the induction threshold, we observe that the case of 50 cells has already exceeded

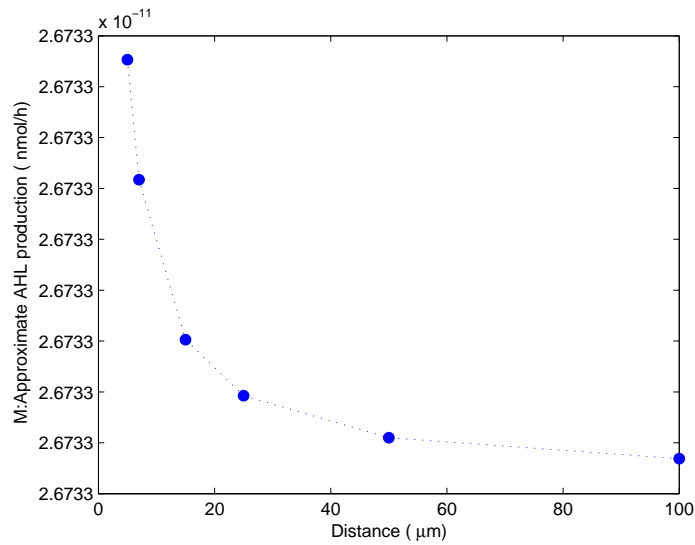
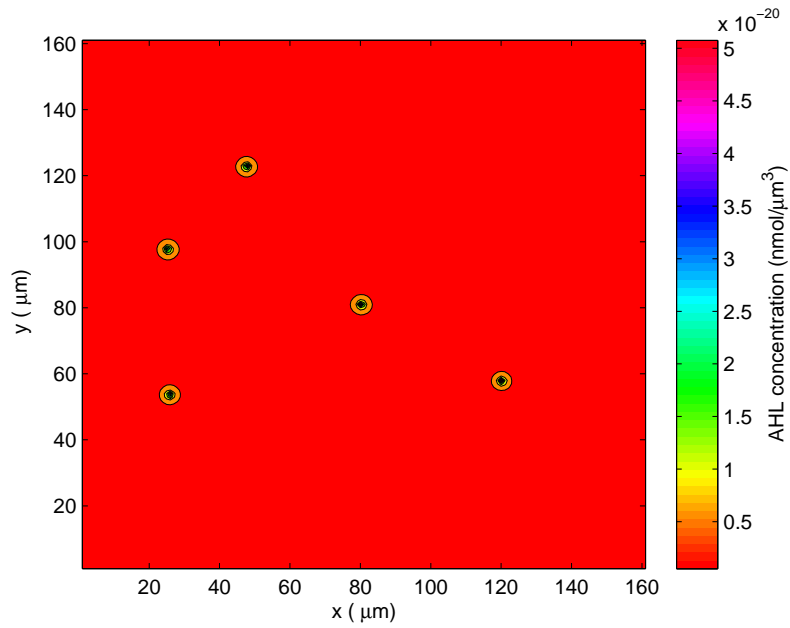


Figure 4.6: Numerical simulation of AHL production for two cells. It is shown that the total amount of AHL production is dependent on the distance between two cells.

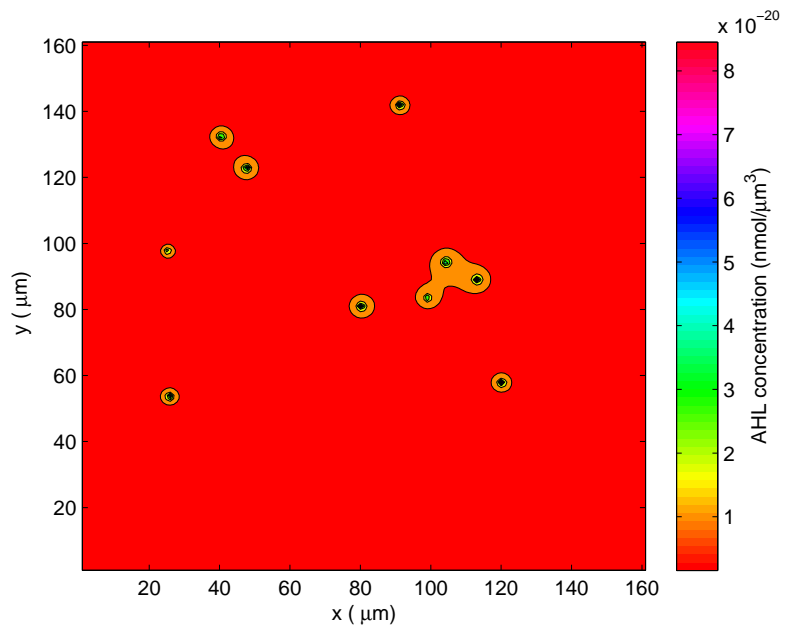
it. Thus, we guess around the population size of the 50 cells is possible to reach to the induction threshold. However, a smaller colony may also reach to the induction threshold for all other spatial structures where the cells are distributed closer to each other.

- Once the population exceeds the threshold, the AHL concentration increases noticeable as shown in the 75 cells case.

4 Spatial Structure of Cells and their Effect on the AHL Concentration

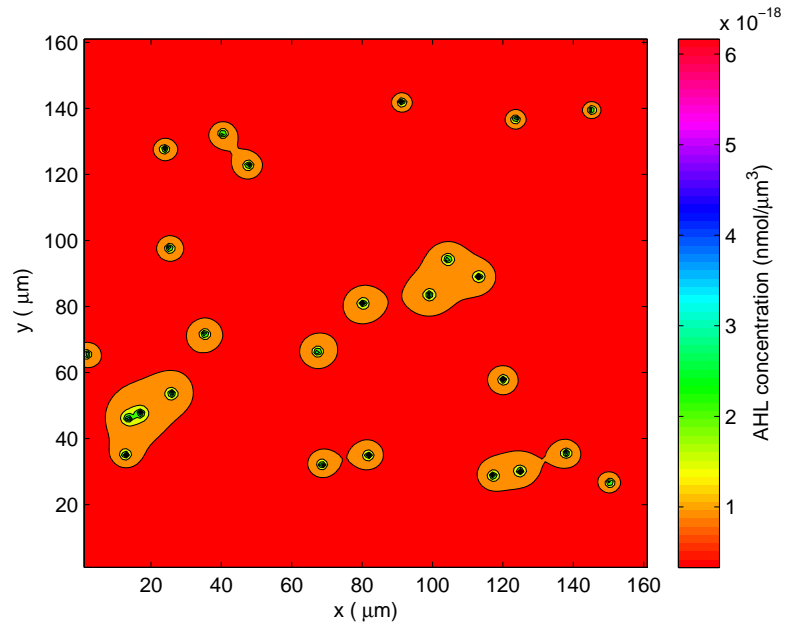


(a) AHL concentration for 5 cells.

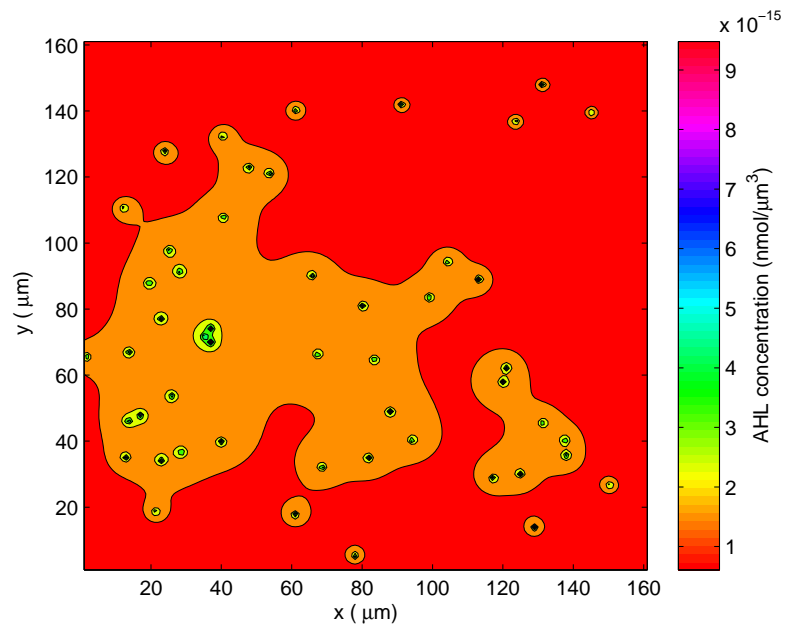


(b) AHL concentration for 10 cells.

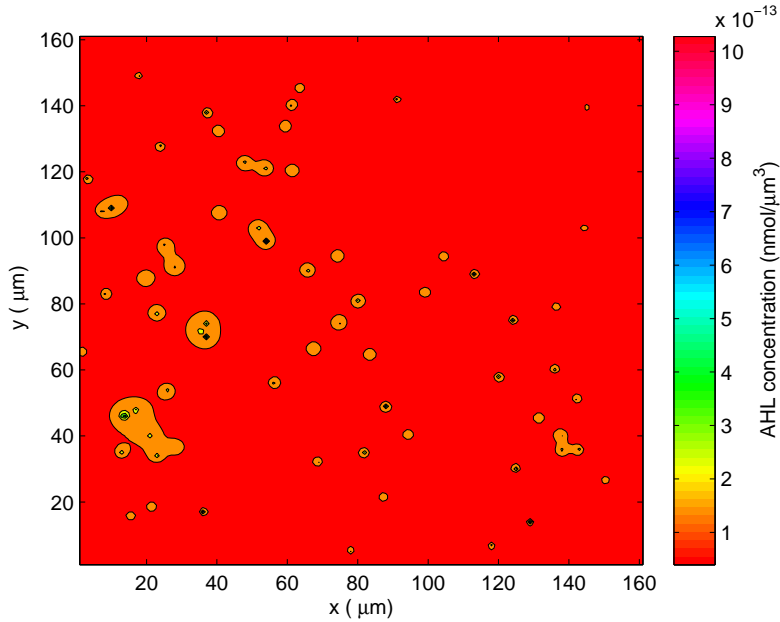
4.5 A Population Model in \mathbb{R}^3 with a Lipschitz Continuous Source Term



(c) AHL concentration for 25 cells.



(d) AHL concentration for 50 cells.



(e) AHL concentration for 75 cells.

Figure 4.7: Numerical simulation of AHL concentration for N cells with an identical cell radius $L = 0.6203\mu m$. It is shown that the AHL production is dependent on the distance between cells.

4.6 Conclusions

In this chapter, we investigated the influence of the spatial structure of a bacterial community on the QS coordinated by AHL molecules. We developed a mathematical model describing the AHL concentration based on a system of non-linear RDEs. We assumed that each cell is able to produce AHL and these AHL molecules freely diffuse through the cell membrane. The reaction term in our model explains the AHL production within the cell which is affected by the available AHL molecules in the cell. The spatially scattered structure of cells causes heterogeneity in the extracellular AHL concentration. For this complex system, analytical solutions are not available in the case of N cells. A necessary fine discretization around each tiny cell may cost a high computational effort for numerical solutions. Therefore, we looked for another possibility and used an approach of the mathematical shrinking of the tiny bacteria to point-size, [45]. This approach enabled us to find

some analytical approximate solutions in the steady state. We also investigated the error between the approximate solution and the exact solution for the single cell case and extended this idea for the N cells case. As expected, the approximate solutions to the steady state complex system show that the interaction of cells are highly dependent on the distance between each other, i.e., a cell efficiently produces AHL, when there exist many cells close to it. Consequently, our analytical results are supported by numerical simulations.

As a future work we are interested in evolving our model in two different directions. First, a flow effect on this spatially scattered cell system may influence the AHL accumulation and increase/decrease the interaction between cells. The analysis of the flow conditions would allow us to examine the response of the bacteria to the changing environmental conditions. Moreover, a model for interacting cells in non-steady state can be formulated by a delay equation, where the delay represents the time needed for sensing the AHL production from the other cells, [44]. This approach can be adapted to our RDE model and finding analytical approximate solutions would help understand the spatio-temporal QS system better.

5 Discussion

In this thesis we have introduced two different approaches for understanding the QS system in Gram-negative bacteria better. We assumed to have a single QS process that can be considered in several levels for mathematical modeling. For example, in the following we summarize in three levels:

- The QS process has a gene regulatory system that includes two essential components: the inducer protein I, (e.g. LuxI) synthesizes the autoinducer molecules AI and the transcriptional regulator protein R, (e.g. LuxR) interacts with the AI molecules, (e.g. AHL) and forms a complex.
- Bacterial growth causes AI accumulation. AI diffuses freely through the cell membrane and outspread spatially. The R-AI complex binds to the promoter of the protein I operon on the DNA to trigger the positive feed-back loop for an increasing production of AIs.
- The R-AI complex does not only activate the positive feed-back of the QS system, but also other gene expressions, which leads to phenotypic changes in bacteria.

We only focused on the last two levels in our modeling approaches: The phenotypic variation of single cells in a bacterial population and AI diffusion and their spatial distribution.

The phenotypic variation of single cells is interesting, because it is difficult to detect AI production of each cell from experiments, individually, even if it has a strong effect on the phenotypic changes. We have investigated the role of the AI concentration on the phenotypical changes in our model, so that we take into account the positive feedback loop that causes an increasing production of AIs in the activated cells. We described the phenotypic change (from the inactive to the active state) stochastically, as it is the case in reality, in combination with a deterministic AI production dependent on the phenotype of the cells. So, we have achieved a model predicting the phenotypic variation on single cell base in a growing bacterial population which was supported by experimental results.

Subsequently, we have needed to understand the AI diffusion and its accumulation better, which actually causes the phenotypic variations. Experimentally, it is not easy to measure the spatially heterogeneous AI concentration in a bacterial colony, but one can e.g. expect that the distance between cells respectively their local density may play an important

role in AI production and distribution due to the QS process. Indeed, the spatial structure of our model has provided to support this expectation quantitatively and predicted the approximate concentration of AIs in the heterogeneous medium. We have achieved this result with an analytical approximation to the spatially heterogeneous AI concentration taking each tiny cell as a point-source of AI. This allows for using a much simpler mathematical model, e.g. also very useful for more realistic simulations.

Bibliography

- [1] K. Anguige, J. R. King, J. P. Ward, and P. Williams. Mathematical modelling of therapies targeted at bacterial quorum sensing. *Mathematical Bioscience*, 192(1):39–83, 2004.
- [2] K. Anguige, J. R. King, and J. P. Ward. Modelling antibiotic- and anti-quorum sensing treatment of a spatially-structured *Pseudomonas aeruginosa* population. *Journal of Mathematical Biology*, 51(5), 2005.
- [3] B. A. Annous, P. M. Fratamico, and J. L. Smith. Quorum sensing in biofilms: Why bacteria behave the way they do. *The Society of Food Science and Technology*, 74(1): 24–37, 2009.
- [4] M. Badiale and E. Serra. *Semilinear Elliptic Equations for Beginners*. Springer, 2011.
- [5] L. J. Bain and M. Engelhardt. *Introduction to Probability and Mathematical Statistics*. Duxbury, Thomas Learning, 1991.
- [6] B. L. Bassler. How bacteria talk to each other: regulation of gene expression by quorum sensing. *Current Opinion in Microbiology*, 2:582–587, 1999.
- [7] B. L. Bassler, M. Wright, R. E. Showalter, and M. R. Silverman. Intercellular signalling in *Vibrio harveyi*: Sequence and function of genes regulating expression of luminescence. *Molecular Microbiology*, 9:773–786, 1993.
- [8] M. Boyer and F. Wisniewski-Dyé. Cell-cell signalling in bacteria: not simply a matter of quorum. *FEMS Microbiology Ecology*, 70:1–19, 2009.
- [9] A. W. Decho, R. L. Frey, and J. L. Ferry. Chemical challenges to bacterial AHL signalling in the environment. *Chemical Reviews*, 111:86–99, 2011.
- [10] J. D. Dockery and J. P. Keener. A mathematical model for quorum sensing in *Pseudomonas aeruginosa*. *Bulletin of Mathematical Biology*, 63:95–116, 2001.
- [11] A. Eberhard. Inhibition and activation of bacterial luciferase synthesis. *Journal of Bacteriology*, 109:1101–1105, 1972.

BIBLIOGRAPHY

- [12] J. Engebrecht and M. Silverman. Identification of genes and gene products necessary for bacterial bioluminescence. *Proceedings of the National Academy of Science*, 81:4154–4158, 1984.
- [13] M. Englmann, A. Fekete, C. Kuttler, M. Frommberger, X. Li, I. Gebefügi, J. Fekete, and P. Schmitt-Kopplin. The hydrolysis of unsubstituted N-acylhomoserine lactones to their homoserine metabolites analytical approaches using ultra performance liquid chromatography. *Journal of Chromatography A*, 1160:184–193, 2007.
- [14] L. C. Evans. *Partial Differential Equations*. American mathematical Society, 2010.
- [15] L. C. Evans, J. Blackledge, and P. Yardley. *Analytic Methods for Partial Differential Equations*. Springer, 2000.
- [16] A. Fekete, C. Kuttler, M. Rothballer, B. A. Hense, D. Fischer, K. Buddrus-Schiemann, M. Lucio, J. Müller, P. Schmitt-Kopplin, and A. Hartmann. Dynamic regulation of N-acyl-homoserine lactone production and degradation in *Pseudomonas putida* IsoF. *FEMS Microbiology Ecology*, 72(1):22–34, 2010.
- [17] M. R. Frederick, C. Kuttler, B. A. Hense, and H. J. Eberl. A mathematical model of quorum sensing regulated eps production in biofilms. *Theoretical Biology and Medical Modelling*, 8:8:e1000819, 2011.
- [18] W. C. Fuqua, S. C. Winans, and E. P. Greenberg. Quorum sensing in bacteria: The LuxR-LuxI family of cell density-responsive transcriptional regulators. *Journal of Bacteriology*, 176:269–275, 1994.
- [19] W. C. Fuqua, S. C. Winans, and E. P. Greenberg. Census and consensus in bacterial ecosystems: the the LuxR-LuxI family of quorum-sensing transcriptional regulators. *Annual Review of Microbiology*, 50:727–751, 1996.
- [20] A. B. Goryachev, D. Toh, K. B. Wee, T. Lee, H. Zhang, and L. Zhang. Transition to quorum sensing in an *Agrobacterium* population: A stochastic model. *PLoS Computational Biology*, 1:0264–0275, 2005.
- [21] E. Gustafsson, P. Nilsson, S. Karlsson, and S. Arvidson. Characterizing the dynamics of the quorum-sensing system in *Staphylococcus aureus*. *Journal of Molecular Microbiology and Biotechnology*, 8:232–242, 2004.
- [22] B. A. Hense, C. Kuttler, J. Müller, M. Rothballer, A. Hartmann, and J. Kreft. Does efficiency sensing unify diffusion and quorum sensing? *Nature Reviews Microbiology*, 5:230–239, 2007.

- [23] B. A. Hense, C. Kuttler, J. Müller, and A. Hartmann. Spatial heterogeneity of autoinducer regulation systems. *Sensors*, 12:4156–4171, 2012.
- [24] R. Hobbie. *Intermediate physics for medicine and biology*. Wiley, 1988.
- [25] A. Isidori. *Lecture Notes in Control and Information Sciences*. Springer, 1985.
- [26] S. James, P. Nilsson, G. James, S. Kjelleberg, and T. Fagerström. Luminescence control in the marine bacterium *Vibrio fischeri*: An analysis of the dynamics of *lux* regulation. *Journal of Molecular Biology*, 296:1127–1137, 2000.
- [27] A. Jayaraman and T. K. Wood. Bacterial quorum sensing: signals, circuits, and implications for biofilms and disease. *Annual Review Biomedical Engineering*, 10:145–167, 2008.
- [28] H. B. Kaplan and E. P. Greenberg. Diffusion of autoinducer is involved in regulation of the *Vibrio fischeri* luminescence system. *Journal of Bacteriology*, 163:1210–1214, 1985.
- [29] T. B. Kepler and T. C. Elston. Stochasticity in transcriptional regulation: origins, consequences, and mathematical representations. *Biophysical Journal*, 81:3116–3136, 2001.
- [30] I. Klapper and J. Dockery. Mathematical description of microbial biofilms. *SIAM REVIEW*, 52(2):000–000, 2010.
- [31] M. S. H. Ko. Stochastic model for gene induction. *Journal of Theoretical Biology*, 153:181–194, 1991.
- [32] A. J. Koerber, J. R. King, J. P. Ward, P. Williams, J. M. Croft, and R. E. Sockett. A mathematical model of partial-thickness burn-wound infection by *Pseudomonas aeruginosa*: quorum sensing and the build-up to invasion. *Bulletin of Mathematical Biology*, 64:239–259, 2002.
- [33] A. J. Koerber, J. R. King, and P. Williams. Deterministic and stochastic modelling of endosome escape by *Staphylococcus aureus*: quorum sensing by a single bacterium. *Journal of Mathematical Biology*, 50(4):440–488, 2005.
- [34] T. Lipniacki, P. Paszek, A. Marciniak-Czochra, A. R. Brasier, and M. Kimmel. Transcriptional stochasticity in gene expression. *Journal of Mathematical Biology*, 238:348–367, 2006.
- [35] A. Lunardi. *Analytic Semigroups and Optimal Regularity in Parabolic Problems*, (*Progress in Nonlinear Differential Equations and their Applications*). Birkhauser, 1995.
- [36] MATLAB. *Version 7.14.0.739 (R2012a)*. The MathWorks Inc., Natick, Massachusetts, 2012.

BIBLIOGRAPHY

- [37] R. C. McOwen. *Partial Differential Equations: Methods and Applications*. Prentice Hall, 2003.
- [38] J. A. Megerle. Cell-to-cell variability of gene expression dynamics in inducible regulatory networks. *Dissertation LMU, 2011*, 2011.
- [39] P. Melke, P. Sahlin, A. Levchenko, and H. Jönson. A cell-based model for quorum sensing in heterogeneous bacterial colonies. *PLoS Computational Biology*, 6:e1000819, 2010.
- [40] A. Meyer, J. A. Megerle, C. Kuttler, J. Müller, C. Aguilar, L. Eberl, B. A. Hense, and J. O. Rädler. Dynamics of AHL mediated quorum sensing under flow and non-flow conditions. *Physical Biology*, 9:026007–10pp, 2012.
- [41] M. B. Miller and B. L. Bassler. Quorum sensing in bacteria. *Annual Review of Microbiology*, 55:165–199, 2001.
- [42] J. Müller. *Imageana, Image Analyses Program*. TU Munich, 2010.
- [43] J. Müller. *SimbTUM, Simulation of Stochastic Processes and ODE Models in Biology*. GNU General Public License Version 3.0, TU Munich, 2012.
- [44] J. Müller and H. Uecker. Approximating the dynamics of communicating cells in a diffusive medium by ODEs-homogenization with localization. *Journal of Mathematical Biology*, DOI 10.1007:s00285–012–0569–y, 2012.
- [45] J. Müller, C. Kuttler, B. A. Hense, M. Rothballer, and A. Hartmann. Cell-cell communication by quorum sensing and dimension-reduction. *Journal of Mathematical Biology*, 53:672–702, 2006.
- [46] J. Müller, C. Kuttler, B. A. Hense, S. Zeiser, and V. Liebscher. Transcription, inter-cellular variability and correlated random walk. *Mathematical Biosciences*, 216:30–39, 2008.
- [47] J. D. Murray. *Mathematical Biology I*. Springer, 2002.
- [48] J. D. Murray. *Mathematical Biology II*. Springer, 2003.
- [49] I. J. Myung. Tutorial on maximum likelihood estimation. *Journal of Mathematical Psychology*, 47:90–100, 2003.
- [50] K. H. Nealson, T. Platt, and J. W. Hastings. Cellular control of the synthesis and activity of the bacterial luminescent system. *Journal of Bacteriology*, 104:313–322, 1970.

- [51] P. Nilsson, A. Olofsson, M. Fagerlind, T. Fagerström, S. Rice, S. Kjelleberg, and P. Steinberg. Kinetics of the AHL regulatory system in a model biofilm system: how many bacteria constitute a "quorum"? *Journal of Molecular Biology*, 309:631–640, 2001.
- [52] National Institute of Allergy and Infectious Diseases. Gram-negative bacteria, 2012. URL <http://www.niaid.nih.gov/topics/antimicrobialresistance/examples/gramnegative/Pages/default.aspx>.
- [53] N. M. Ozisik. *Heat Conduction*. Wiley Interscience Publication, 1993.
- [54] T. G. Platt and C. Fuqua. What 's in a name? The semantics of quorum sensing. *Trends Microbiology*, 18:383–387, 2010.
- [55] R. J. Redfield. Is quorum sensing a side effect of diffusion sensing? *The Society of Food Science and Technology*, 10:365–370, 2002.
- [56] M. Renardy and R. C. Rogers. *An Introduction to Partial Differential Equations*. Springer, 2004.
- [57] A. Steidle, M. Allesen-Holm, K. Riedel, G. Berg, M. Givskov, S. Molin, M. Luciao, and L. Eberl. Identification and characterization of an N-acylhomoserine lactone-dependent quorum-sensing system in *Pseudomonas putida* IsoF. *Applied Environmental Microbiology*, 68:6371–6382, 2002.
- [58] B. L. Jr. Vaughan, B. G. Smith, and D. L. Chopp. The influence of fluid flow on modeling quorum sensing in bacterial biofilms. *Bulletin of Mathematical Biology*, 72(5):1143–65, 2010.
- [59] J. P. Ward, J. R. King, A. J. Koerber, P. Williams, J. M. Croft, and R. E. Sockett. Mathematical modelling of quorum sensing in bacteria. *IMA Journal of Mathematics Applied in Medicine and Biology*, 18:263–292, 2001.
- [60] C. M. Waters and B. L. Bassler. Quorum sensing: cell-to-cell communication in bacteria. *Annual Review of Cell and Developmental Biology*, 21:319–46, 2005.
- [61] P. Williams. Quorum sensing, communication and cross-kingdom signalling in the bacterial world. *Microbiology*, 153:39233938, 2007.
- [62] K. Yosida. *Functional analysis*. Springer, 1980.
- [63] E. Zauderer. *Partial Differential Equations of Applied Mathematics*. Wiley, 1989.
- [64] J. Zhu, M. B. Miller, R. E. Vance, M. Dziejman, B. L. Bassler, and J. J. Mekalanos. Quorum-sensing regulators control virulence gene expression in *Vibrio cholerae*. *PNAS*, 99:3129–3134, 2002.